Master's Theses

Spring 2020

Nearshore Sedimentology of Eroding Microtidal Estuaries: Bon Secour Bay, Alabama and Perdido Bay, Florida

Jennifer Simpson

NEARSHORE SEDIMENTOLOGY OF ERODING MICROTIDAL ESTUARIES:

BON SECOUR BAY, ALABAMA AND PERDIDO BAY, FLORIDA

by

Jennifer L. Simpson

A Thesis
Submitted to the Graduate School,
the College of Arts and Sciences
and the School of Biological, Environmental, and Earth Sciences
at The University of Southern Mississippi
in Partial Fulfillment of the Requirements
for the Degree of Master of Science

Approved by:

Dr. Franklin T. Heitmuller, Committee Chair
Dr. T. Markham Puckett
Dr. Carl A. "Andy" Reese
Dr. Davin J. Wallace

_____	_____	_____
Dr. Franklin T. Heitmuller	Dr. Jacob Schaefer	Dr. Karen S. Coats
Committee Chair	Director of School	Dean of the Graduate School

May 2020

THE UNIVERSITY OF SOUTHERN MISSISSIPPI®

ABSTRACT

Estuarine shorelines along the northern Gulf of Mexico are dynamic geologic
settings that provide numerous ecological and economic benefits. By definition, estuaries
are semi-enclosed bodies of water that receive sediment from two sources: (1) fluvial
systems feeding into the estuary and (2) sediment transported by wave action and tidal
currents from adjacent marine sources. Erosion of estuarine shorelines resulting from
rising sea level, storm impact, and anthropogenic influence has been increasingly evident
in the microtidal Gulf Coast over recent decades. This study collects quantitative and
qualitative data to better understand sedimentary dynamics associated with contemporary
estuarine shoreline erosion in Bon Secour Bay, Alabama and Perdido Bay, Florida.
Historical aerial imagery compared with modern imagery indicates an average land loss
rate of $0.30 - 0.67$ m yr^{-1} at Bon Secour Bay (1992–2018) and 0.55 m yr^{-1} at Perdido Bay
(1994–2018). Selection of these two sites is based on their similar microtidal, sandy,
forested, undeveloped, northwest-to-southeast trending shorelines; albeit Bon Secour Bay
has a considerably longer fetch and greater fluvial sediment input as it is part of the
greater Mobile Bay estuarine system. Particle size of five nearshore sediment cores
(~$0.75 - 1.00$ m below seafloor) are dominated by fine- to medium-grained sand with
intervals of very fine and coarse sand and silt (rare). Sedimentological characteristics of
nearshore cores and surface sediment suggest eroding shorelines are being directly
deposited to the nearshore. Occurrences of shell material, wood fragments, coarser
particles, and reduced sorting quality at the base of some core locations indicate facies
change and possible ravinement surfaces that have been buried by sediment from a
Holocene transgression.

ii

ACKNOWLEDGMENTS

ACKNOWLEDGMENTS

I would like to express great appreciation to my committee chair and advisor, Dr. Frank Heitmuller, whose guidance and encouragement through this thesis has been irreplaceable. His positive attitude and unwavering willingness to help me through this challenging process has been a lesson in and of itself that I will take with me into my future ventures.

I would also like to extend my gratitude to my committee members, Dr. Mark Puckett, Dr. Andy Reese, and Dr. Davin Wallace, whose collective generosity of equipment, advice, and extensive knowledge in their respective fields have contributed to the development and success of this project.

Additionally, I would like to thank Dr. Scott Phipps and Shannon Walker from Weeks Bay National Estuarine Research Reserve; and Arthur Stiles with the Florida Department of Environmental Protection for their help in the facilitation of site locations for this project. I am also thankful for the support and camaraderie of the faculty and fellow students in the geology department at the University of Southern Mississippi.

Finally, I am grateful for the inspiration, motivation, and confidence I unrelentingly received from my family and friends throughout this journey.

TABLE OF CONTENTS

LIST OF TABLES

LIST OF ILLUSTRATIONS

CHAPTER I – INTRODUCTION

1.1 Introduction

Holocene sea-level rise has been extensively studied and has led to the shoreline

configuration observed today (Bruun, 1962; Schwartz, 1965; Leatherman et al., 2000;

Morton et al., 2004; Zhang et al., 2004; Anderson and Rodriguez, 2008). Accelerated sea-

level rise over the last few decades has been the primary contributing factor to

contemporary shoreline erosion and retreat. Eroding coastal shorelines include those of

barrier islands, mainland beaches, marshland, and margins of deltas, bays, lagoons, and

estuaries. This study focuses on nearshore clastic sedimentology of Bon Secour Bay,

Alabama and Perdido Bay, Florida, where there are two actively eroding microtidal

estuaries situated on the northern coast of the Gulf of Mexico (GOM) (Figure 1.1).

Coastlines along the northern GOM are of low topographic relief and experience diurnal

microtidal (< 2 m) regimes. Because of these characteristics, northern GOM shorelines

are particularly vulnerable to erosion from global sea-level rise and storm events.

Measurements for linear rates of relative sea-level rise (RSLR) assessed from the

Permanent Service for Mean Sea Level (PSMSL) tide gauges at locations along the

northern GOM vary from 2.0 mm yr^{-1} to greater than 9.5 mm yr^{-1} (Kolker et al., 2011).

As observed from historical aerial imagery, there has been an estimated average shoreline

retreat rate of 0.30 – 0.67 m yr^{-1} at Bon Secour Bay (1992 – 2018) and 0.55 m yr^{-1} at

Perdido Bay (1994 – 2018). Previous investigations using remote sensing and satellite

imagery of coastal Alabama quantified shoreline erosion rates ranging from 0 – 1.52 m

yr^{-1} along much of the eastern shore of Mobile Bay, including Bon Secour Bay (Hardin et

al., 1976). With evidence for erosion and land loss provided by previous workers and

historical imagery, the research conducted for this study characterizes nearshore

sedimentary cores to serve as a potential geologic indicator to assess estuarine shoreline

erosion.
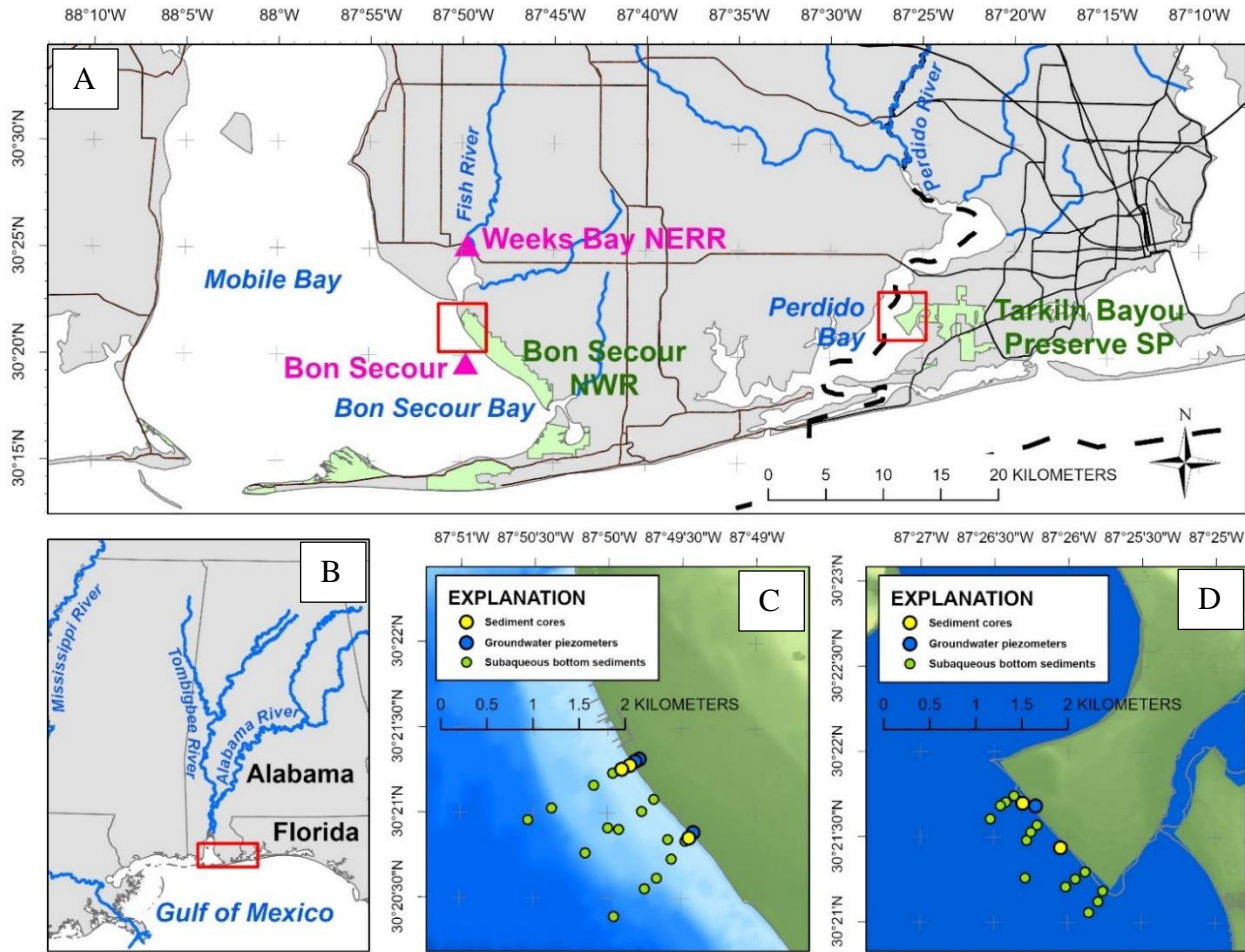
Figure 1.1 A). Inset map of northern Gulf of Mexico study area. B) Regional map of study area. C). Bon Secour Bay study area inset map with sample locations plotted. D). Perdido Bay study area inset map with sample locations plotted. (Map originally rendered by Dr. Frank Heitmuller in ArcPro GIS software in February 2020).

1.2 Research Questions

Historical imagery available for recent decades shows evidence of erosion and land loss along the clastic shorelines of Bon Secour Bay, Alabama and Perdido Bay, Florida. Because of low-relief topography, microtidal regimes, and often saturated shorelines resulting from high precipitation rates, estuaries of the northern Gulf Coastal Plain are especially vulnerable to damaging effects caused by storms and rising global sea level. Traditional transgressive estuarine sedimentary models include facies with input exclusively from marine and fluvial sources (Dalrymple et al., 1992). A more recent facies model for transgressive wave-dominated coasts includes deposition of tidal mud flats, channels, and sandy beaches of estuarine margins (Boyd, 2010). The sandy beach margin of the estuary and its erosion is the environmental focus for this study. Questions addressed by this research include:

(1) Are sediments eroded from the shoreline re-distributed in recognizable depositional patterns in submerged nearshore settings?

(2) What is the sedimentological variability of nearshore deposits in the vicinity of eroding estuarine shorelines? Does variability of these nearshore deposits correspond with sedimentary characteristics of the shoreline zone or further offshore?

(3) Is ground saturation particularly effective at eroding estuarine shorelines and re-distributing sediment?

The primary objective of this study is to determine if there is an identifiable sedimentary profile for actively eroding microtidal estuarine shorelines along the transgressing Gulf Coastal Plain. Secondary objectives will (1) analyze sedimentological

4

variability of eroding clastic microtidal estuarine shorelines between two different estuarine basins; (2) identify how responsive shallow groundwater levels are to rainfall events along low-relief, microtidal estuarine shorelines; (3) determine if water table levels contribute to shoreline instability; and (4) determine if short-term (monthly) shoreline erosion measurements are reflective of long-term (decadal) erosion rates.

1.3 Hypothesis

Given the evidence for shoreline erosion and transgression observed from historical imagery and literature of the northern Gulf Coast, I believe a coarsening upward sequence will be present over finer grain sediment in the nearshore cores of the estuarine margin. Furthermore, the source of the coarse overlying sediment will be from the proximal eroding shoreline, as supported by sedimentological analysis. Because erosion is presumed to be occurring as a result of transgression, there is a possibility of active formation of an erosional unconformity known as a ravinement surface (Boyd, 2010; Bache et al., 2014). Identifying a definitive ravinement surface in this study is likely not possible because the surface in question is still actively eroding and not well preserved.

Longitudinal variation of sediment as compared between Bon Secour Bay and Perdido Bay will likely show similar abundance of sand and mud. However, because of differences in watershed lithology (and associated mineralogy), the Bon Secour Bay sediment cores should have a greater heavy mineral content than Perdido Bay sediment cores (Northwest Florida Water Management District, 2017). Also expected is higher organic matter content in Bon Secour Bay cores because of the proximity to fluvial influence and the associated greater nutrient inputs from larger rivers compared to

5

Perdido Bay sediment (Hummell and Parker, 1995). Oyster farming in Bon Secour Bay and vicinity could result in greater carbonate content in those sediments than in Perdido Bay sediments.

Highly permeable sandy shorelines and regular saturation from rainfall events should promote rapid responses in shallow groundwater levels at both locations (Tolhurst et al., 2006). Sandy shoreline sediment combined with a rapid rise in the water table from rainfall could exacerbate coastal erosion, especially during a meteorological event when wind, waves, and storm surge have increased influence.

Short-term erosion rates could be highly variable from month to month. Seasonal effects need to be taken into consideration, as well as natural shoreline replenishment. In estuarine settings, natural shoreline replenishment is not nearly as significant a geomorphologic factor as it is in open-marine settings (Van Rijn and Barr, 1990). Short-term erosion measurements can be indicative of a general trend; however, the quantitative values of monthly measurements might be "noisy" when compared to a decadal trend.

Results from this research, if reasonable and applicable, could be used to propose re-analysis of coastal depositional environments in the geologic record. Specifically, consideration could be made for the existence of a transgressive estuarine facies without evidence of a ravinement surface.

1.4 Thesis Scope

The scope of this thesis includes interpretations based on sediment cores, sediment samples, and groundwater samples collected in the field; piezometer, groundwater-level sensor, and erosion pin installations in the field; laboratory analyses of sedimentological parameters and water quality; ancillary data analysis; and statistical

analyses of sedimentological data. Field data collection trips occurred between May 2018

and November 2019; laboratory analyses occurred between July and September 2019;

and ancillary and statistical analyses occurred between October 2019 and February 2020.

CHAPTER II – LITERATURE REVIEW

2.1 Geologic Setting

Bon Secour Bay, Alabama and Perdido Bay, Florida are situated within the

northeastern portion of the Gulf Coastal Plain physiographic province (DuBar, 1991). In

the United Sates, the Gulf Coastal Plain extends 2,350 km from the Mexico border to the

southern end of Florida. Discussed hereinafter are the geologic units pertinent to the

study and does not include units further upstream where influence is marginal for the

study locations. Figure 2.1 is a stratigraphic column of outcropping units on the Gulf

Coastal Plain in the study area. The Pliocene-Pleistocene Citronelle Formation commonly

occurs along ridges or flat upland areas of southern Mobile and Baldwin Counties,

Alabama and is spatially variable in lithology (Matson, 1916). The Citronelle is less than

a meter to 60 m thick with unconformable contacts, and typically consists of orange-red,

weathered, unconsolidated to poorly consolidated silty-sandy to gravelly-sandy fluvial

upland deposits with few paralic or marine fossils (Matson, 1916; Isphording and Lamb,

1971, Hummell, 1996). The Citronelle contains chert and quartz pebbles and lenticular

beds of red, purple, yellow, and gray clays that are typically mottled (Raymond et al.,

1988). South of the Citronelle along the coastline are the Pleistocene-age Prairie and

Gulfport Formations. The pre-Holocene deposits range from less than one meter to 46 m

thick and directly underlie an unconformable boundary identified by seismic and

vibracores from Mobile Bay. The Pleistocene age formations are alluvial, coastal, and

terrace deposits characterized by stiff, oxidized clay-rich sediment that is yellowish

orange, brown, gray, and greenish gray in color, or semi- to unconsolidated sands, muddy

sands, and gravelly sands that are yellowish brown, olive gray, greenish gray, and brown

in color (Marsh, 1966; Hummell, 1996). The Prairie Formation consists of fine to coarse sand and silty sand with occasional gravel and lignite. The Gulfport Formation is a thin belt along the outermost seaward margin and is comprised of poorly to moderately sorted shoreface sands (Otvos, 1991). Pleistocene sediment in the northeastern region of the Gulf Coastal Plain is generally less than 30 m thick and grades seaward at 0.2 to 3.0 m/km. The aquifer and groundwater supply of southern Baldwin County, Alabama consist of geologic units from Citronelle Formation and Holocene alluvial, low terrace, and coastal deposits (Chandler, et al., 1985).

Perdido Bay is in Escambia County, Florida, and occurs in the narrow 10–12-mile-wide Coastal Lowlands topographic region of the Gulf Coastal Plain. Escambia County subsurface geology is like that of coastal Alabama as previously discussed (Work et al., 1991). Marine terraces of Pleistocene age are a distinctive feature of the Escambia County coastal plain. Terrace remnants are preserved as upland plateaus, low coastal plains, flat-topped hills, and benches.
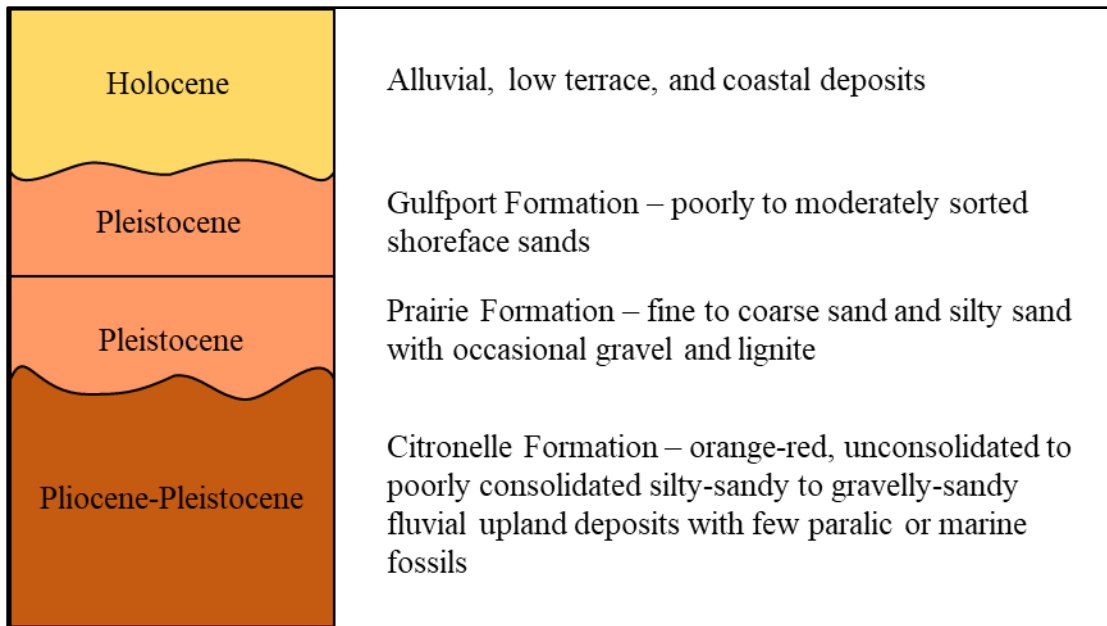
Figure 2.1 Stratigraphic column of Alabama-Florida Gulf Coastal Plain.

During the Late Pleistocene Wisconsinan glacial maximum, around 18 ka, relative sea level was approximately 120 m lower than present day (Morton et al., 2004). Low sea level and relatively high stream discharge rates allowed for incision of river valleys along the Gulf Coastal Plain, extending out to the present-day continental shelf (DuBar, 1991; Hollis et al., 2019). Subsequent glacial melting resulted in inundation and partial sediment-fill of the incised river valleys, forming bays and bayhead deltas. Rising sea levels from melting glaciers reached their current position approximately 4 ka, leading to the creation of coastal features including Bon Secour Bay and Perdido Bay (Milliken et al., 2008). The most recent Holocene highstand resulted in approximately 3 m of sea level rise in the ancestral Mobile River valley complex, about 6,000 to 7,000 years before present to the current time (Isphording and Flowers, 1990; Hummell, 1996). Previous work has constrained the antecedent topography and depositional history of Mobile Bay using vibracores, rotary drill cores, and seismic data (Rodriguez et al., 2008). Seismic

10

reflectors from a cross-section of Mobile Bay show an unconformity at varying depths between approximately 6 and 18 m below sea level. A sharp contact is seen in cores that sample the unconformity that consists of clay, peat, and rip-up clasts overlying an oxidized clay layer, characterizing it as an erosional unconformity. This erosional unconformity delineates the Pleistocene-Holocene boundary in Mobile Bay.

Tectonic activity along the outer region of the northeastern Gulf Coastal Plain, including Bon Secour Bay and Perdido Bay, has been relatively stable during the Quaternary. Evidence for minor tectonic activity includes surficial expressions of sub-surface growth faulting, Pleistocene outcrop faulting and fracturing, and Holocene shore-parallel shallow fracture systems (Ewing, 1991).

2.2 Depositional History

The Gulf Coastal Plain is primarily comprised of siliciclastic sediment ranging in size from clay to sand (McBride and Byrnes, 1995). Unconsolidated and eroded sediment from the Pliocene-Pleistocene aged Citronelle Formation supplies a considerable amount of the surficial sediment transported downstream to coastal Alabama and western Florida from upland areas of the lower Gulf Coastal Plain.

The Mobile-Tensaw bayhead delta system provides fluvial input to the Mobile Bay estuary complex. The watershed for this delta system is more than 110,000 km^2 including parts of Alabama, Mississippi, Georgia, and Tennessee; and discharges into Mobile Bay through various distributaries at an average rate of over 1,750 m^3/sec (Isphording and Flowers, 1990; Hummell and Parker, 1995; Rodriguez et al., 2008). Major rivers contributing discharge and sediment in the watershed include the Tombigbee, Alabama, Black Warrior, Tallapoosa, and Coosa (the latter three are

tributaries of the first two). Included in the watershed drainage is sediment originating

from the southeastern Piedmont Province, the southern Appalachian Mountains of the

Ridge and Valley and Blue Ridge Provinces, the Cumberland Plateau, and sediment from

within the Gulf Coastal Plain Province. The Fish and Magnolia Rivers are local minor

contributing watershed streams that discharge directly to Bon Secour Bay. Reworked

siliciclastic sediment from the Gulf Coastal Plain contributes to most of the sediment

volume for the entirety of Mobile Bay.

The Perdido River and Bay watershed supplies fluvial inputs to Perdido Bay.

Covering 3,238 km^2 in parts of Alabama and Florida, the Perdido River and Bay

watershed is much smaller than the Mobile-Tensaw watershed. The Perdido River is the

primary contributing stream in the watershed, discharging at an average rate of 22 m^3/sec

into Perdido Bay (Northwest Florida Water Management District, 2017). The Perdido

River has several tributary streams including the Styx River, Blackwater Creek, Boggy

Creek, and Brushy Creek, among others. Elevenmile Creek and Bayou Marcus are other

contributing streams discharging directly to Perdido Bay, but with much lower volumes

than the Perdido River. Sediment deposited into Perdido Bay from lithologic formations

within the Perdido River and Bay watershed are nearly pure quartz sand with minor

heavy mineral sand (Northwest Florida Water Management District, 2017).

2.3 Climate

The Gulf Coastal Plain experiences a warm, humid, and subtropical climate with

strong meteorological influence from the Gulf of Mexico. The northern Gulf Coast

receives a higher amount of precipitation than most other locations in the United States

(NOAA, 2019). Bon Secour Bay and Perdido Bay occur within the isopleth contour of

150 – 200 cm of mean annual precipitation. The wettest time of year along the Gulf Coast is typically during the late winter and throughout the summer months. Snowfall and snowmelt are not significant contributors of precipitation in this region. Bon Secour Bay and Perdido Bay regularly experience seasonal tropical storm activity. This high occurrence of storm activity is especially impactful to low-relief shorelines which lack a buffer to rapid flooding otherwise provided by higher-relief shorelines.

2.4 Transgressive Systems Tract

This study analyzes facies and facies change, particularly in a transgressive regime. Figure 2.2 displays a sequence for a siliciclastic system such as the estuarine deposits of this study. Although not all systems tracts, surfaces, and strata architecture in the schematic are present in the nearshore sediment cores of this study, select characteristics are important to note for contextualization of interpretations made given the results. By definition, a sequence is "a succession of strata deposited during a full cycle of change in accommodation or sediment supply" (Catuneanu et al., 2009). A transgressive systems tract (TST) is a subdivision of a sequence that occurs when sea level rises more rapidly than sediment accumulates. During a marine transgression in a formerly subaerial environment, an erosional surface known as a ravinement surface can be produced in the coastal zone by encroaching wave or tidal action. A regime reversal is marked by turnaround point known as maximum flooding surface (MFS). The MFS is a stratigraphic feature that separates a TST from a highstand systems tract where the shoreline is at its furthest landward point.
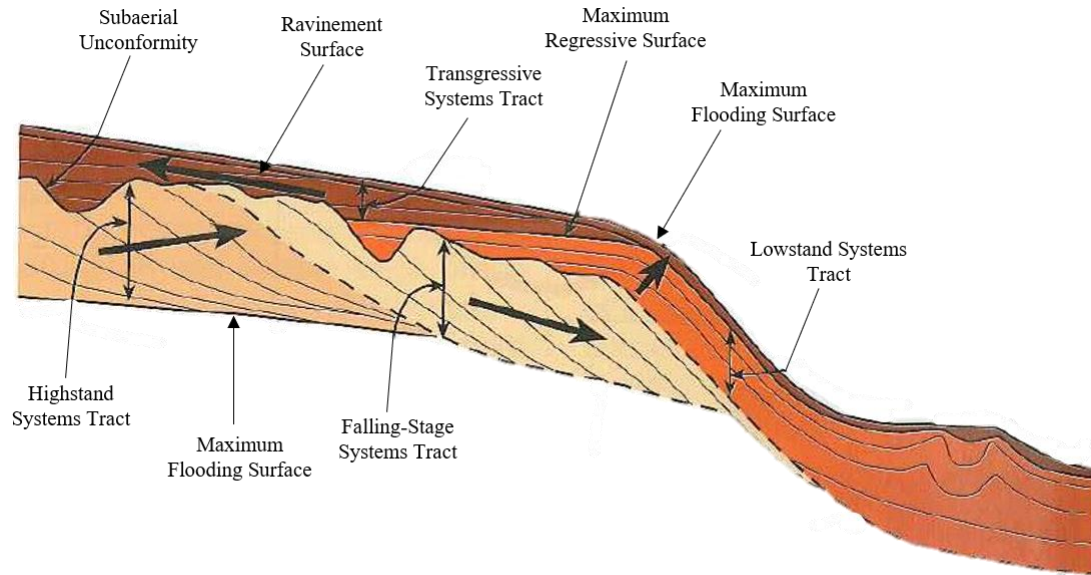
Figure 2.2 Schematic dip section for a siliciclastic system (From Dalrymple, 2010).

2.5 Estuary Model

Estuaries are transitional inlet environments where continental land meets the sea.
Estuaries develop best along mid-latitude coastal plains with submerged continental
shelves (Reinson, 1992). The northern GOM and its affiliated estuaries have
transgressive, wave-dominated coastlines as a response to the balance between sea-level
rise, coastal sediment flux, and geographic location (Boyd, 2010). Wave-dominated
coasts are often westward facing shorelines with persistent winds and relatively low tidal
power in temperate regions between latitudes 35 – 60° N and S (Boyd, 2010). The
northern GOM estuarine coasts in this study do not perfectly fit the geographic definition
given by Boyd (2010); however, they are indeed more strongly affected by waves than
tides, which are almost negligible, thus are categorized as wave-dominated shorelines.

The classic facies model for wave-dominated microtidal estuaries (See Figure 2.3)
like those along the northern Gulf Coast is tripartite and developed with respect to the

14

sedimentological sequence along the estuary axis (Dalrymple et al., 1992; Reinson, 1992; Roy, 1994).
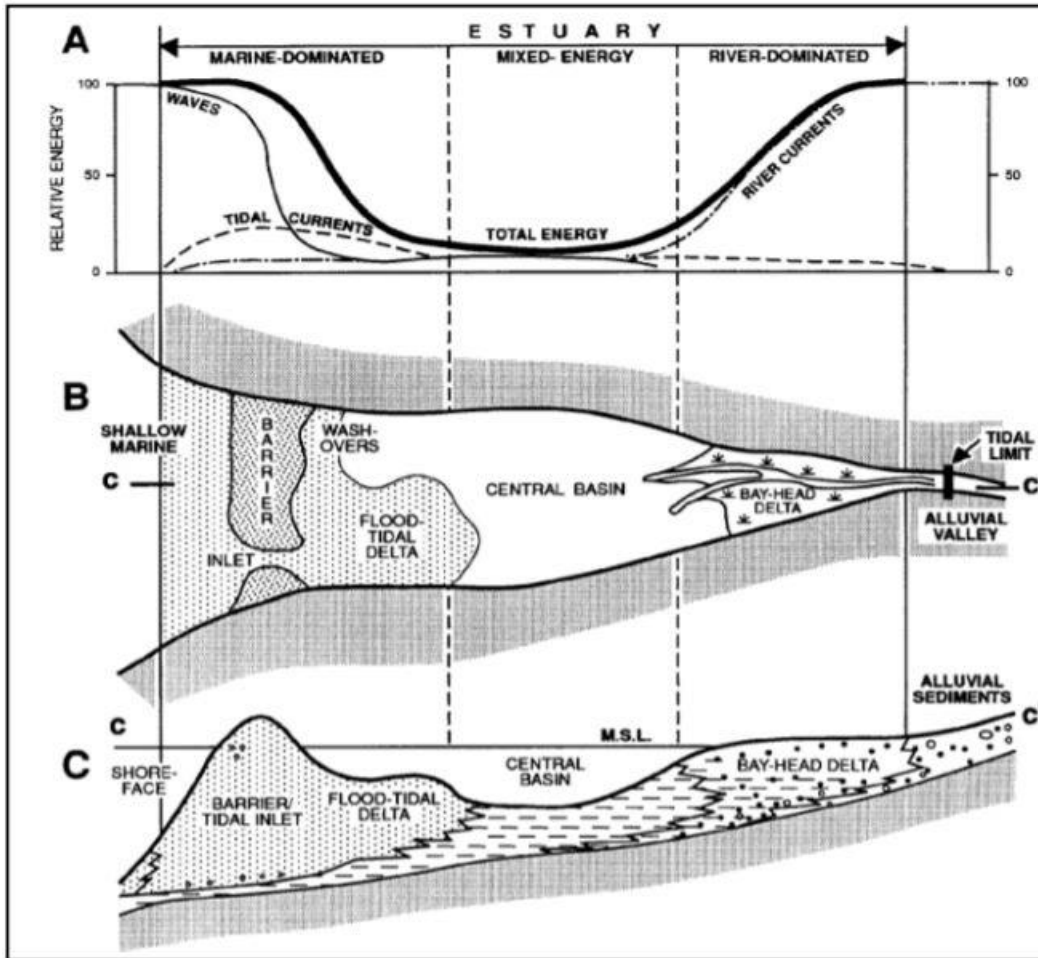
Figure 2.3 Classic conceptual model of a wave-dominated estuary. (A) Energy regime, (B) morphological units, (C) facies association. From Dalrymple et al., (1992).

Estuarine sediment accumulation is dependent on waves, tides, river discharge, wind, and precipitation (Nichols and Biggs, 1985). Beginning at the landward margin, the three-part model consists of reworked fluvial sand and gravel facies in the bayhead delta, then transitions to a fine-grained sediment facies in the central basin, then to coarse-grained marine sediment facies from washover, barrier island, and tidal deposits in the seaward margin. The margin around the central basin of Mobile Bay is characterized as

15

nearshore facies (Hummell, 1996). The nearshore facies is a transitional environment between open bay and the beach, and therefore deposits are composed of features such as shells, wood, rip-up clasts, and peat balls in addition to varying proportions of sand, silt, and clay. Sand-sized particles are from the proximal eroding shoreline and winnowing of finer grained material from wave activity. Present-day nearshore facies are being deposited in Mobile Bay at water depths of 1 – 2 m (Hummell, 1996).

Estuarine margins are comprised of tidal channels, mud flats, and sandy beaches with deposits that typically coarsen upward with shoreline progradation (Boyd, 2010). When estuarine shorelines erode because of storms, sea level rise, or otherwise, sediment is often reworked and deposited in environments that do not reflect original deposition. For example, the presence of coarse-grained siliciclastic sediment over a fining upward sequence in a central estuary facies may be evidence for an eroding shoreline along the estuary margin. It is also important to consider the preservation potential of sedimentological sequences, both modern and ancient. Evidence of reworking and erosion of sediment after deposition may not be obvious or present in the geologic record, making detection of a transgressive estuarine depositional facies a complex and uncertain endeavor. Figure 2.4 is a model of facies profiles for transgressive wave-dominated coasts containing shore-parallel and shore-perpendicular sections. This model represents more facies possibilities than the classic model for wave-dominated estuaries.
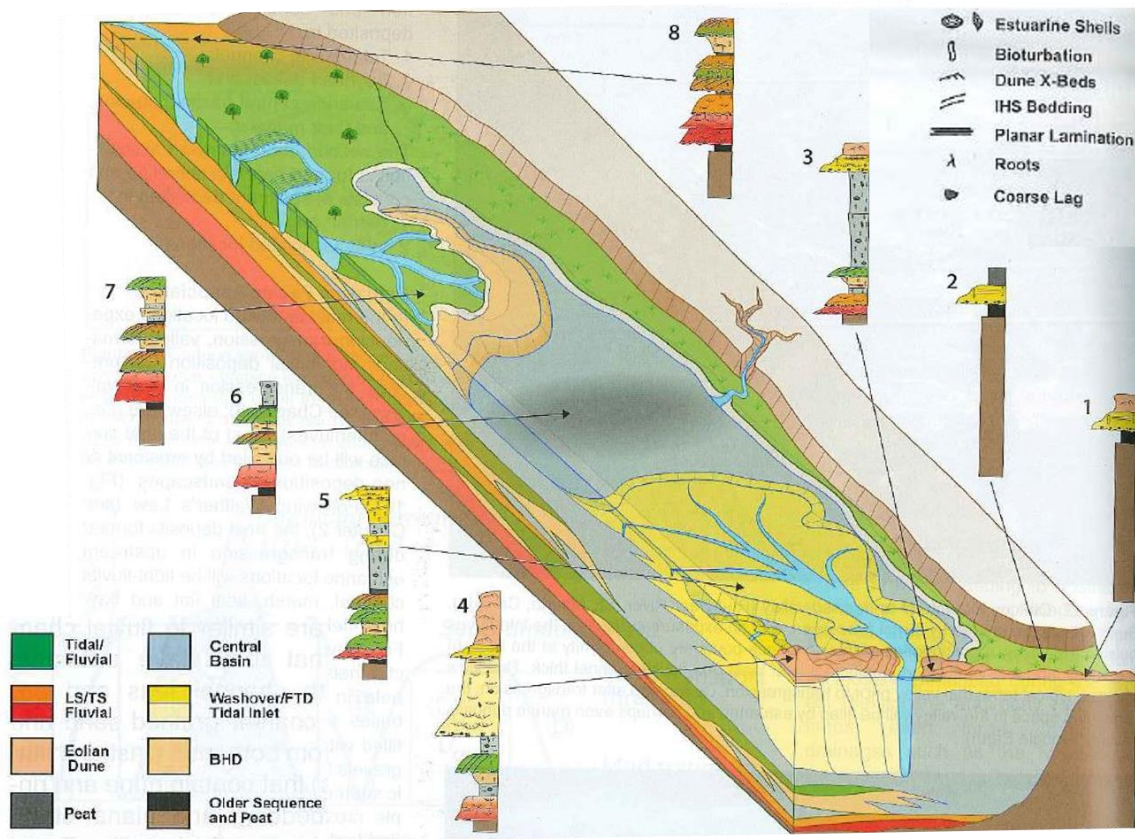
Figure 2.4 Facies model for transgressive wave-dominated coasts (From Boyd, 2010).

2.6 Previous work

The studies summarized below document estuarine shoreline erosion along the Atlantic seaboard, which provides context for rates of erosion along the northern Gulf Coast. Those studies, however, did not directly associate erosion rates with nearshore sedimentological characteristics. Thus, one of the primary contributions of this study is to contextualize reworked sediment in the nearshore zone with erosional rates along the adjacent shoreline.

2.6.1 Cedar Island, North Carolina

A case study of Cedar Island, North Carolina, was made by Cowart et al. (2010) detailing estuarine shoreline change using aerial photography and available data sets. The

study focuses on understanding variation of rates of shoreline change along Cedar Island

which is part of the Albemarle-Pamlico estuarine system, the second-largest estuary in

the United States (Martin et al., 1996). Estuarine emergent wetland is the dominant land-

use land-cover (LULC) type of the Cedar Island shoreline analyzed in this study. Cedar

Island is sheltered from ocean processes and experiences astronomical tides of less than

10 cm making it a microtidal estuary (Benninger and Wells, 1993). Results of the study

using digitized aerial photographs from 1958 and 1998 showed a range of –1.89 to 1.74

m yr^{-1} with an average shoreline change of –0.24 m yr^{-1}. Erosion occurred at 88% of the

shoreline measurement points, 10% were characterized by shoreline accretion, and 2% of

the shoreline did not change. Erosion was significantly controlled by shoreline

composition (elevation and vegetation type) rather than wave energy, which did not

correlate with the rate of shoreline change. Statistical analysis concluded there was a

significant difference in mean shoreline change rates at elevations greater than 1.2 m (< –

0.60 m yr^{-1}) and elevations lower than 1.2 m (–0.18 to –0.26 m yr^{-1}). The evergreen forest

and scrub/shrub portions of the estuarine shoreline comprise a much smaller area of the

Cedar Island study area, however the study shows the mean shoreline change rates are –

0.40 m yr^{-1} and –0.39 m yr^{-1}), respectively—higher than estuarine emergent wetland.

2.6.2 Chesapeake Bay, Maryland

Chesapeake Bay is the largest estuary in the United States and has an average

depth of 8.5 m. The bay runs northwest-southeast with a dendritic shoreline pattern. Tidal

range varies from 0.3 to 1 m. The orientation of Chesapeake Bay allows for long wave

fetch and wind-forced surface waves, typically less than 1 m in height. Shoreline bank

heights range from marsh to cliff (over 30 m). A recent study was conducted analyzing

the influences of wave forcing and sea-level fluctuations on shoreline erosion along

Chesapeake Bay (Sanford and Gao, 2017). The study showed wave forcing was a

dominant factor in erosion and that bank shorelines eroded at a slower rate than marshy

shorelines exposed to the same wave power. Some shore regions are experiencing severe

erosion rates of over 2.4 m yr^{-1}. Between 1850 and 1950, land loss from shoreline erosion

measured 1.9 x 10^8 m^2 (Slaughter, 1967). Erosion rates have been magnified by sea-level

rise, subsidence, and increased shoreline development (Halka et al., 2005).

CHAPTER III – STUDY AREA

3.1 General Study Area

The broad study area is located on the Gulf Coastal Plain near the Alabama-

Florida state line. Comparing the two study sites of Bon Secour Bay (BSB) and Perdido

Bay (PB), BSB is a larger bay and receives a greater volume of fluvial input from the

Mobile-Tensaw watershed and is less sheltered from storms by surrounding land (i.e.,

longer fetch). PB receives most of its fluvial input from the smaller Perdido River

watershed and is relatively protected from storm impact by surrounding land (i.e., shorter

fetch). Table 3.1 gives an overview about each site location.

Table 3.1 Study site location information.

Onshore study site	GPS coordinates	General site characteristics	Data types collected
Bon Secour Bay #1	30.355024180 -87.830308919	Primarily forested wetland; low relief with exposed undermined tree roots along the sandy shoreline	Nearshore sediment cores (2); erosion pins (2); piezometer borehole sediment (2); groundwater; bottom samples (16 total in BSB)
Bon Secour Bay #2	30.348174841 -87.823635359	Primarily swamp with fewer trees than BSB site #1; low relief with exposed undermined tree roots along the sandy shoreline	Nearshore sediment core (1); erosion pins (2); piezometer borehole sediment (1); groundwater; bottom samples (16 total in BSB)
Perdido Bay	30.361391776 -87.436972692	Open forested wetlands and scrub lands, sandier beaches than BSB sites	Nearshore sediment cores (2); piezometer borehole sediment (1); groundwater; bottom samples (14)

3.1.2 Bon Secour Bay

Bon Secour Bay is a southeastern contiguous subsidiary of Mobile Bay, with shorelines along the southern portion of Baldwin County, Alabama. Bon Secour Bay is restricted from the Gulf of Mexico by the Fort Morgan Peninsula to the south and Dauphin Island to the southwest. The bay is bell-shaped, approximately 18 km at its widest point, and 17 km at its greatest length, tapering west to east. The average water depth is 3-4 m (Hummell, 1996). The BSB study site is along the Swift Tract of Weeks Bay National Estuarine Research Reserve (NERR) which is 56 km SE of Mobile, AL on the eastern shore of Mobile Bay. The Swift Tract spans 615 acres on the northern coastline of BSB in southern Baldwin County, AL, and is one of 13 tracts of state-owned land at Weeks Bay NERR. The Swift Tract is comprised of undeveloped forested wetlands and swamps that are commonly inundated during storm events. This area includes two study sites; the first is approximately 3.3 km SE of the mouth of Weeks Bay, and the second location is approximately 4.3 km SE of the mouth of Weeks Bay along the shoreline (Figure 3.1). The first site is primarily forested wetland and the second site is primarily swamp with fewer trees than the first site (Figure 3.2). Both locations have low relief with exposed undermined tree roots along the sandy shoreline.
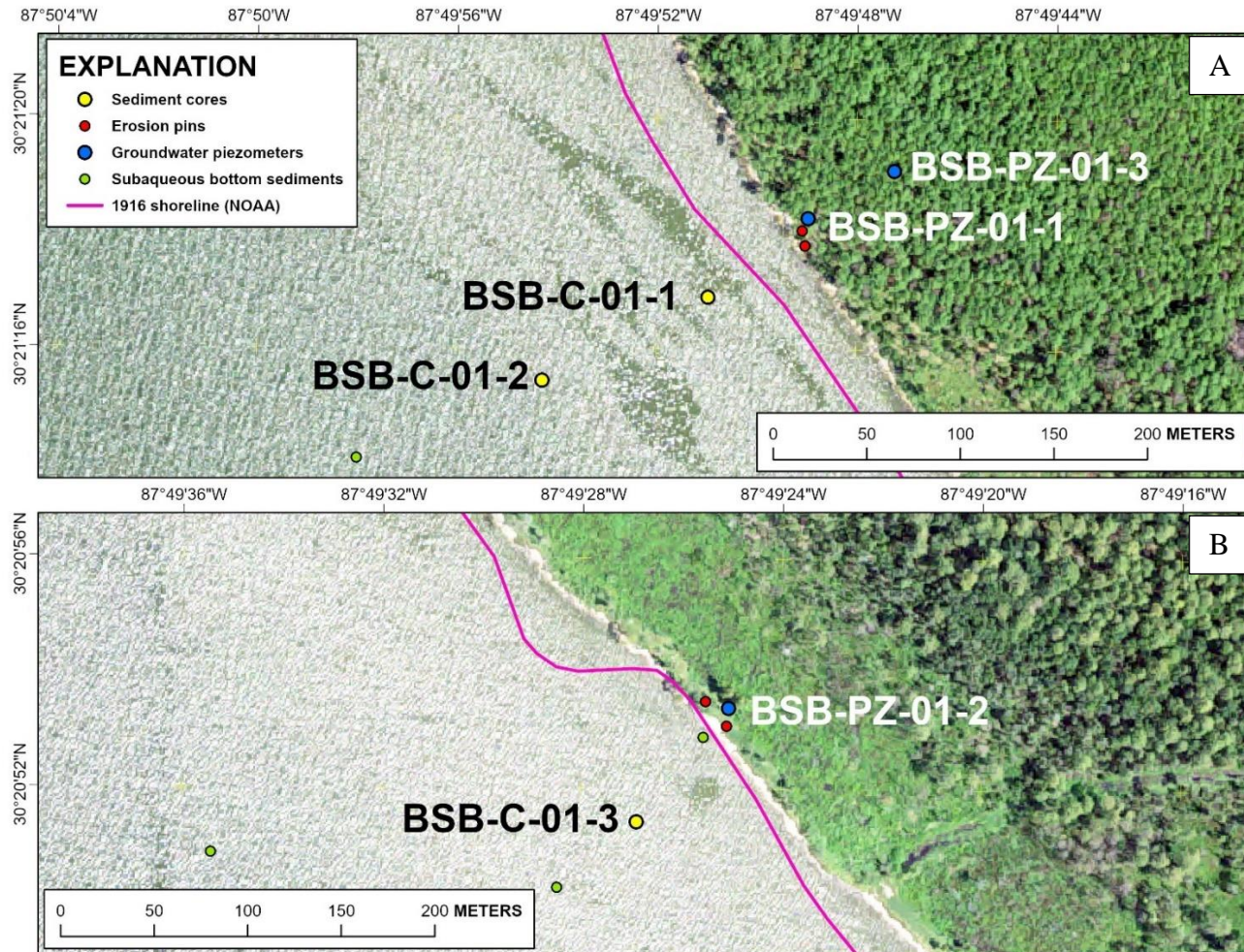
Figure 3.1 A) BSB site location 1. B) BSB site location 2 (Map originally rendered by Dr. Frank Heitmuller in ArcPro GIS software in February 2020).

Figure 3.2 Bon Secour Bay study site 1 (A) and site 2 (B).

3.1.3 Perdido Bay

Perdido Bay is located on the western edge of the Florida Panhandle in Escambia County, and is bisected by the Alabama-Florida state line. The elongate and narrow bay is 53 km in length along the sinuous centerline, has an average width of 4 km, and average water depth of 2 m. Perdido Pass and Big Lagoon connect Perdido Bay with the Gulf of Mexico. The Perdido Bay (PB) site is on a peninsula of Tarkiln Bayou Preserve State Park (Tarkiln) (Figure 3.3). Tarkiln is 22 km W of Pensacola, FL, and encompasses over 4000 acres of open forested wetlands (wet prairie) and scrub lands. Tarkiln is 45 km east of Weeks Bay NERR. The one PB site (0.7 km SE of DuPont Point) for this study includes sandier beaches compared to BSB sites. Tarkiln regularly experiences prescribed burns to manage growth of prairie and scrub lands (State of Florida, 2018). The last recorded burn occurred on March 27, 2019 and targeted 665 acres including the Tarkiln Bayou Peninsula (Carter, 2019).

Figure 3.3 Close-up map of Perdido Bay study site (Map originally rendered by Dr. Frank Heitmuller in ArcPro GIS software in February 2020).

Figure 3.4 Perdido Bay study site. Image A was taken northwest of Image B along the shoreline at Tarkiln Peninsula.

CHAPTER IV – METHODOLOGY

The methodological approach for this study includes preliminary assessments of

the study areas using aerial imagery and GPS data collected in the field; field data

collection trips to install erosion pins, piezometers, and deploy groundwater level and

temperature sensors; field data collection trips to collect nearshore sediment cores,

estuarine bottom sediment samples, onshore borehole sediment samples, and discrete

groundwater samples; field data collection trips to download sensor data; laboratory

analyses of sediment and groundwater samples; online retrieval of ancillary datasets; and

statistical analyses of sedimentary parameters.

4.1 Preliminary Assessments Using Aerial Imagery

Historical and short-term shoreline change measurements are used for estimating

erosion rates at the Bon Secour Bay and Perdido Bay study sites. Figure 4.1 compares

shoreline positions for each site over the past ~25 years, with an estimated shoreline

retreat rate of 0.3 to 0.67 m/yr at Bon Secour Bay (1992 – 2018) and 0.55 m/yr at Perdido

Bay (1994 – 2018). Historical shoreline retreat rates in the study areas were determined

from Google Earth images acquired by satellite and aircraft (Google, 2019) and positions

of the high-tide shoreline surveyed in 2018 using a Trimble GeoXH GPS (Centimeter

edition) and Zephyr Model 2 antenna mounted to a survey pole. Field positions were

subsequently processed in Trimble Pathfinder software using differential correction to the

nearest CORS base station (Foley, AL). Historical shoreline position changes in Google

Earth were computed by plotting high-tide shoreline GPS positions on the most current

images for each study site. Then by using the oldest available historical image for each

site, the Google Earth ruler tool was utilized to determine the distance between the oldest

and most recent high-tide shoreline position points plotted on the image. The World

Geodetic System 1984 (WGS84) datum was used for GPS survey points and Google

Earth images.
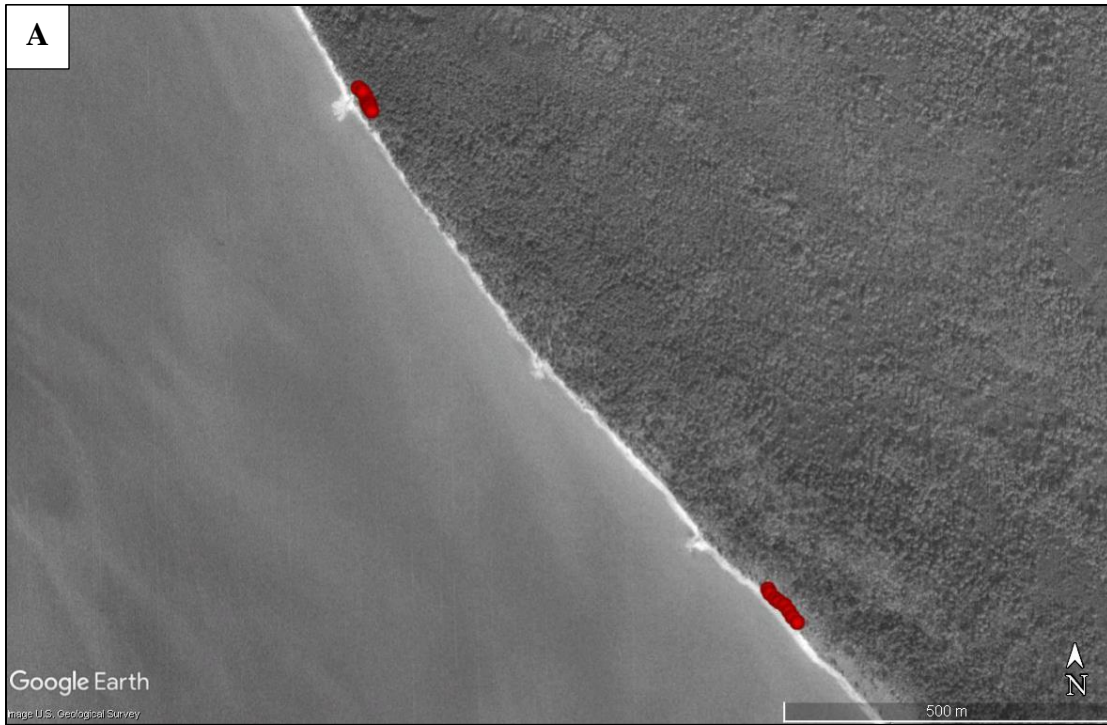
Figure 4.1 Comparison of historical shoreline imagery (Google, 2019) overlain by recent high-tide shoreline GPS points (red dots) surveyed in October 2018. (A) Bon Secour Bay site image from 1992, B) Perdido Bay site image from 1994.

4.2 Field Sampling and Data Collection

Collection and characterization of five shallow nearshore sediment cores from Bon Secour Bay and Perdido Bay are the primary data in this study. Contextualization of the cores using a suite of ancillary data including onshore sediment samples from piezometer boreholes, subaqueous bottom-sediment samples of the adjacent nearshore and central estuarine basin margins, shallow groundwater levels and groundwater quality, short-term shoreline erosion field measurements, and erosion assessments made from historical aerial imagery. Sampling and data collection occurred intermittently from May 2018 through November 2019. GPS positions using a Trimble GeoXH (Centimeter edition) and Zephyr Model 2 antenna were obtained at each coring location and other sample locations as described below.

4.2.1 Sample Locations

Three cores were taken at BSB: two at the first site, and one at a second site 1.2 km southeast of the first site (Figure 4.2 A). Two nearshore sediment cores were collected at PB equidistant from the shoreline (Figure 4.2 B). Three piezometers were installed at BSB: two at the first site, and one at the second site (Figure 4.6 A). One piezometer was installed at the PB site (Figure 4.6 B). At the BSB location, 16 grab samples of bottom sediment were collected from the nearshore and margin of the central estuary basin using a Ponar sampler (Figure 4.9 A). At PB, 14 grab samples of bottom sediment were collected from the nearshore and margin of the central estuary basin (Figure 4.9 B). Two erosion pins were installed at each BSB sub-location, and no erosion pins at PB (Figure 4.10). One barometric pressure logger was installed at Weeks Bay NERR.

4.2.2 Nearshore Sediment Cores

The primary source of analytical data for this study comes from five nearshore subaqueous sediment cores. Three cores (BSB-C-01-1, BSB-C-01-2, BSB-C-01-3) were extracted in the nearshore waters along the Swift Tract of the Weeks Bay NERR at Bon Secour Bay. Two cores (PB-C-02-1, PB-C-02-2) were extracted in the nearshore waters of Tarkiln Bayou Preserve State Park along a peninsula that protrudes into Perdido Bay. See Figure 4.2 and Table 4.1 for location information. In Bon Secour Bay, BSB-C-01-1 and BSB-C-01-3 are nearer to the shoreline, where BSB-C-01-2 is more distal and was selected to compare the shallower locations with a slightly deeper location.

Table 4.1

Core locations and depths.

Core	Water depth (m)	Core length (m)	Distance from shore (m)[b]
BSB-C-01-1	0.75	0.78	55
BSB-C-01-2	0.95	0.875	155
BSB-C-01-3	0.70[a]	0.76	62
PB-C-02-1	0.68[a]	0.95	73
PB-C-02-2	0.70[a]	0.845	84

[a] Estimations based on surrounding grab sample depths.

[b] Approximated from Google Earth Pro measurement tool.

Figure 4.2 Nearshore core locations at Bon Secour Bay (A) and Perdido Bay (B) (Google, 2020).

Nearshore sediment cores were extracted using a gravity-coring device with a piston sampler modified from the Livingstone gravity corer design (Livingstone, 1955). The coring device is lightweight, manually operated, and can accommodate up to one meter of sediment. See Figure 4.3 for the corer in operation. The corer is typically used in fine-grained lake sediment, which is finer than the sandy nearshore sediment in the study area. The relatively coarse particles made it difficult to move the gravity corer down through the sediment. Although the coring sleeve can accommodate one meter of material, none of the five cores were able to reach that depth because of the quantity of sand in the column. The shallowest core was the third core from Bon Secour Bay (BSB-C-01-3) and it reached a depth of 76 cm below water bottom. The deepest core was the second core from Perdido Bay (PB-C-02-1), which reached a depth of 95 cm below water bottom. After returning from the field, the cores were cut in half lengthwise using a table saw, with one half becoming the working half and the second half for future analyses. See Figure 4.4 for sawed core cross-sections. Sediment cores were photographed, sketched, and analyzed at one-centimeter increments for particle size, organic matter content, carbonate content, and analyzed at 5-cm increments for magnetic susceptibility (see Section 5.1 below).

Figure 4.3 Gravity coring device in use at Bon Secour Bay (A) and Perdido Bay (B).

Figure 4.4 Nearshore sediment cores during laboratory preparation.

Note: Cores were photographed at different camera distances, affecting photo scale from core to core.

4.2.3 Piezometers

A piezometer is a perforated standpipe in a borehole to sample shallow groundwater levels and water quality in the field. Piezometers were installed as part of the study to better understand the influence of groundwater table fluctuations on shoreline erosion. The piezometers were constructed using 2-inch PVC pipe perforated on the bottom half-meter, screen around the perforated interval to prevent sediment entry, a galvanized bolt at the bottom of the pipe to ensure consistent sensor position, backfill consisting of gravel and excavated borehole material, and a bentonite clay seal near the surface to prevent surface water infiltration. See Figures 4.7 and 4.8 for piezometer construction and installation. Boreholes were excavated using a 3-inch diameter soil auger until the water table was reached. The PVC pipe was set into the borehole and anchored into place with gravel, sand, excavated material, and bentonite clay. GPS positions at the base and cap of each piezometer were acquired and post-processed by the same procedures as outlined above.

Sediment samples were collected incrementally at different depths below the surface (measured with a folding rule) during the augering process. Collection intervals varied due to inconsistent recovery amounts while augering. These samples were bagged, labeled, and subsequently analyzed for particle size, organic content, carbonate content, and magnetic susceptibility (see Section 4.3 below). Laboratory and statistical analyses of borehole sediment samples are used to compare with sediment collected from the nearshore cores to match facies and, thus, facilitate interpretation of the nearshore cores.

Four piezometers were installed to monitor water table levels and shallow groundwater quality along the shorelines of BSB and PB. Groundwater level fluctuations

and, specifically, prolonged high levels could contribute to shoreline instability and erosion when combined with wave impact. See Table 4.2 and Figure 4.6 for piezometer location information. Three piezometers were installed at Bon Secour Bay: two along the high-tide shoreline (BSB-PZ-01-1, BSB-PZ-01-2) and one approximately 50 m landward from the shoreline in a forested swamp area (BSB-PZ-01-03). Piezometers BSB-PZ-01-1 and BSB-PZ-01-2 were installed in May 2018, and piezometer BSB-PZ-01-3 was installed in October 2018. Groundwater logging sensors (pressure transducers) for water levels and temperatures (see below) were not deployed in the BSB piezometers until October 2018 when the transducers became available. The fourth piezometer is located at Perdido Bay along the high-tide shoreline (PB-PZ-02-1). The piezometer at Tarkiln Bayou was affected by the prescribed fire and the PVC pipe received damage, however the logging device was not damaged. The PB piezometer was installed in November 2018 after receiving permit approval from the Florida Department of Environmental Protection (See Appendix B). At that time, the groundwater sensor being used in BSB-PZ-01-3 was removed and re-deployed at PB-PZ-02-1. Because of this, groundwater level data for BSB-PZ-01-3 is only available from October 14, 2018 to November 15, 2018.

Groundwater logging sensors deployed in each piezometer recorded groundwater temperature (°C) and pressure (kPa) every 30 minutes. Groundwater pressure values have been compensated for atmospheric pressure (kPa). For this study, we used Solinst Levelogger (in BSB-PZ-01-1, BSB-PZ-01-03, and PB-PZ-02-1) and In-Situ Rugged Troll 100 (in BSB-PZ-01-2) logging sensors. A Solinst Barologger barometric pressure sensor was deployed on an existing weather station tower at the Weeks Bay NERR in October 2018 and was used to compensate for barometric pressure (kPa) (i.e., subtract

atmospheric pressure from total pressure) to compute groundwater levels (i.e., residual pressure difference). Barometric compensation was done in Solinst Levelogger software for the Solinst groundwater sensors; it was done using Microsoft Excel for the In-Situ groundwater sensor. Where necessary, data was converted from daylight savings time to Central Standard Time.

Groundwater was periodically sampled from each piezometer using a bailer and was bottled for subsequent water-quality analysis. Water-quality analysis is important for determining if groundwater at each site is primarily from fresh (rainfall recharge) or marine (estuarine) sources. Water quality analyses in the laboratory at USM used a calibrated YSI multi-parameter instrument to measure oxidation-reduction potential (mV), pH, conductivity (mS/cm^2), total dissolved solids (mg/L), and dissolved oxygen (%).

Figure 4.5 Piezometer locations at BSB (A) and PB (B) (Google, 2020).

Table 4.2

Piezometer borehole depths and adjacent ground surface elevations.

Piezometer	Borehole depth (m)	Elevation (m)[a]
BSB-PZ-01-1	1.43	0.206
BSB-PZ-01-2	1.31	0.189
BSB-PZ-01-3	0.85	-
PB-PZ-02-1	1.49	0.537

[a]GNSS height provided by GPS measured at base of piezometer. BSB-PZ-01-3 elevation unavailable due to tree canopy obscuration.
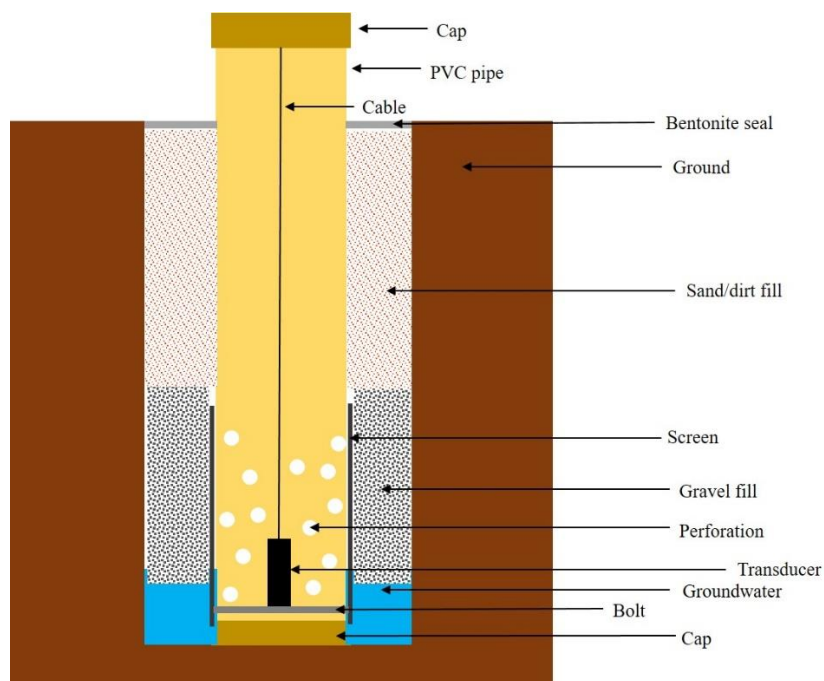
Figure 4.6 Piezometer construction and installation.

Note: Schematic not to scale.

Figure 4.7 Piezometer construction and installation.

Note: A) Bottom portion of PVC pipe with perforations and screen. B) Collecting GPS position at BSB-PZ-01-1.

4.2.4 Bottom Sediment Samples

Subaqueous bottom sediment samples, also referred to as Ponar samples, were collected using a Ponar sampler deployed from a boat. See Figure 4.9 and Table 4.3 for sample collection depths and locations. Bon Secour Bay bottom samples were collected in October and November 2018. All Perdido Bay bottom samples were collected October 2018. Bottom sample depths were calibrated using a folding rule and the Garmin depth sounder mounted on the transom of the boat. The depths were adjusted to mean sea level with NOAA tide tables using the Weeks Bay, Mobile Bay, AL Station 8732828 (for Bon Secour Bay samples) and the Pensacola, FL Station 8729840 (for Perdido Bay samples). Samples were collected along nearshore-to-basin margin transects. Samples were analyzed for particle size, organic content, carbonate content, and magnetic susceptibility in laboratories at USM (see Section 4.3 below). GPS positions were acquired for each Ponar sample site using equipment and procedures outlined above. Laboratory and statistical analyses of Ponar samples are compared with sediment collected from nearshore cores to match facies and, thus, facilitate interpretation of the nearshore cores.
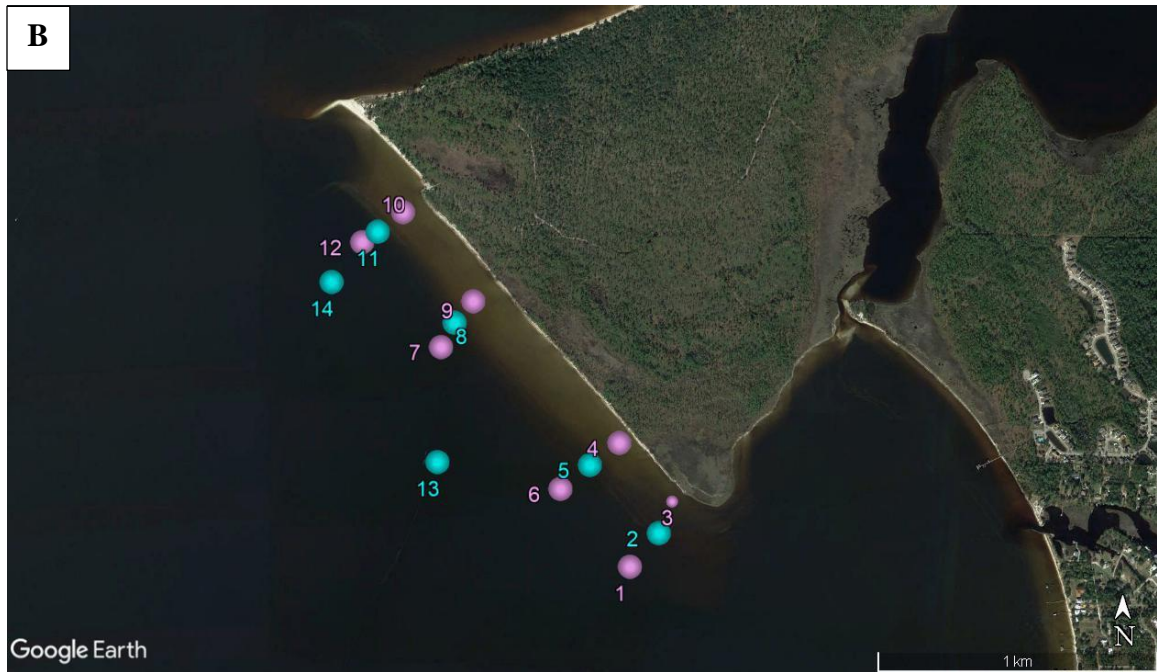
Figure 4.8 Bottom sediment sample locations at BSB (A) and PB (B) (Google, 2020).
Due to the close proximity of points, change in colors are for clarity of each location.

Table 4.3

Subaqueous bottom sample depths.

BSB grab sample	Water depth (m)	PB grab sample	Water depth (m)
1	0.52	1	2.04
2	0.94	2	1.28
3	1.39	3	0.92
4	2.57	4	0.70
5	1.82	5	1.22
6	1.27	6	1.98
7	0.93	7	2.20
8	0.76	8	1.28
9	0.70	9	0.73
10	0.91	10	0.70
11	1.29	11	1.68
12	1.60	12	2.35
13	2.46	13	3.17
14	1.81	14	3.22
15	1.10		
16	0.86		

4.2.5 Erosion Pins

Monitoring of short-term shoreline erosion at the study sites occurred intermittently over a 17-month period (May 2018 – November 2019) through the use of what are commonly referred to as erosion pins, which were inserted at the high-tide shoreline. Short-term measurements are used to interpret storm-induced changes and seasonal variability along the shorelines. Qualitative interpretations are limited because of infrequent measurement intervals and brevity of this study. The erosion pins for this study are 4-foot long sections of half-inch diameter rebar rods that were driven into the ground with a slide hammer until secure. The exposed length was measured with a folding rule and recorded during each site visit. GPS positions were acquired at each erosion pin installation location using equipment and procedures outlined above. Four erosion pins were installed at Bon Secour Bay in May 2018: two at the first BSB site and two at the second BSB site. See Figure 4.10 for a location map. No erosion pins were installed at Perdido Bay because the site is on Tarkiln Bayou Preserve State Park property, which is partly designated for recreation and experiences a fair amount of visitation to the shoreline. The metal erosion pin protruding from the sand would likely have been tampered with and would pose a potential tripping hazard to park visitors.

Figure 4.9 Erosion pin locations at the first BSB sub-location (A) and second BSB sub-location (B) (Google, 2019). Nearshore cores are plotted in green for location reference.

4.3 Laboratory Analyses

Laboratory analysis was done for nearshore sediment cores, piezometer sediment samples, groundwater, and water bottom grab samples. Laboratory work was conducted in The University of Southern Mississippi Sedimentology Laboratory with Dr. Franklin Heitmuller, the Biogeography Laboratory with Dr. Carl (Andy) Reese, and the Coastal Hazards Laboratory with Dr. Davin Wallace in the School of Ocean Science and Engineering at Stennis Space Center, Mississippi. Core sediment samples were analyzed at 1-cm increments for particle size, organic matter content, and carbonate content. Magnetic susceptibility was analyzed at 5-cm increments, with some bottom-core increments measuring less than 5-cm. Piezometer borehole sediment samples were analyzed with depth but at non-uniform increments. Subaqueous bottom sediment samples were analyzed individually and not incrementally.

The cores were first divided into 1-cm increments, then individually transferred to beakers and dried, then disaggregated, weighed, transferred to crucibles and placed in the furnace to undergo organic matter loss on ignition (OM LOI). After OM LOI the samples were re-weighed, and then underwent calcium carbonate loss on ignition ($CaCO_3$ LOI). After $CaCO_3$ LOI, the samples were re-weighed and a small scoop of sediment from each crucible was removed and placed in 15-mL centrifuge tubes to be used in particle size analysis. The remaining samples were bagged at 5-cm intervals and used to determine magnetic susceptibility. Bottom samples and piezometer sediment samples were also treated identically, although not at 1-cm intervals.

Sediment particle size (mm) was determined for Dx (0) through Dx (100) with the median particle size Dx (50) being graphically represented in the following sections.

Particle size sorting (dimensionless) was determined using the equation ($\sqrt{}$ (Dx 75/Dx 25)) and categorized as "well" (< 2.5), "normal" (2.5 – 4.5), or "poor" (> 4.5) as determined from Trask (1930) (Friedman, 1962). Magnetic susceptibility is represented as χ (chi), which is expressed in units of 10^{-6} m^3 kg^{-1}. See Figure 4.11 for typical ranges for tested geologic material at room temperature (Dearing, 1999). Organic matter and calcium carbonate values are percentage of mass lost after LOI. Groundwater samples collected during piezometer installation were evaluated for oxidation-reduction potential, pH, conductivity, total dissolved solids, and dissolved oxygen using a Mettler Toledo pH meter and YSI multi-parameter water-quality probe and are reported in Section 3.1.1. Also reported here are the recorded measurements for four erosion pins installed at Bon Secour Bay. See Appendix Tables A.1 through A.8 for select particle size percentiles, OM %, $CaCO_3$ %, and MS for every sediment sample.

4.3.1 Sediment Particle Size

Sediment particle size was measured by the laser diffraction method using a Malvern Mastersizer 3000 particle analyzer and software paired with the Hydro LV wet dispersion unit. Because of mechanical constraints of the instrument (also referred to as the Malvern), only particles with diameters of 1 mm or smaller were measured by laser diffraction. In order to integrate the fraction greater than 1 mm, each sample was weighed, then sieved through a 1 mm mesh, and the sieved fraction was weighed and recorded. An equation was formulated in Microsoft Excel software and applied to the percentile raw data spreadsheets to adjust for the sieved fraction. New percentile values were manually selected from the adjusted data and are used in the presented results. This method was done for all samples, except for core BSB-C-01-1. There were no clogging

or mechanical issues with the Malvern when processing BSB-C-01-1, which was the first core to be analyzed. The absence of a mechanical issue could possibly be explained by the minimal amount of coarse particles in the core. However, clogging did occur when analyzing core BSB-C-01-2, which prompted the procedural change.

4.3.2 Organic Matter

For further characterization of depositional environments and conditions, organic matter (OM) content of each sample was determined using the loss-on-ignition (LOI) method (Heiri et al., 2001). Samples were initially dried in glass beakers at 105 °C overnight, weighed using a calibrated Ohaus digital scale (in grams), disaggregated with a mortar and pestle, transferred to pre-weighed 5 mL ceramic crucibles, and placed in a muffle furnace at 550 °C for four hours. Finally, samples were cooled and reweighed to measure a loss of mass percentage.

4.3.3 Calcium Carbonate

Calcium carbonate ($CaCO_3$) content of sediment samples was measured using the LOI method. After undergoing LOI for OM, the reweighed samples were returned to the muffle furnace at 1000 °C for two hours. After this duration, samples were cooled and reweighed to measure a loss of mass percentage.

4.3.4 Magnetic Susceptibility

Magnetic susceptibility of sediment samples was measured to broadly interpret mineralogy, provenance, and environmental geochemistry. Because of the amount of volume required to measure magnetic susceptibility (MS) and the limited amount of sample available from the 1-cm increments of nearshore sediment cores, measurements were made with homogenized 5-cm sample intervals. Onshore borehole and subaqueous

bottom sediment samples included enough sediment to avoid this problem. A Bartington

MS2B Dual Frequency Sensor with the Bartington MS3 Magnetic Susceptibility Meter

system was used to measure MS. A calibration check of the equipment was done prior to

analyzing samples. Measurements were made using volume-specific program settings

with a 10 cm^3 plastic container. Because not all nearshore sediment core lengths

measured to a multiple of five, some bottom increments include less than 5-cm of core

length. For example, core BSB-C-01-1 has sample increments of 0 – 5 cm, 6 – 10 cm

…71 – 75 cm, and 76 – 78 cm. Figure 4.11 shows MS readings commonly representative

of geological material. Sedimentary rocks typically range between 0.001 – 0.01 * 10^{-6} m^3

kg^{-1}. Sediment containing iron-bearing minerals such as magnetite that remain

magnetized in the absence of a magnetic field will exhibit a ferrimagnetic behavior and

result in a high MS reading. Weakly susceptible minerals such as manganese and iron

ions that are only magnetized in the presence of a magnetic field are referred to as

paramagnetic. If MS values are negative and weak when introduced to a magnetic field,

then the sample contains minerals that do not contain iron minerals such as quartz and

CaCO$_3$ and it is referred to as diamagnetic.
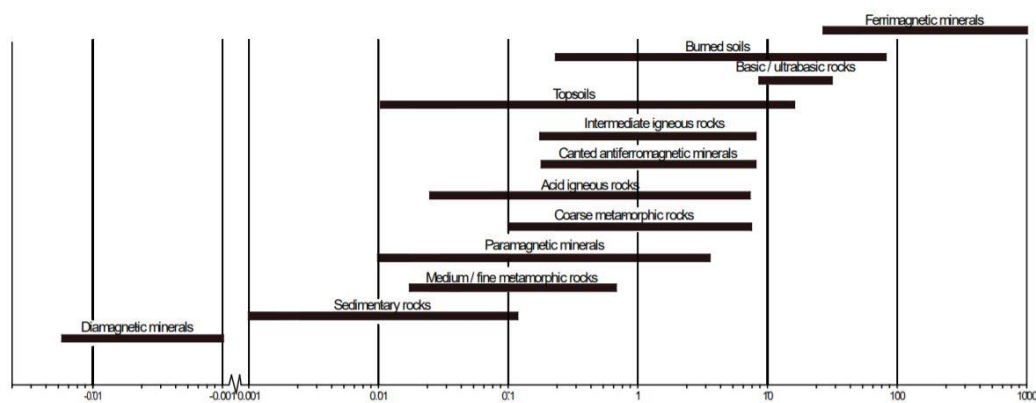
Figure 4.10 Typical ranges of magnetic susceptibility values for environmental materials
and minerals measured at room temperature. From Dearing (1999).

4.4 Statistical Analysis

Statistical analyses of sedimentary parameters were done using IBM SPSS

Statistics 26 software. Discriminant analysis was used to determine significant

differences amongst the five nearshore sediment cores. Based on those results, T-tests

were done to analyze the significance between two cores at a time. Cores were then tested

for similarity to subaqueous bottom and onshore borehole sediment samples using

statistical and laboratory results to match facies and the likelihood of erosional sources of

sediment to the nearshore zone. Variables used in the analyses are particle size

percentiles Dx (10), Dx (16), Dx (25), Dx (50), Dx (75), Dx (84), and Dx (90), OM

percentage, and $CaCO_3$ percentage. Because magnetic susceptibility samples encompass

5-cm increments where the other testable parameters are 1-cm increments, MS is not

included in these statistical analyses.

5.1 Laboratory Results

5.1.1 Nearshore sediment cores
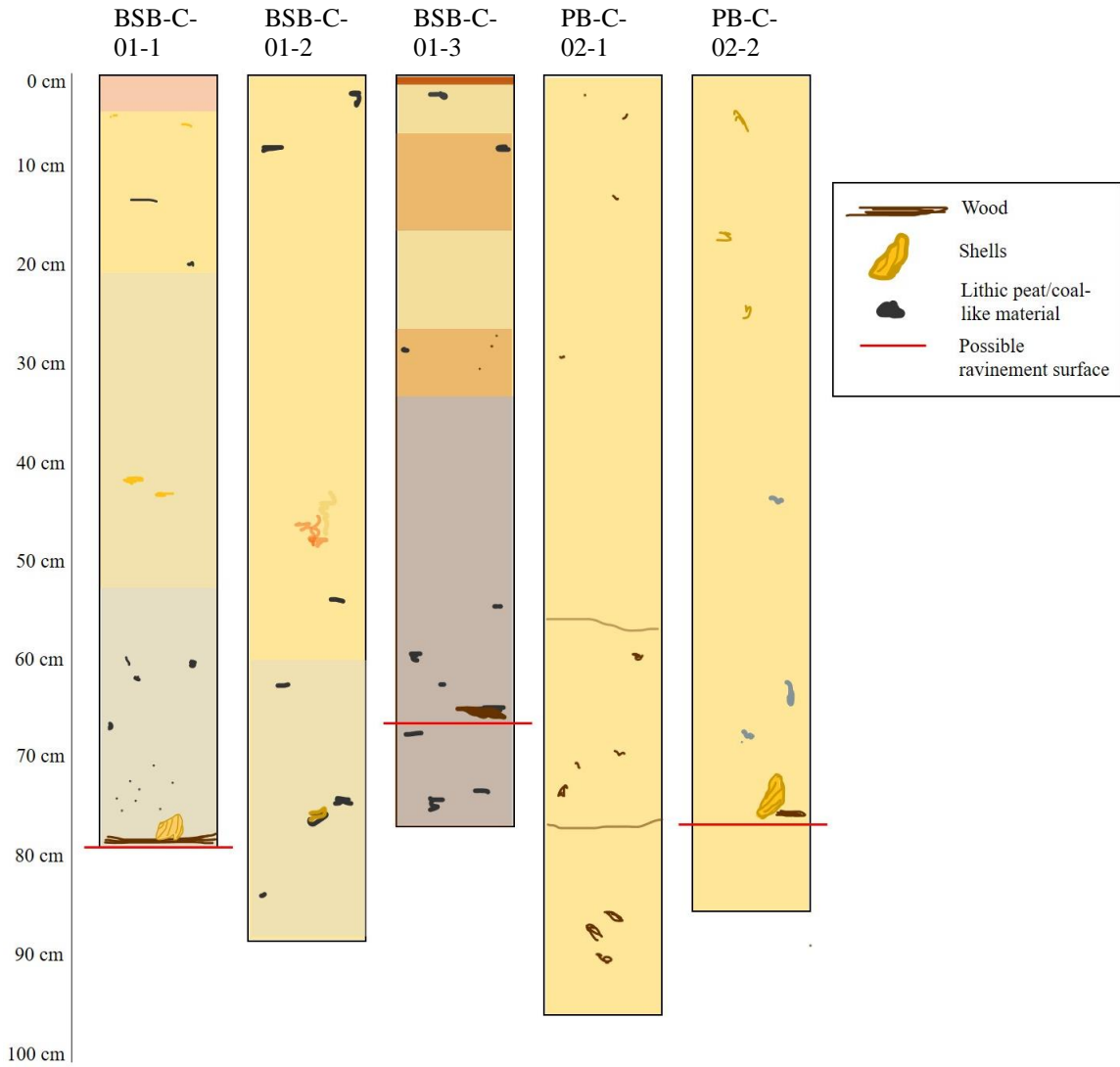
Figure 5.1 Nearshore sediment core lithologs.

Note: BSB-C-01-1 top is 75 cm below median sea level (MSL); BSB-C-01-2 top is 90 cm below MSL; BSB-C-01-3 top is 70 cm

below MSL; PB-C-02-1 top is 70 cm below MSL; PB-C-02-2 top is 70 cm below MSL.

5.1.1.2 BSB-C-01-1
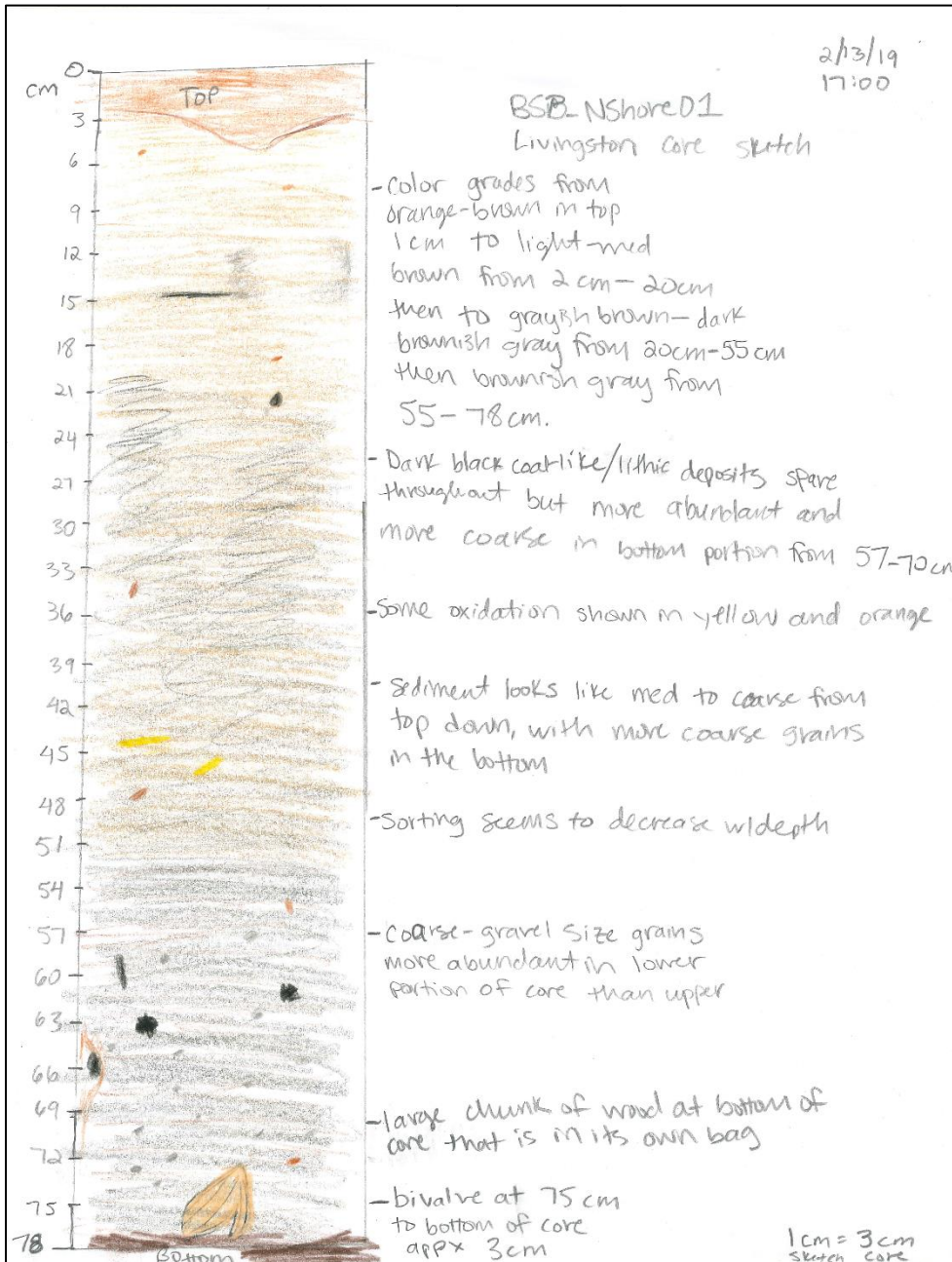
Figure 5.2 Sketch of nearshore sediment core BSB-C-01-1.

Core BSB-C-01-1 was extracted 55 m offshore of the first BSB site in the nearshore zone and is 78 cm long. Upon initial extraction in the field, large pieces of woody material were observed to be lodged in the bottom of the coring sleeve. After the core was split in half, large bivalve shell material was also observed at the same location at the bottom of the core where the wood was lodged (See Figures 5.2 and 5.3). Figure 5.4 displays the laboratory results for core BSB-C-01-1. Dx (50) particle size remains within the sand-size fraction throughout the core length. From 0 – 23 cm, Dx (50) ranges between very fine to medium sand. From 24 – 77 cm, Dx (50) fluctuates between medium and coarse-sized sand with two very coarse sand layers at 27 cm and 37 cm measuring 1.00 mm and 1.26 mm, respectively. Dx (50) is fine sand (0.24 mm) at 78 cm. Sorting for the entire core length is classified as well-sorted, except at 8 cm where sorting is normal with a calculated value of 2.7. Organic matter content is minimal and measures less than 5% at all depths of the entire core length, except at 35 cm where the maximum OM content is 6.25%. Calcium carbonate is minimal and fluctuates from 0 – < 3% with a maximum of 2.7% at 56 cm. MS ranges from $0.001 – 0.017 *10^{-6} \, m^3 \, kg^{-1}$ for the length of BSB-C-01-1. The final magnetic susceptibility (MS) increment is from 76 – 78 cm and it is where the core reaches a maximum χ value of $0.017 * 10^{-6}$. The presence of shells, wood, coarse grains, higher abundance of heavy minerals at the base of the core suggest the presence of an erosional surface buried by cleaner shoreface sands (i.e. a ravinement surface).
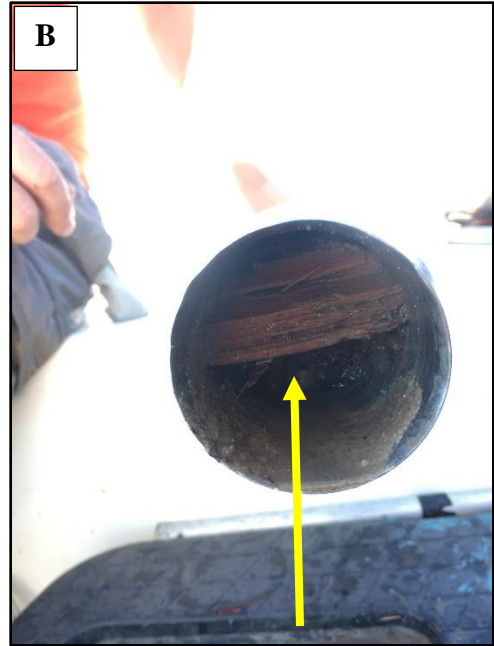
Figure 5.3 Shell (A) and wood (B) fragments at the bottom of core BSB-C-01-1.
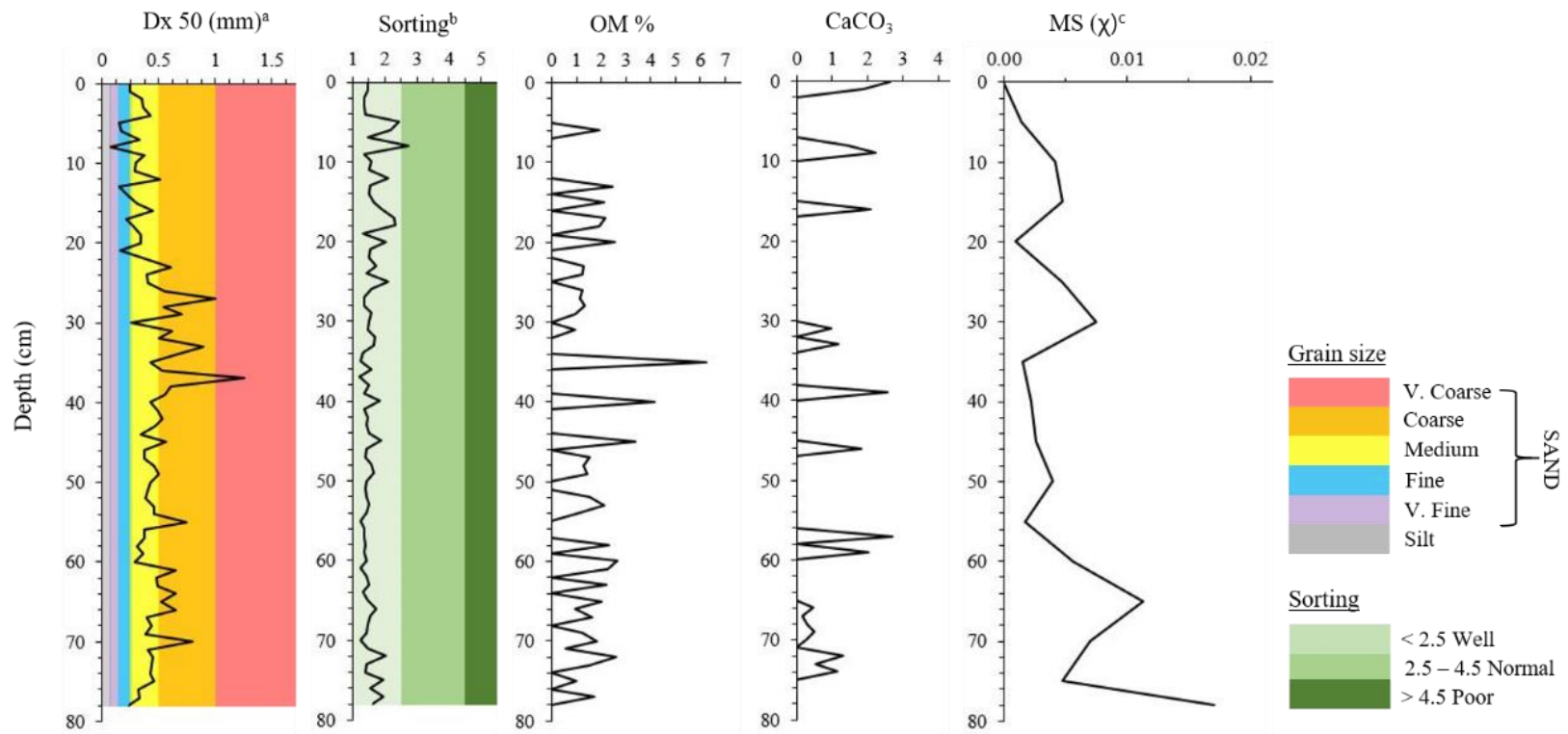
Figure 5.4 Laboratory analysis results for core BSB-C-01-1.

Note: Core length = 78 cm, water depth = 75 cm.

[a]Some 50th percentiles are +/- 0.5% due to calculation adjustments after correcting for sieved portion > 1mm. [b]Sorting is calculated from Trask (1930). [c]Values are *10[-6].

5.1.1.3 BSB-C-01-2

The sketch shows a sediment core with a depth scale in cm (0 to 87.5 cm) along the left side. Handwritten notes to the right read:

- Color is fairly uniform from top to bottom of core. Becomes more gray with depth, but only slightly.
  Munsell: 0-17 cm 10YR 6/3
  17-87.5 cm 10YR 5/2

- grain size is fairly uniform throughout med-coarse sand w/o hand lense. Some clay

- some orange-yellow coloration around 50 cm

- some dark lithic material between 54-83 cm

- few large gravel-size grains present in deeper portions of core

- brown streaks are not present in core

not perfectly to scale   1cm = ~3cm cor

Figure 5.5 Sketch of nearshore sediment core BSB-C-01-2.

57

Figure 5.6 displays the laboratory results for core BSB-C-01-2. This core was extracted 155 m offshore of the first BSB site in the nearshore zone and is 87.5 cm long. Dx (50) particle size increases and decreases between fine and coarse sand from the top of the core to 66 cm where there is a sharp excursion from medium sand to silt, followed by a coarsening upward trend to the bottom of the core. The coarsest interval is at 87 cm where Dx (50) is 0.68 mm. The core is well to normally sorted from top to bottom until 84 cm where sorting is classified as poor with a measurement of 5.13. Organic matter content stays below 2% for the entire length of the core, with a maximum measurement of 1.39% at 78 cm. Carbonate content measures below 1% for the entire core length, the highest measurement being 0.52% at 82 cm. MS ranges from $0 - 0.005 *10^{-6}\,m^3\,kg^{-1}$ and shows a decreasing trend with depth. A maximum MS value of $0.009 * 10^{-6}$ occurs in the first $0 - 5$ cm interval. Overall BSB-C-01-2 is homogeneous throughout the depth of the core with no notable trends or composition changes.
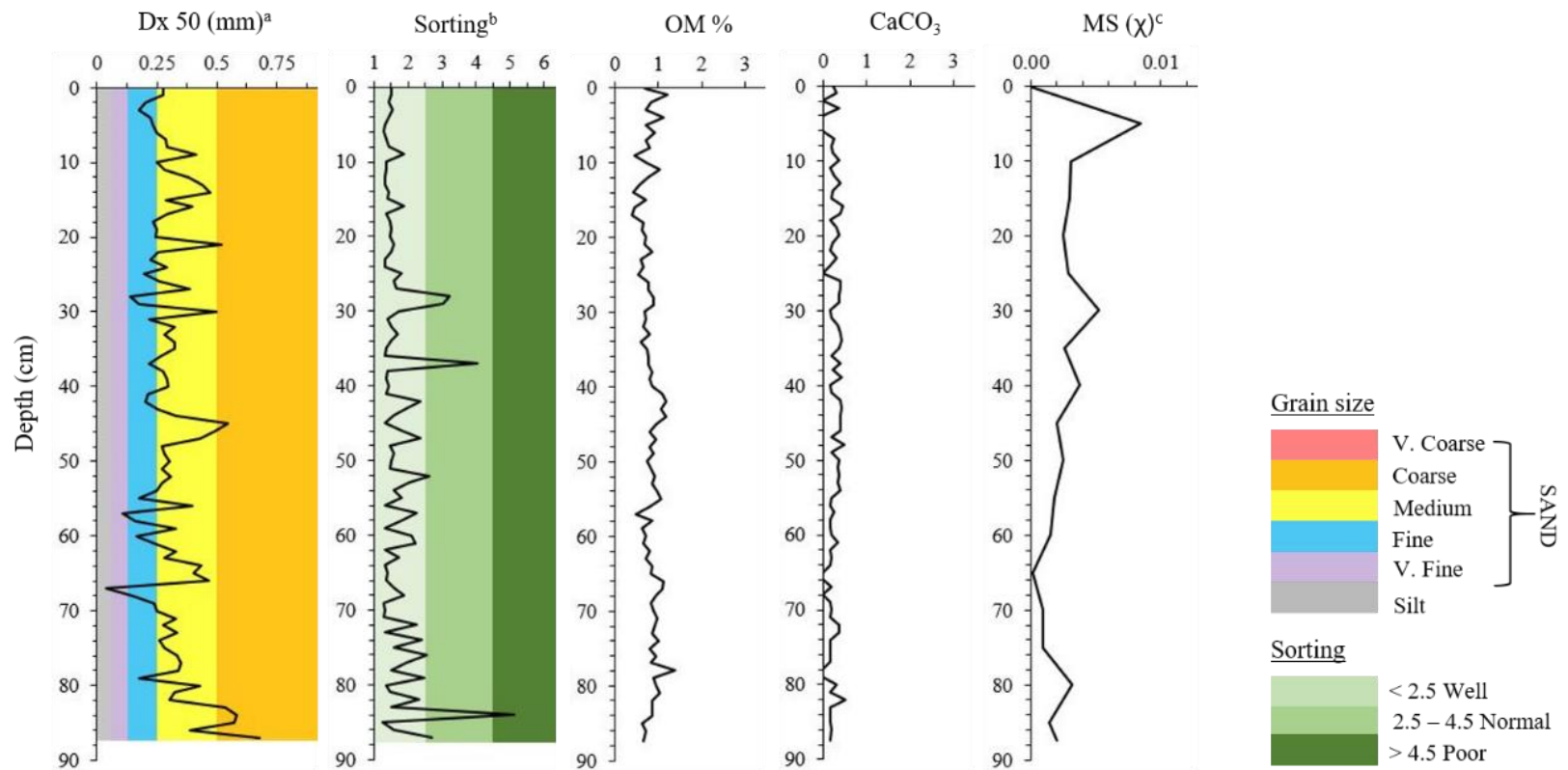
Figure 5.6 Laboratory analysis results for core BSB-C-01-2.

Note: Core length = 87.5 cm, water depth = 95 cm.

[a]Some 50th percentiles are +/- 0.5% due to calculation adjustments after correcting for sieved portion > 1mm. [b]Sorting is calculated from Trask (1930). [c]Values are *10[-6].

59

5.1.1.4 BSB-C-01-3

The sketch shows a sediment core measured from 0 cm to 76 cm with the following handwritten notes:

- Very mottled color throughout core.
- Varies from light brown to yellowish brown to medium gray/grayish brown
- Becomes darker and more gray w/depth
- Some dark lithic-like material throughout, but more abundant in deeper core
- Subrounded-rounded throughout
- Yellowish film — clay? 27-33 cm
- Orange color around 30-54 cm could be from oxidation

Munsell: 0-2cm 10YR 5/4
2-15cm 10YR 6/4
15-27cm 10YR 5/2
27-33 cm 5YR 6/2
33-55 cm 10YR 4/2
55-76cm 10YR 4/1

- Abundant black lithic-woody material from ~55-61 cm
- Sidewall portion partially missing from 56-61cm. Still enough to take samples.
- Wood chunk at 68 cm
- grain size is medium-coarse throughout w/ a few more coarse grains in deeper portion ~40cm?

1cm = ~3cm core

Figure 5.7 Sketch of nearshore sediment core BSB-C-01-3.

Figure 5.8 displays laboratory results for core BSB-C-01-3. This core was extracted 62 m offshore of the second BSB site in the nearshore zone and is 76 cm long. Overall, Dx (50) particle size is the finest compared to the other four nearshore sediment cores. Dx (50) particle size stays between medium and very fine sand for the length of the core except for a coarse sand measurement of 0.54 mm at 16 cm and a silt-size measurement of 0.045 mm at 62 cm. Sorting ranges from well to normal except at 43 cm it is classified as poor with a measurement of 4.6. OM remains under 4% for the entire depth of the core with a maximum of 3.45% at 61 cm. $CaCO_3$ is under 1% at all core depths with a maximum of 0.72% at 63 cm. MS ranges from $0 – 0.014 *10^{-6} \, m^3 \, kg^{-1}$. The maximum MS value $0.014 * 10^{-6}$ occurs at the $65 – 70$ cm interval. Looking at this core from a top – down perspective, OM %, and MS increase, and particles become less well sorted with depth. As with BSB-C-01-1, these sedimentological features in BSB-C-01-3 could be indicative of a buried ravinement surface.
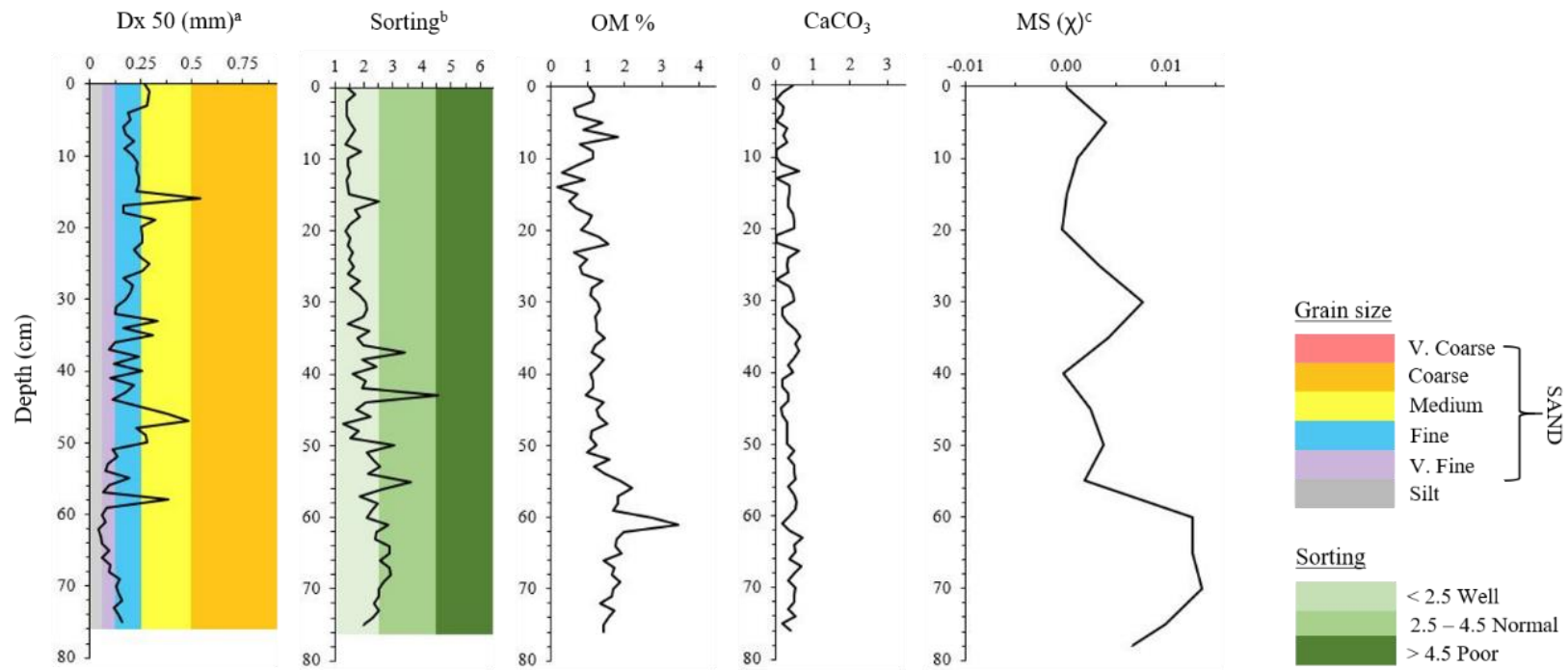
Figure 5.8 Laboratory analysis results for core BSB-C-01-3.

Note: Core length = 76 cm, water depth = 70 cm (estimated from nearby Ponar sample depths).

[a]Some 50th percentiles are +/- 0.5% due to calculation adjustments after correcting for sieved portion > 1mm. [b]Sorting is calculated from Trask (1930). [c]Values are *10[-6].

5.1.1.5 PB-C-02-1

- not much distinct color variation with depth
- coarse grain sand with some clay/lithics in spots

- dark brownish/gray spots intermittently dispersed

- Munsell: 0-33cm 10 YR 7/3
                34-95cm 10YR 6/3

- distinct dark brown/gray line at ~54-55 cm

- distinct dark brown/gray line at ~71 cm

- hiatus spots on backside of core from ~76-93cm

- hiatus on frontside of core from ~83-95 cm which will significantly reduce amount of sample

1 cm = ~3 cm core

Figure 5.9 Sketch of nearshore sediment core PB-C-02-1.

63

Figure 5.10 displays laboratory results for core PB-C-02-1. This core was extracted 73 m offshore of the Tarkiln study shoreline in the nearshore zone and is 95 cm long. Dx (50) particle size remains between fine and coarse sand throughout the core and is medium sand-sized on average. The maximum Dx (50) is 0.824 mm occurring at 23 cm, and the minimum Dx (50)is 0.176 mm occurring at 91 cm. Sorting is well to normal for the length of the core. OM is below 2% with the highest amount being 1.2% at 83 cm. $CaCO_3$ also is below 2% with a maximum of 1.56% at 84 cm. MS remains within the typical range for clastic sediments at a range of -0.009 – 0.007 $*10^{-6}$ m^3 kg^{-1} , with a maximum value occurring at the 45 – 50 cm interval. This core is homogenous throughout with no trends or sedimentary structures indicated.
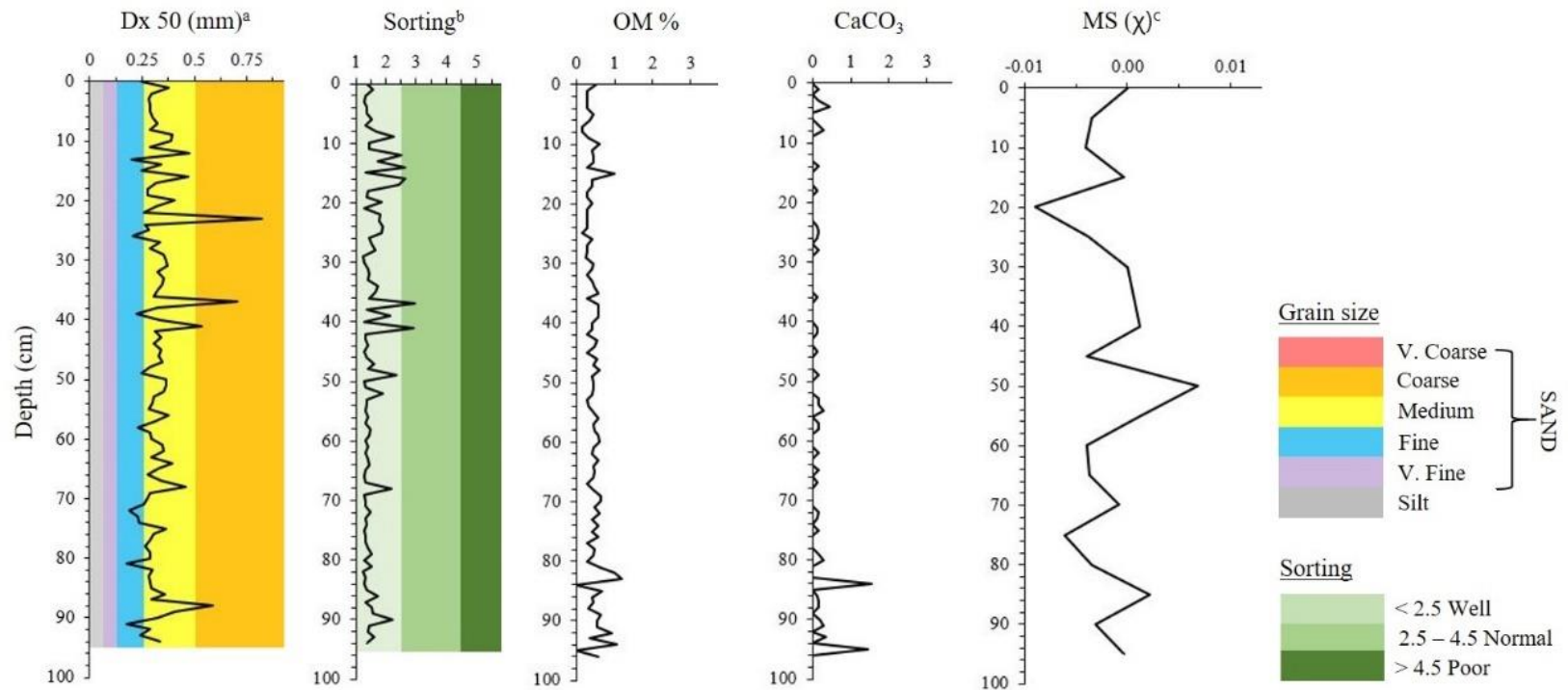
Figure 5.10 Laboratory analysis results for core PB-C-02-1.

Note: Core length = 95 cm, water depth = 68 cm (estimated from nearby Ponar sample depths).

[a]Some 50th percentiles are +/- 0.5% due to calculation adjustments after correcting for sieved portion > 1mm. [b]Sorting is calculated from Trask (1930). [c]Values are *10[-6].

5.1.1.6 PB-C-02-2
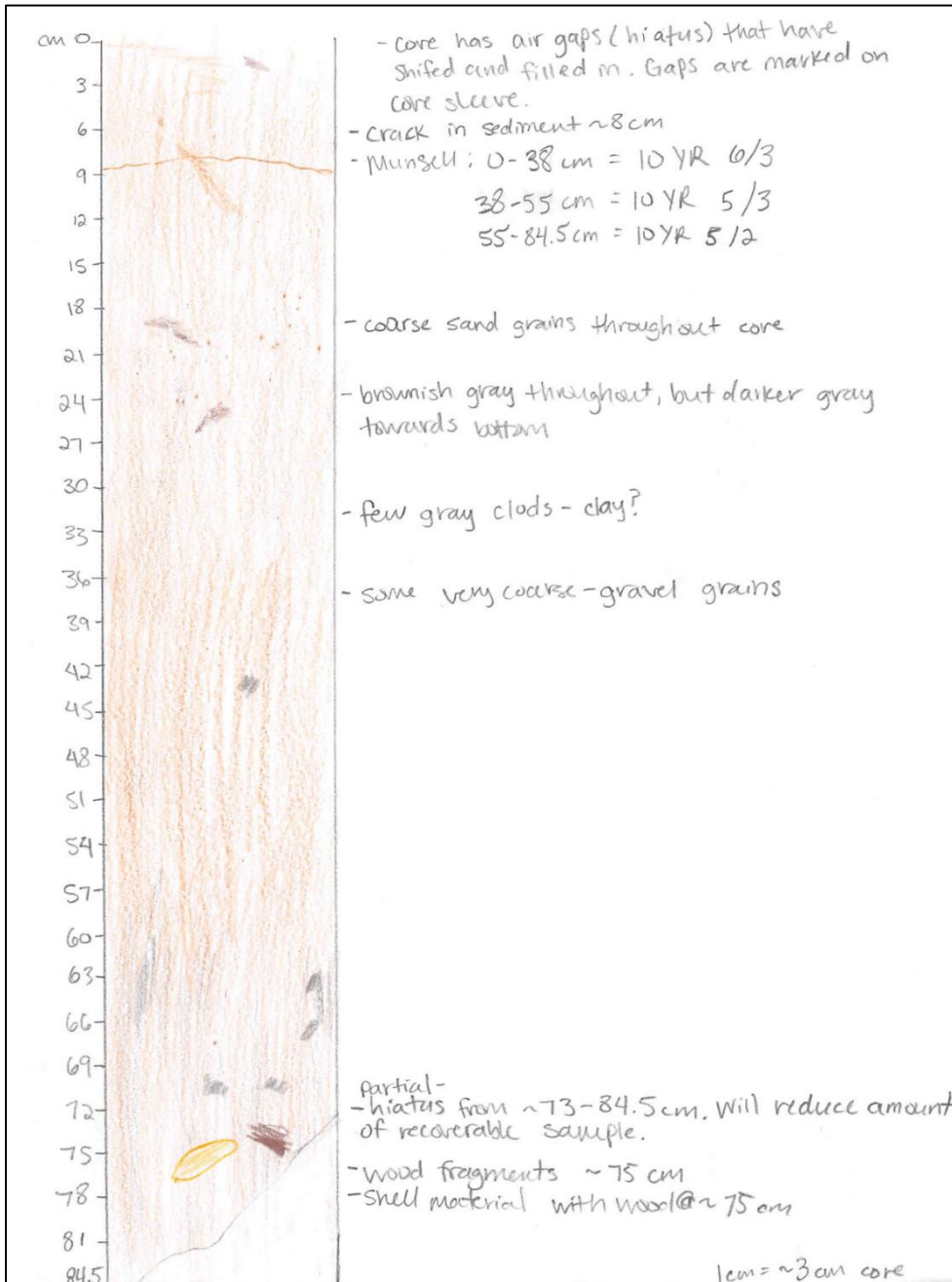
Figure 5.11 Sketch of nearshore sediment core PB-C-02-2.

Figure 5.12 displays the laboratory results for core PB-C-02-2. This core was extracted 84 m offshore of the Tarkiln study shoreline in the nearshore zone and is 84.5 cm long. When the core was cut lengthwise and opened, shell hash and wood fragments were present in the bottom portion (See Figure 5.11). Dx (50) particle size ranges between fine and medium sand size and is mostly medium sand. The maximum Dx (50) value is 0.429 mm at 64 cm, and the minimum is 0.194 mm at 76 cm. There is no particle size or sorting data for the 17 cm interval because the sample was flushed from the Malvern before analyzing. Sorting is classified as "well" throughout the length of the core. OM is below 1% with a maximum of 0.9% at 75 cm. Carbonate content results for PB-C-02-2 on the first LOI analysis produced several relatively large negative percentages, perhaps because of a mistake in arranging the ceramic crucibles in the muffle furnace and were found to be unreliable. A second analysis was conducted which produced more reasonable results. Results from the second analysis show $CaCO_3$ content remained under 2% for the length of the core, with a maximum of 1.6% at 76 cm. Because of a lack of remaining sample available from the working half of the core, no $CaCO_3$ data is available for 77, 78, and 81–84.5 cm. MS values are weakly negative, which is expected with samples that do not contain much iron, but have abundant quartz (Dearing, 1999). Surface samples have a maximum MS value of 0. However, MS decreases with depth to a minimum negative value of $-0.005 * 10^{-6}$ m^3 kg^{-1} at 70 cm for PB-C-02-2.
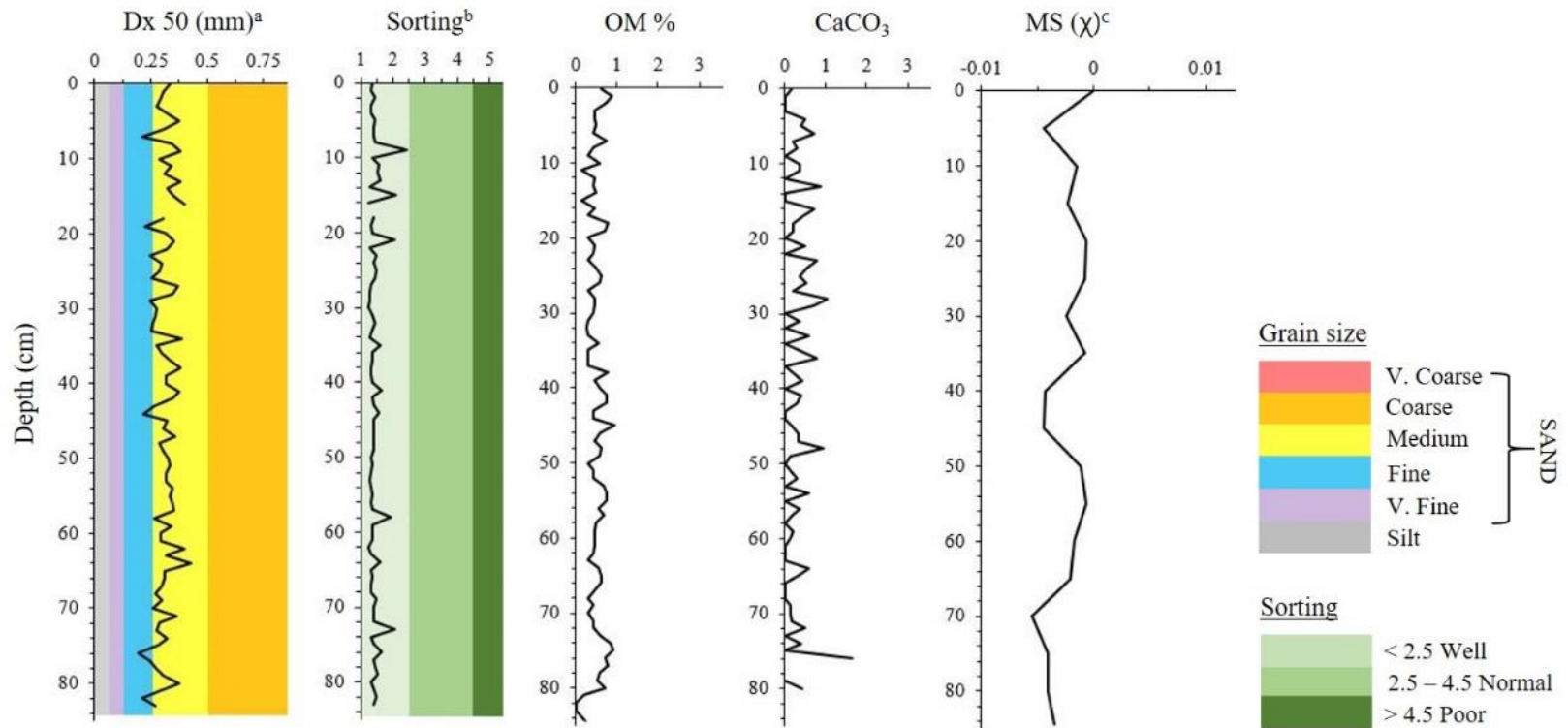
Figure 5.12 Laboratory analysis results for core PB-C-02-2.

Note: Core length = 84.5 cm, water depth = 70 cm (estimated from nearby Ponar sample depths). No particle size or sorting data for 17 cm. No CaCO$_3$ data for 77, 78, 81-84.5 cm.

[a]Some 50th percentiles are +/- 0.5% due to calculation adjustments after correcting for sieved portion > 1mm. [b]Sorting is calculated from Trask (1930). [c]Values are *10^{-6}.

5.1.2 Piezometers

Four boreholes were made at onshore sites to serve as piezometers for groundwater level and temperature sensors (see Section 4.2). Three piezometers are located at the Bon Secour Bay study area and one piezometer at the Perdido Bay study area. Sediment was collected and recorded at various intervals. The following sections document the laboratory results for the sediment samples and time series of groundwater levels and temperatures.

5.1.2.1 BSB-PZ-01-1

5.1.2.1.1 BSB-PZ-01-1 sediment

Figure 5.13 displays the laboratory results for borehole sediments at BSB-PZ-01-1. This piezometer borehole is located on the shoreline berm of the first Bon Secour Bay study site. Sampling intervals include the surface (0 cm), 0 – 52 cm, 52 – 76 cm, 76 – 91 cm, 91 – 113 cm, 113 – 116 cm, and 116 – 143 cm. Dx (50) particle size values indicate a decrease with depth from medium sand to silt. The maximum median particle size is 0.623 mm at 52 cm and the minimum is 0.041 mm at 143 cm. The core is well sorted from the top down until a transition to normal sorting in the 52 – 76 cm interval. Organic matter remains below 2% with a maximum value of 1.6 %. Calcium carbonate is minimal throughout the core and was highest at 0 – 72 cm with a measurement of 0.27%. Magnetic susceptibility was weakly magnetic, beginning as paramagnetic from the surface to 113 cm then shifting to diamagnetic (weak negative values) from 113 – 116 cm, and back to paramagnetic to the bottom. MS values stayed in range typical of clastic sediments. Maximum MS is $0.014 * 10^{-6}$ m^3 kg^{-1}.
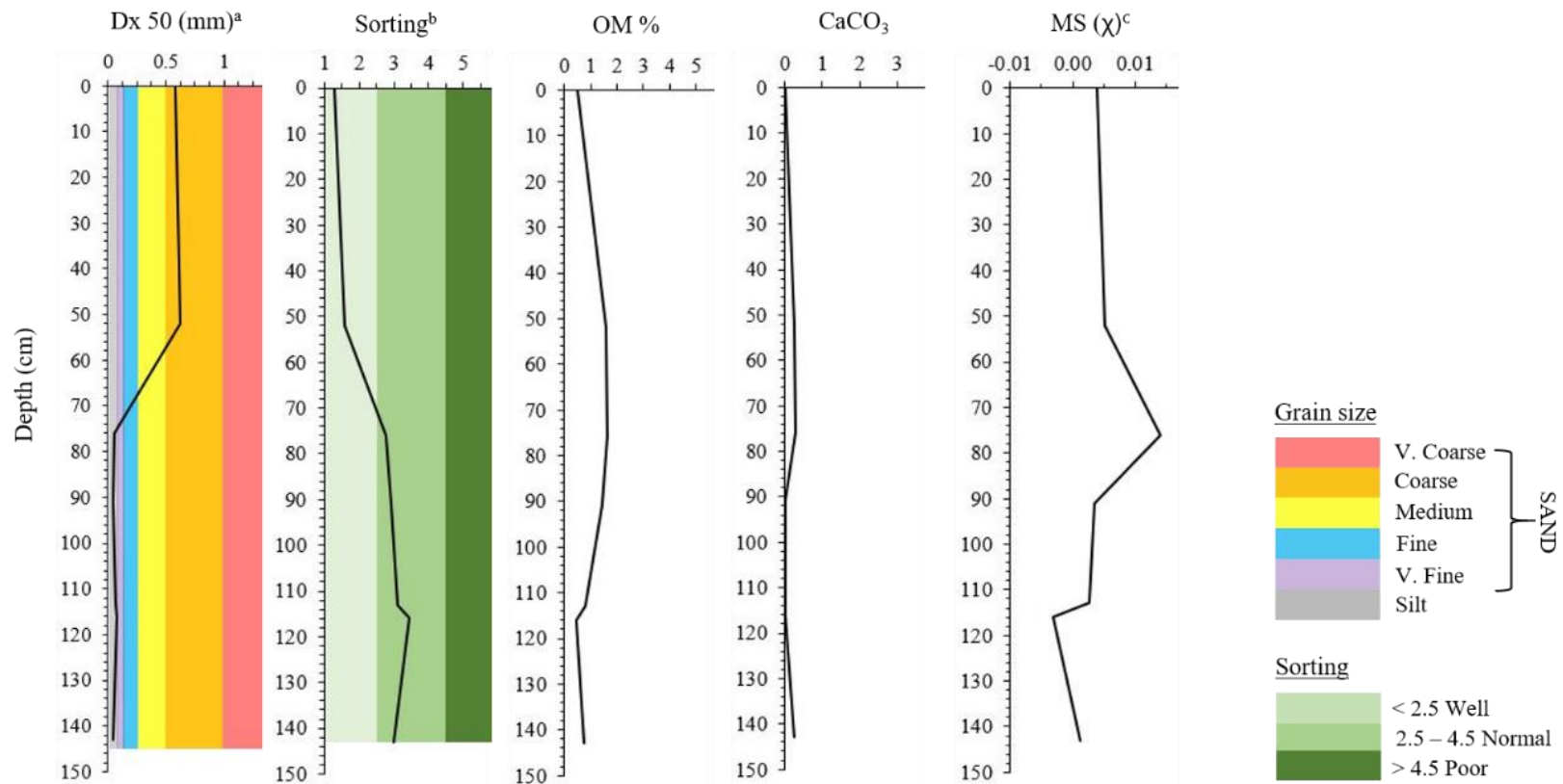
Figure 5.13 Laboratory analysis results for borehole sediment samples of BSB-PZ-01-1.

Note: Borehole depth = 143 cm. [a]Some 50th percentiles are +/- 0.5% due to calculation adjustments after correcting for sieved portion > 1mm. [b]Sorting is calculated from Trask (1930).

[c]Values are *10-6.

5.1.2.1.2 BSB-PZ-01-1 groundwater level

      Average daily groundwater levels and temperature at BSB-PZ-01-1 from October 2018 to October 2019 are graphically represented in Figure 5.14 The time series indicates frequent episodes of recharge followed by a gradual staggered decrease in water level. The lowest reading recorded was of 0.22 m of water depth above the sensor on July 8, 2019. The highest water level recorded was three days later on July 11, 2019 with a measurement of 0.89 m of water depth above the sensor.
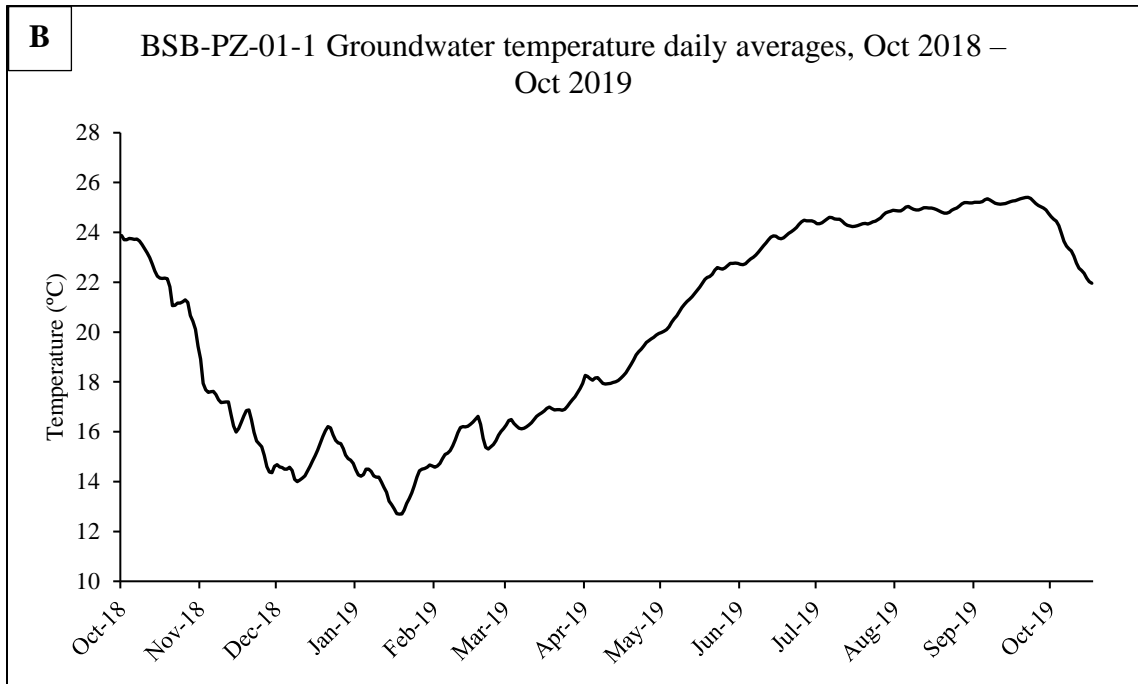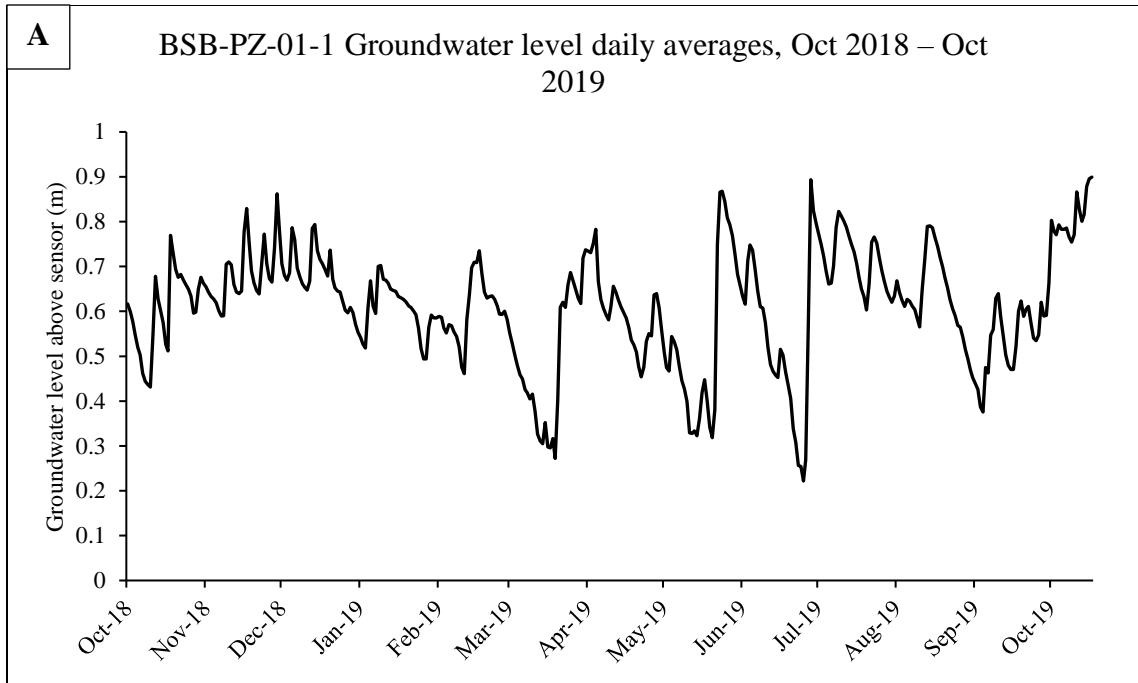
Figure 5.14 Groundwater levels (A) and temperature (B) at BSB-PZ-01-1, October 2018 – October 2019.

5.1.2.2 BSB-PZ-01-2

5.1.2.2.1 BSB-PZ-01-2 sediment

Figure 5.15 displays laboratory results for borehole sediments at BSB-PZ-01-2. This piezometer borehole is located on the shoreline berm at the second BSB study site. Sampling intervals include the surface, 0 – 46 cm, 46 – 64 cm, 64 – 81 cm, 81 – 83 cm, 83 – 107 cm, 107 – 119 cm, and 119 – 131 cm. Dx (50) particle size values widely range between very coarse sand to silt. Maximum Dx (50) is 1.69 mm at the 46 – 64 cm interval. There is a sharp sand-OM contact in the 64 – 82 cm interval. The sample was separated into the sand section and the OM section and lab tested individually. Minimum Dx (50) for the borehole sediments is 0.053 mm and is from the OM section of sediment from the 64 – 82 cm interval. Sorting is well to normal. OM is relatively abundant in sediment of the deeper portion of the borehole. The highest OM value of 12.7% correlates with the sand-OM contact at the 64 – 82 cm interval. $CaCO_3$ is low but is most abundant in the 64 – 82 cm interval with a maximum value of 1.45%. MS stays within range of typical clastic sediment values and has a maximum value of $0.009 * 10^{-6} \text{ m}^3 \text{ kg}^{-1}$ at surface.
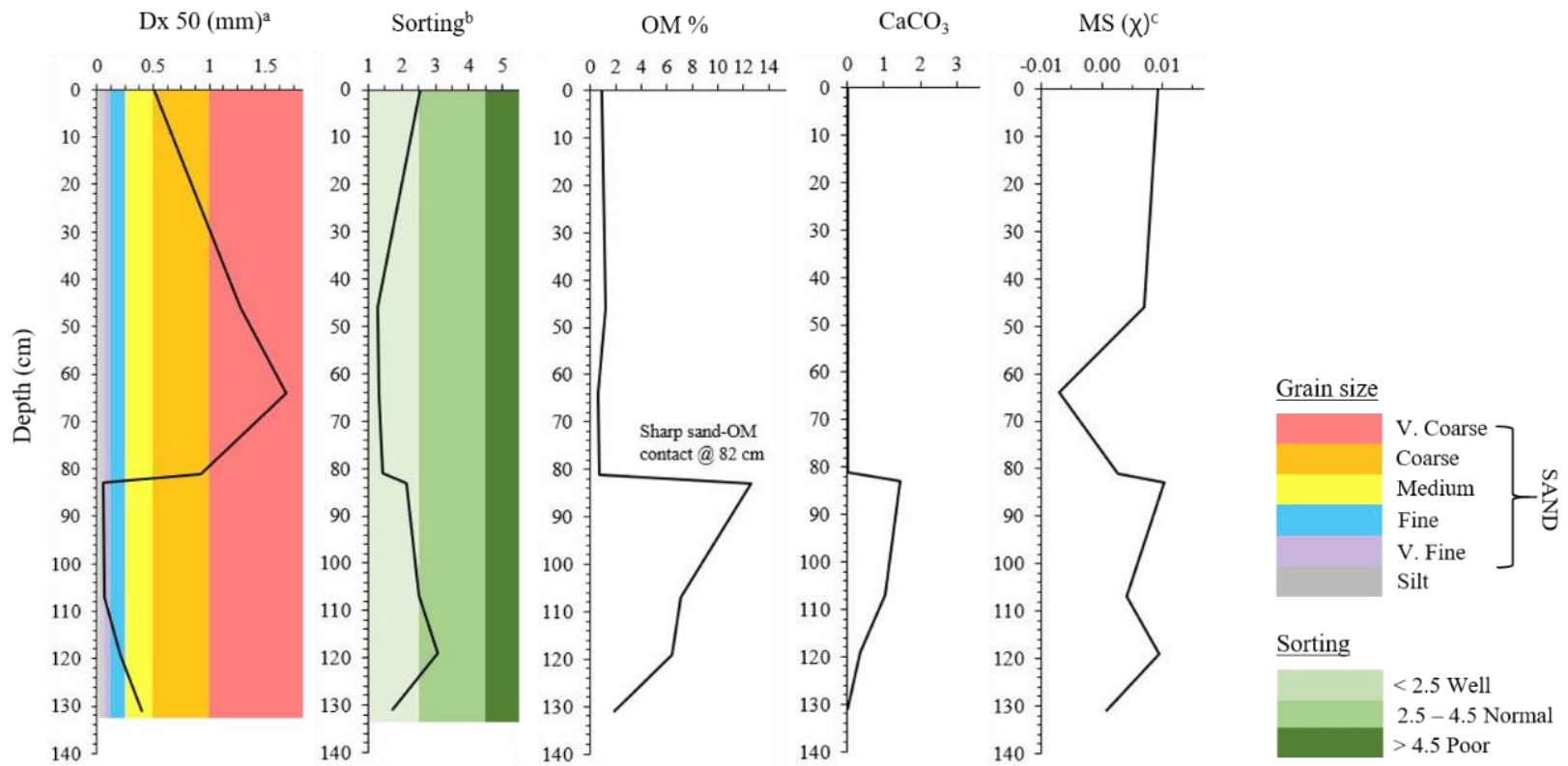
Figure 5.15 Laboratory analysis results for borehole sediment samples of BSB-PZ-01-2.

Note: Borehole depth = 131 cm. [a]Some 50th percentiles are +/- 0.5% due to calculation adjustments after correcting for sieved portion > 1mm. [b]Sorting is calculated from Trask (1930).
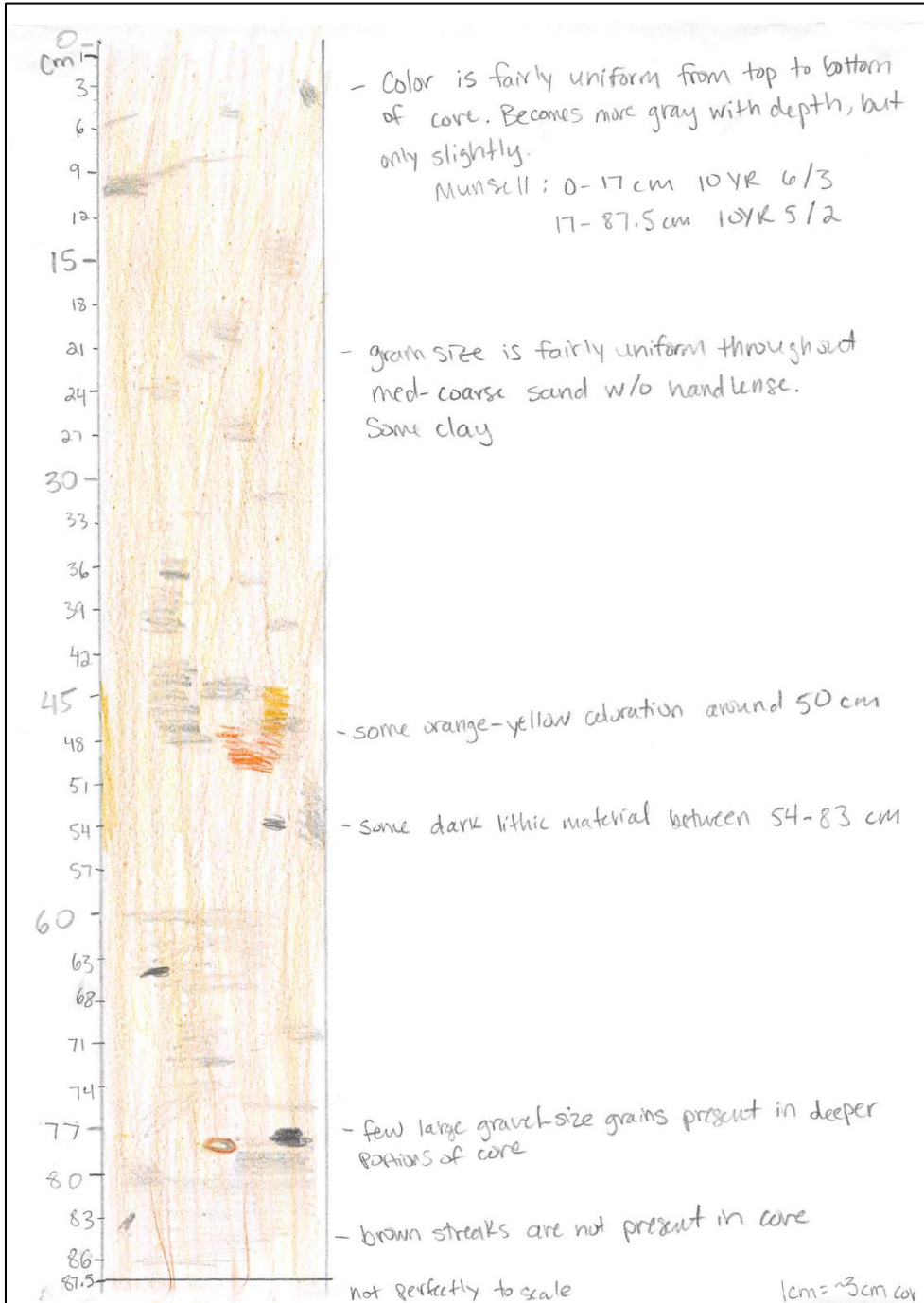
[c]Values are $*10^{-6}$.

5.1.2.2.2 BSB-PZ-01-2 groundwater level

Average daily groundwater levels and temperature for BSB-PZ-01-2 are graphically represented in Figure 5.16. The time series follows a similar pattern as BSB-PZ-01-1 groundwater levels, however the water table levels decline at a slower rate at this location. Groundwater levels fluctuate less and have a smoother, less erratic curve at this piezometer as compared to BSB-PZ-01-1. The lowest level recorded was 0.46 m of water depth above the sensor on July 11, 2019. The highest level recorded was 0.86 m above the sensor on December 14, 2018.
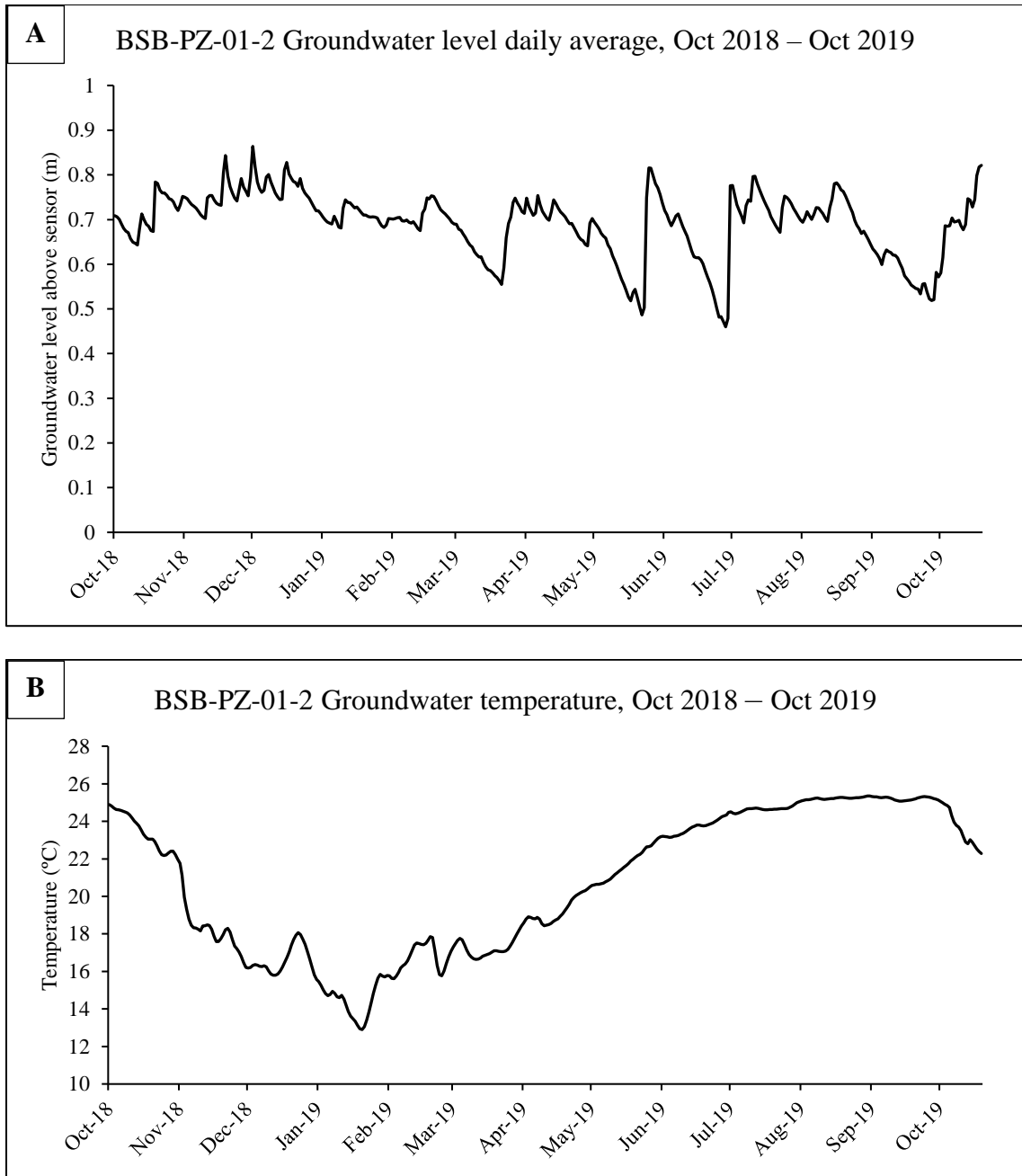
Figure 5.16 Groundwater levels (A) and temperature (B) at BSB-PZ-01-2, October 2018 – October 2019.

5.1.2.3 BSB-PZ-01-3

5.1.2.3.1 BSB-PZ-01-3 sediment

Figure 5.17 displays laboratory results for borehole sediments at BSB-PZ-01-3. This piezometer is in the wooded swamp area of the first BSB study site. The location was selected to compare groundwater levels of an area that is more distant from wave action at the shoreline. Sample intervals include the surface, 0 – 5 cm, 5 – 35 cm, 35 – 55 cm, 55 – 68 cm, and 68 – 85 cm. Dx (50) particle size is comparatively finer than the piezometers closer to the shoreline. Dx (50) ranges from medium sand to silt. Maximum Dx (50)is 0.39 mm at the 0 – 5 cm interval which is below the forest duff layer. Silt is dominant through the middle section of the borehole with the finest Dx (50) measuring 0.035 mm at the 55 – 68 cm interval. Sorting starts as normal at surface and transitions to well with increasing depth. Organic matter content is highest in the top portion of the borehole with a value of 9.09% at the 0 – 5 cm interval. Calcium carbonate is also highest in this interval reading 1.25%. MS is consistently paramagnetic with a maximum value of 0.011 * 10^{-6} m^3 kg^{-1} and is within range of typical clastic sediment values.
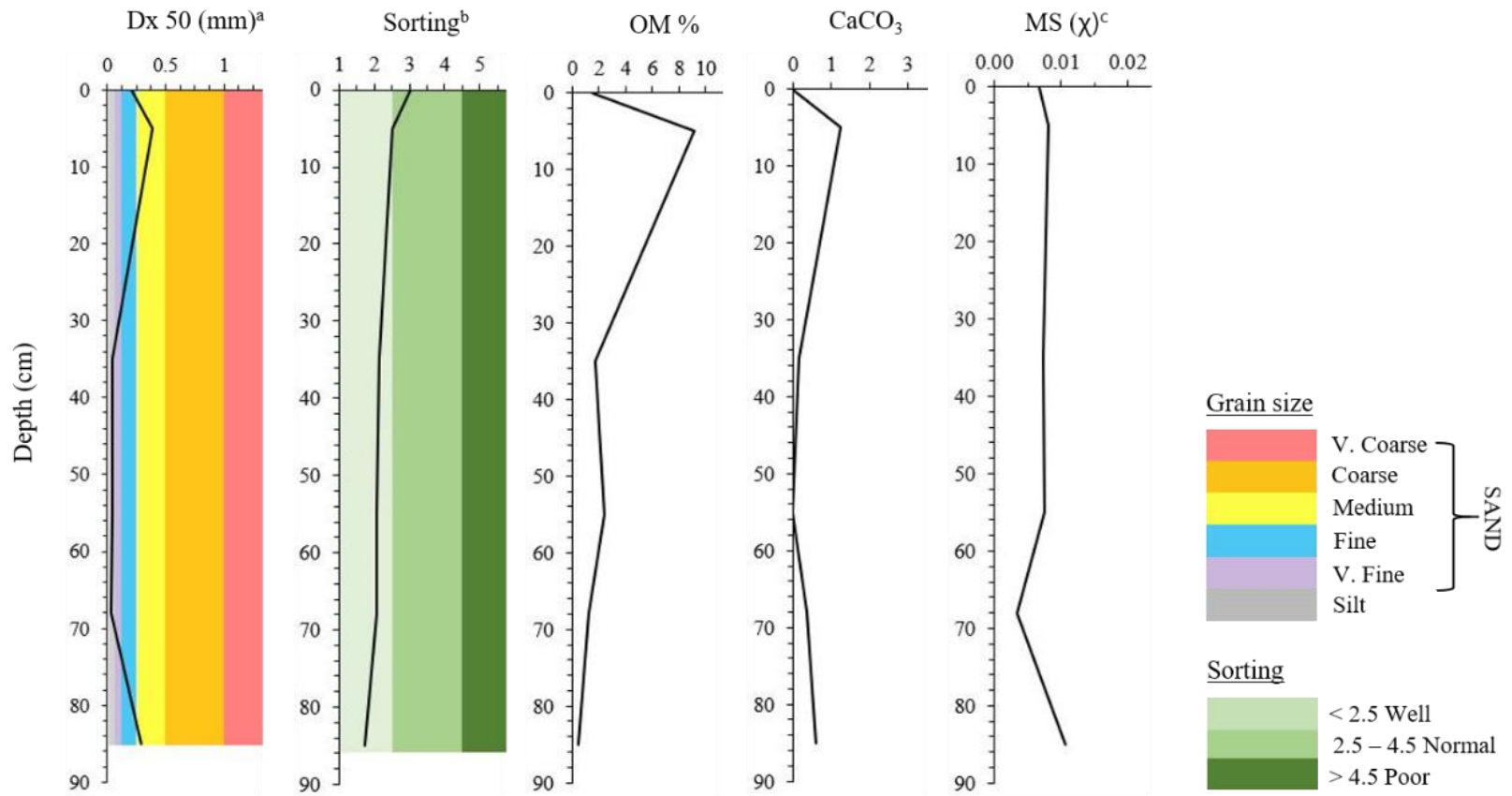
Figure 5.17 Laboratory analysis results for borehole sediment samples of BSB-PZ-01-3.

Note: Borehole depth = 85 cm. [a]Some 50th percentiles are +/- 0.5% due to calculation adjustments after correcting for sieved portion > 1mm. [b]Sorting is calculated from Trask (1930).
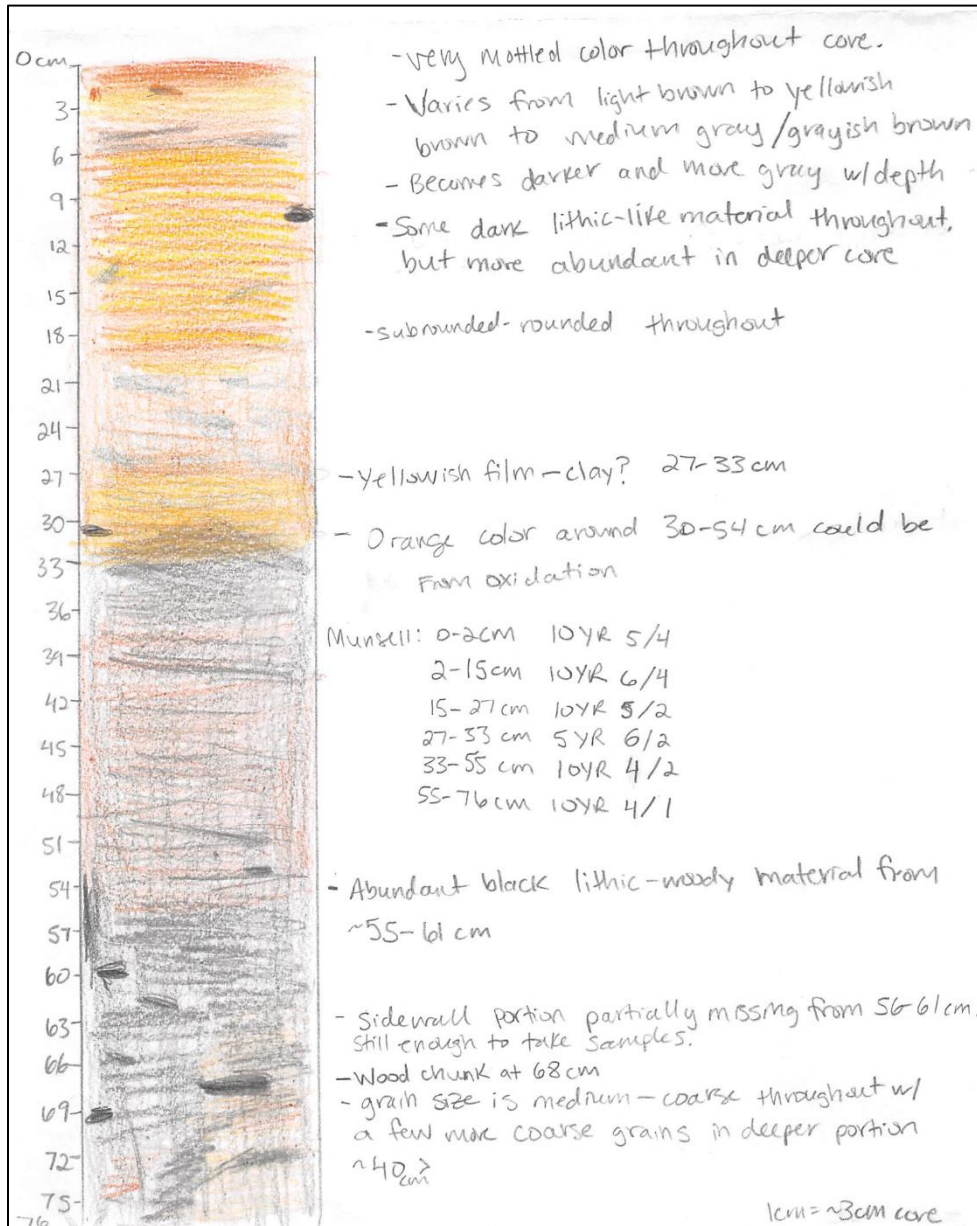
[c]Values are $*10^{-6}$.

5.1.2.3.2 BSB-PZ-01-3 groundwater level

      The average daily groundwater level and temperature recordings for BSB-PZ-01-3 are graphically represented in Figure 5.18. Groundwater levels at this location were monitored for a one month period from October 2018 to November 2018, when at that time the sensor was moved to the Perdido Bay piezometer. Because the time frame for logging at this location is relatively brief, the daily average water level curve is comparatively smooth and less variable. Recharge and depletion trends display similar slopes and therefore rates, respectively. The lowest level was 0.28 m of water depth above the sensor on October 24, 2018. The highest level measured was 0.75 m water depth on November 2, 2018.
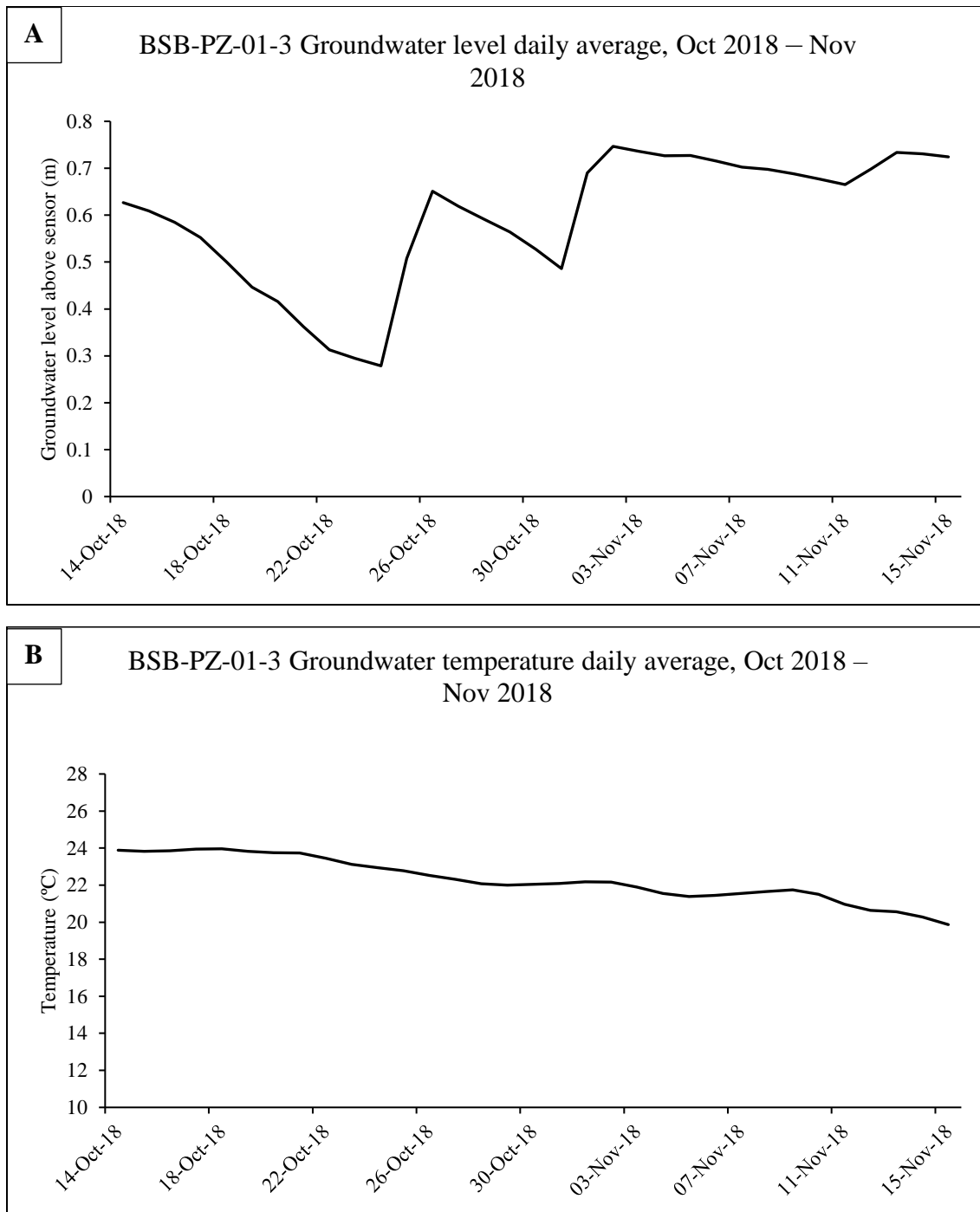
Figure 5.18 Groundwater levels (A) and temperature (B) at BSB-PZ-01-3, October 2018 – November 2018.

5.1.2.4 PB-PZ-02-1

5.1.2.4.1 PB-PZ-02-1 sediment

Figure 5.19 displays laboratory results for borehole sediments at PB-PZ-02-1. This borehole is located on the shoreline berm at the Perdido Bay site. Sampling intervals include the surface, 0 – 29 cm, 29 – 37 cm, 37 – 47 cm, 47 – 57 cm, 73 – 74 cm, 74 – 97 cm, 97 – 108 cm, 108 – 112 cm, 112 – 130 cm, and 130 – 149 cm. Dx (50) particle size values vary between coarse sand and very fine sand for the entire depth of the borehole. Maximum Dx (50)is 0.96 mm at the 73 – 74 cm interval. Minimum Dx (50)is 0.11 mm at the 37 – 47 cm interval. Sorting is well to normal. Organic matter content has a maximum value of 18.1% at the 29 – 37 cm interval. OM stays below 7% for the remaining intervals. $CaCO_3$ is minimal with a maximum value of 1.33% at 47 – 57 cm. MS fluctuates between paramagnetic and diamagnetic with a maximum value of $0.007 * 10^{-6}$ m^3 kg^{-1} at 29 – 37 cm.
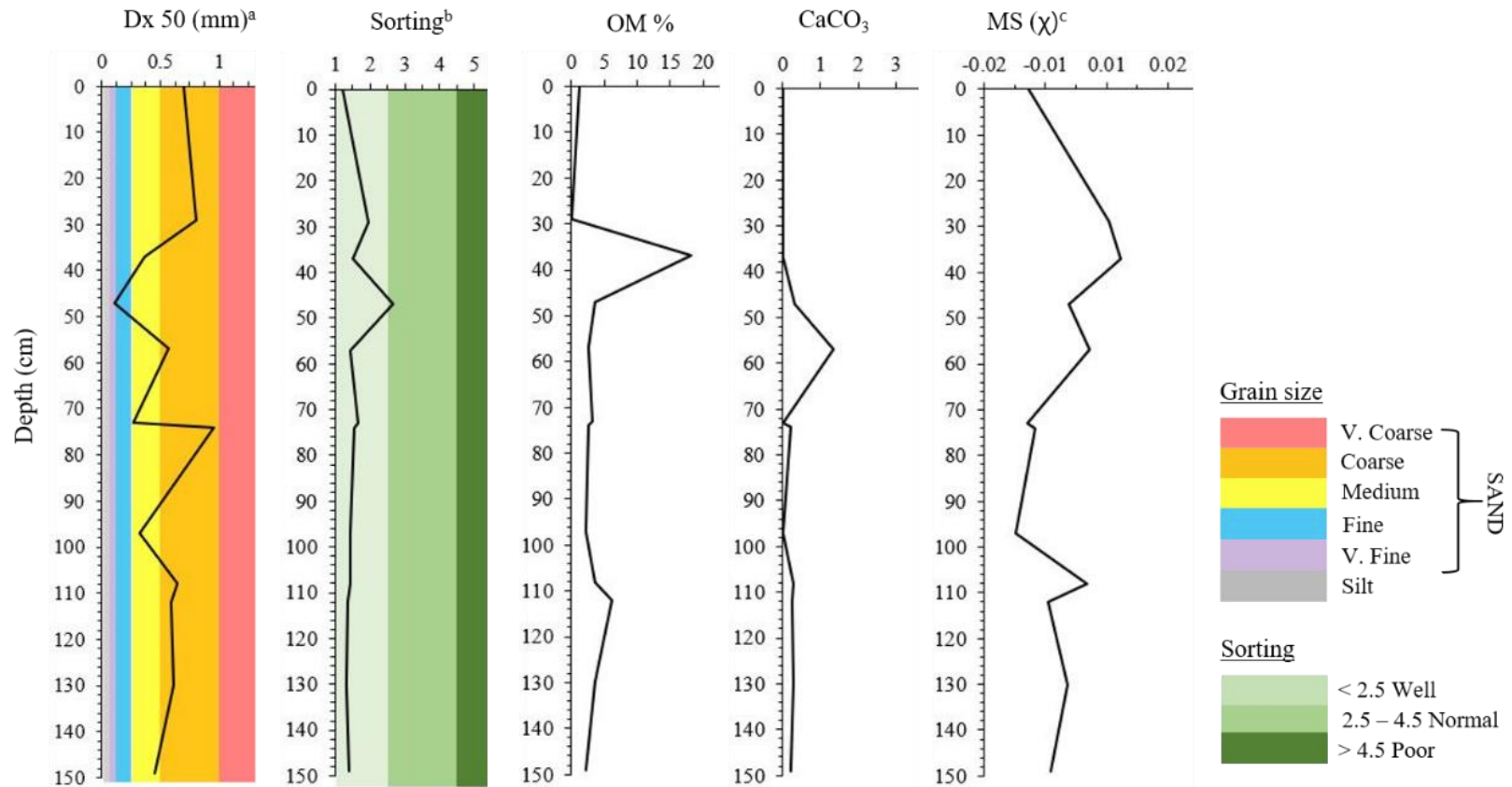
Figure 5.19 Laboratory analysis results for borehole sediment samples of PB-PZ-02-1.

Note: Borehole depth = 149 cm. [a]Some 50th percentiles are +/- 0.5% due to calculation adjustments after correcting for sieved portion > 1mm. [b]Sorting is calculated from Trask (1930). [c]Values are $*10^{-6}$.
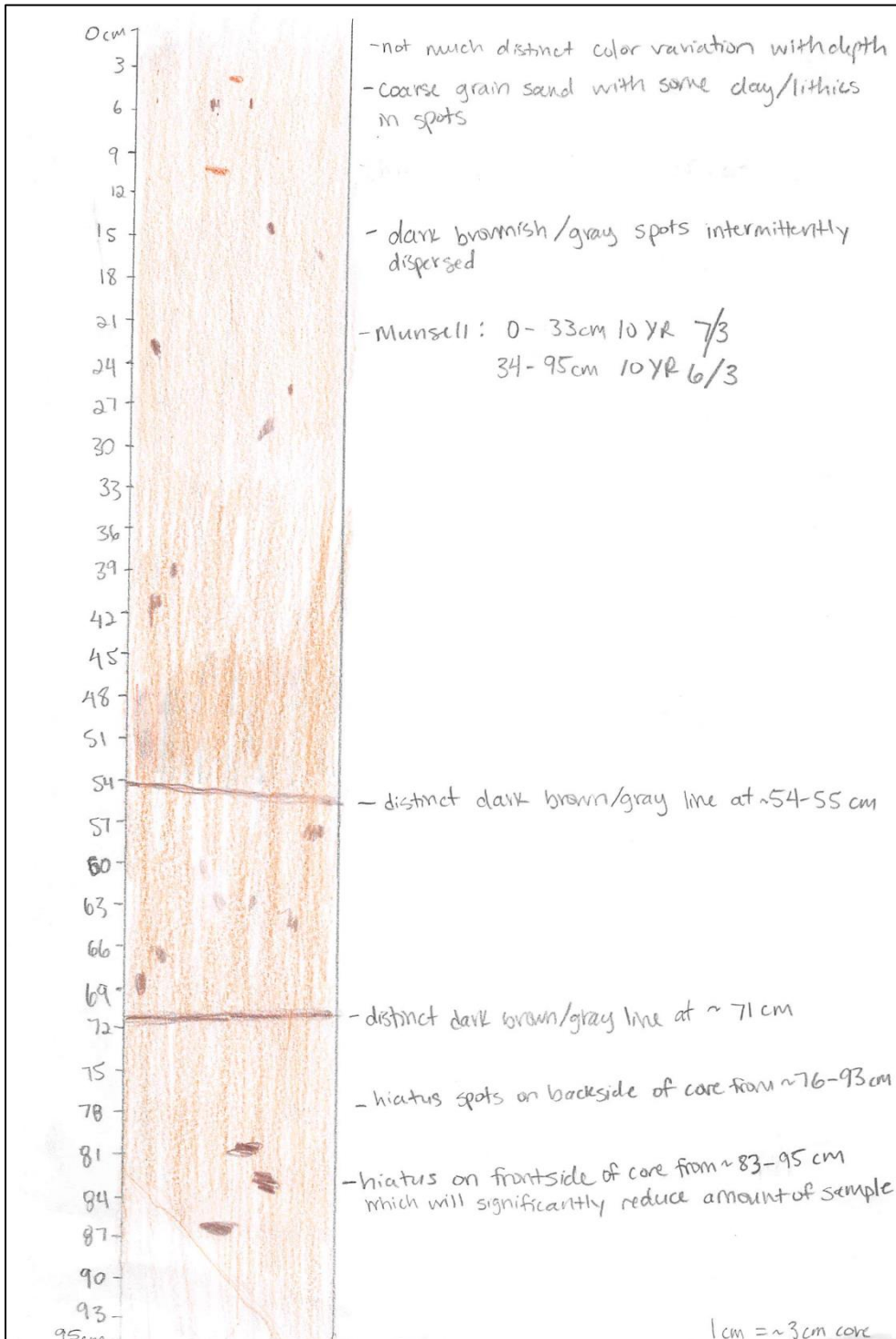
5.1.2.4.2 PB-PZ-02-1 groundwater level

      Average daily groundwater and temperature trends for PB-PZ-02-1 are

graphically represented in Figure 5.20. The time series indicates a more variable and

responsive shallow groundwater table at this location. Relatively large fluctuations are

evident from day to day. The lowest recording was 0.11 m water depth above the sensor

on March 7, 2019. The highest recording was 0.68 m of water above the sensor on June

9, 2019. However, this value may not be completely accurate because it occurred after

damages from the March prescribed burn were incurred by the piezometer standpipe

above the ground surface. When the sensor was checked in November, the piezometer

PVC housing had been melted and bent over, pulling the sensor a few centimeters up the

borehole. Even if the values have shifted, the water level trend is still reliable.
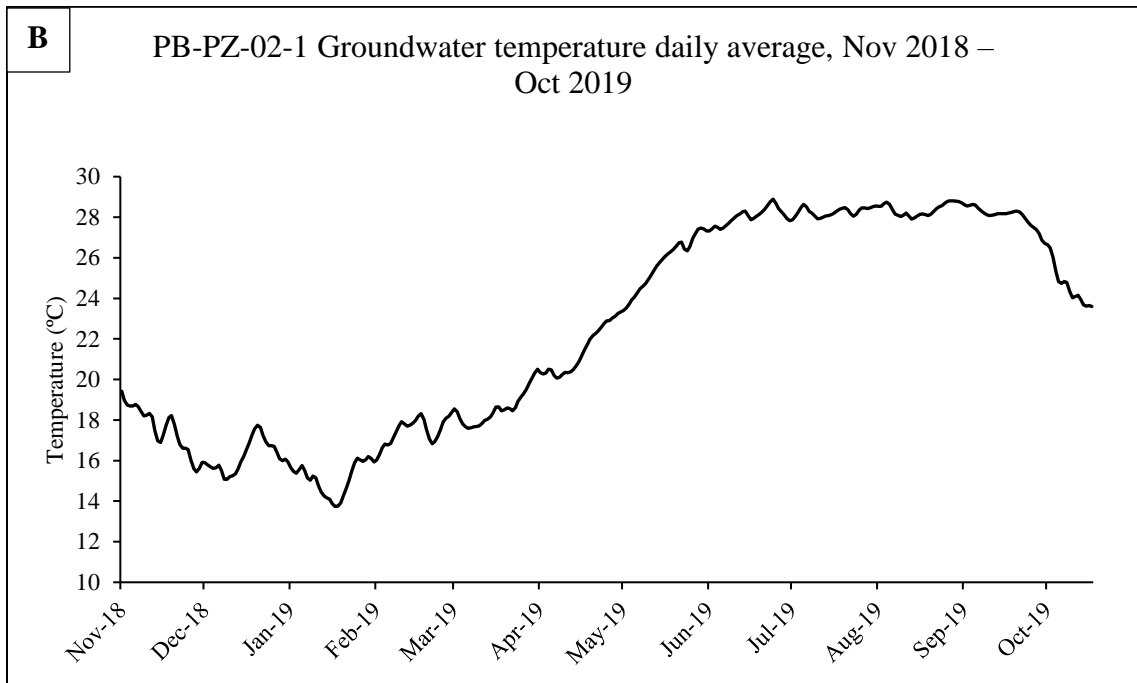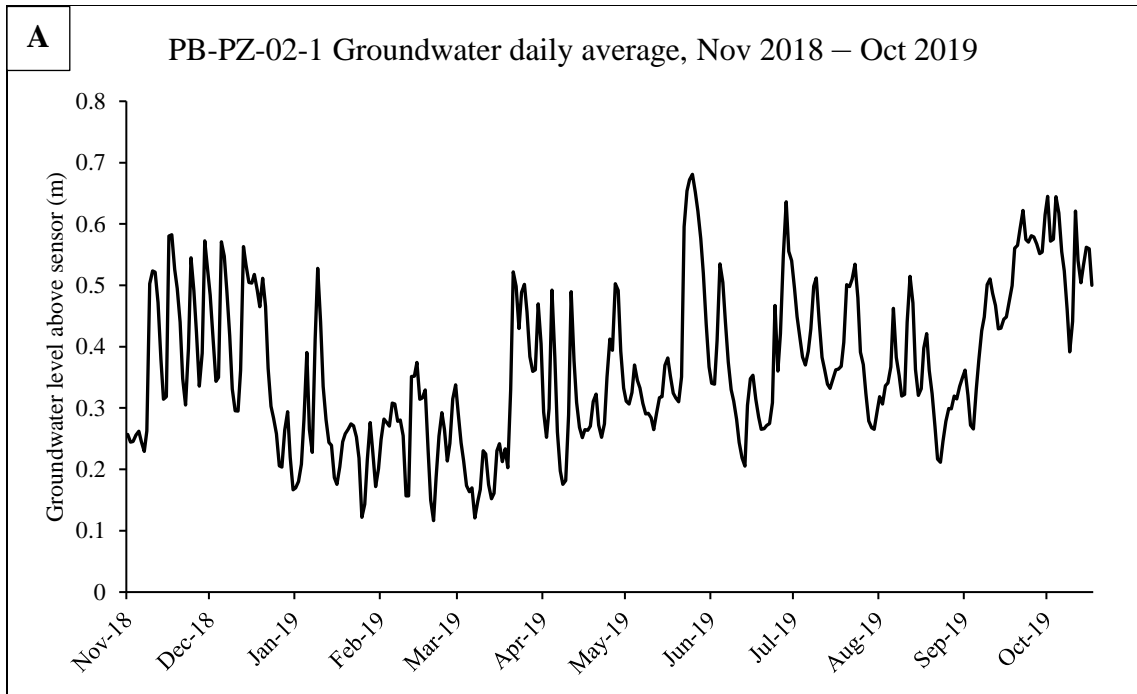
Figure 5.20 Groundwater levels (A) and temperature (B) at PB-PZ-02-1, November 2018 – October 2019.

5.1.3 Groundwater quality

Upon installation of each piezometer, groundwater that had infiltrated during installation was collected with a bailer and bottled for subsequent laboratory analysis of water quality (Table 5.1). Samples A and B are from BSB-PZ-01-1 and were collected during two different site visits. Sample C is from BSB-PZ-01-2, Sample D is from BSB-PZ-01-3, and Sample E is from PB-PZ-02-1. Oxidation-reduction potential (ORP), also known as redox potential, is approximately 200 mV for all samples, indicating a low oxygen content. The reading for dissolved oxygen percentage (DO %) supports this because DO is around 0.1% for all samples. ORP is positive and is therefore has oxidizing potential (Striggow, 2017). Water pH for all samples is acidic, which is primarily a result of tannic acids exuded by decomposing organic matter from the surrounding wetlands and pine forests, which subsequently percolate into the shallow groundwater.

Conductivity is a measurement of ions released from dissolved salts. Conductivity and salinity measurements are related, whereas an increase in dissolved ions produces an increase in salinity and therefore conductivity; however, there is no quantitative salinity measurement for this study. Conductivity for all samples is above the highest typical value of 2000 micro Siemens per centimeter (μS cm^{-1}) for freshwater (SWRCB, 2002). Higher groundwater conductivity values are to be expected at the study sites because of the proximity to the brackish water of the estuaries and tidal influence. Groundwater conductivity and other water quality parameters can readily fluctuate at any given time of measurement at the study locations. In the event of high precipitation, groundwater conductivity will decrease due to a flush of freshwater, or conversely, storm surge from

encroaching estuarine water would increase conductivity. As an example, Samples A and B were sampled from the same piezometer borehole at BSB site 1. At each time of measurement, water table levels were almost identical, however Sample B conductivity levels and ORP levels had decreased and pH had increased (became less acidic) as compared to Sample A, which was captured one month prior to Sample B. A local increase in a freshwater source (i.e., rainwater and/or runoff) is a viable cause of these different groundwater quality readings at the same piezometer. Total dissolved solids (TDS) correlate with conductivity, where the former is the sum of all ion particles as well as dissolved organic matter and other dissolved compounds smaller than two microns (EPA, 2012). TDS values and trends mimic conductivity values for all samples at the study sites. TDS for freshwater has an upper limit of 2000 mg L^{-1} (SWRCB, 2002).

Table 5.1

Water quality laboratory results from piezometer boreholes.

Sample	A	B	C	D	E
Water table level (cm)	97	95	108	43	-
ORP (mV)	227	188	213	211	209
pH	2.78	3.45	3.01	3.05	3.08
Conductivity (μS cm^{-1})	8673	3684	5985	4576	3308
TDS (mg L^{-1})	5863	2496	4063	3114	2243
DO%	0.09	0.1	0.09	0.09	0.1

Note: Sample A: BSB-PZ-01-1 from Oct 2018. Sample B: BSB-PZ-01-1 from Nov. 2018. Sample C: BSB-PZ-01-2 from Nov. 2018. Sample D: BSB-PZ-01-3 (swamp) from Nov. 2018. Sample E: PB-PZ-02-1 from Nov. 2018. No water table level data available for Sample E. Samples were measured at room temperature (~22 ºC).

5.1.4 Bottom sediment samples

Subaqueous bottom sediment samples in the nearshore zone and margin of the central estuarine basin were collected using a Ponar grab sampler. Sample locations

follow a transect pattern from nearshore cores out toward the deeper basin margin. See

Figure 4.8 for sample locations at each study site.

5.1.4.1 Bon Secour Bay bottom sediment

Table 5.2 provides laboratory results for BSB bottom sediment samples, which

indicates that median particle size generally becomes finer as depth increases. Samples 1

and 13 have the most similar particle size characteristics, however Sample 1 is nearest to

shoreline of the second BSB site and Sample 13 is farthest away on the nearshore to

central basin transition. Dx (50) particle size of both samples is silt-sized and they have

the highest OM and $CaCO_3$ content of all the bottom samples in BSB. OM for Sample 1

is 10.6% and Sample 13 is 10.1%. $CaCO_3$ for Sample 1 is 3.0% and Sample 13 is 4.2%.

For the remaining samples, Dx (50) particle size is fine to medium sand, and OM and

$CaCO_3$ are considerably lower compared to Samples 1 and 13. Sorting is well to normal

for all samples. MS is weakly negative (diamagnetic) to weakly positive (paramagnetic)

for all samples.

Table 5.2

Laboratory results for BSB bottom sediment samples.

Sample	Water depth (m)	Dx 50 (mm)	Sorting	OM %	CaCO$_3$ %	MS
1	0.52	0.060 (slt)	2.1	10.6	3.0	0.077
2	0.94	0.224 (f)	1.3	0.9	0.2	0.001
3	1.39	0.253 (m)	1.3	0.8	0.2	-0.002
4	2.57	0.171 (f)	1.8	4.1	1.8	0.036
5	1.82	0.253 (m)	2.2	2.7	0.7	0.012
6	1.27	0.260 (m)	1.3	0.7	0.2	0.004
7	0.93	0.257 (m)	1.3	0.8	0.3	0.006
8	0.76	0.259 (m)	1.3	1.1	0.2	0.005
9	0.70	0.335 (m)	1.3	0.7	0.2	-0.003
10	0.91	0.228 (f)	1.4	1.2	0.2	-0.002
11	1.29	0.342 (m)	1.3	1.1	0.0	0.002
12	1.60	0.286 (m)	1.3	1.0	0.3	0.006
13	2.46	0.045 (slt)	2.3	10.1	4.2	0.077
14	1.81	0.183 (f)	1.9	3.3	1.1	0.027
15	1.10	0.243 (f)	1.4	1.3	0.2	0.001
16	0.86	0.305 (m)	1.4	0.7	0.5	-0.001

Note: slt = silt; vf = very fine sand; f = fine sand; m = medium sand; c = coarse sand. MS is $*10^{-6}$.

5.1.4.2 Perdido Bay bottom sediment

Table 5.3 provides laboratory results for Perdido Bay bottom sediment samples. Dx (50) particle size for samples in this area are fine to medium sand with very fine sand in the deepest part of the area. Sample 14 is the finest particle size sample and is located beyond the nearshore to central basin transition. Sample 14 also has the highest OM content with 10.2% and highest CaCO$_3$ content at 2.9%. Sample 1 is coarse sand that is located near the southern point of the Tarkiln peninsula. The proximity to the higher energy environment of a point or spit is likely the reason for the coarse particle size.

Sorting is well to normal for all sample locations. Magnetic susceptibility is weakly

negative (diamagnetic) to weakly positive (paramagnetic) for all samples. MS values are

generally larger when evaluating bottom sediment samples at no depth increment versus

samples at 5-cm depth increments with the nearshore cores. This is true for both Bon

Secour Bay and Perdido Bay samples.

Table 5.3

Laboratory results for PB bottom sediment samples.

Sample	Water depth (m)	Dx 50 (mm)	Sorting	OM %	CaCO₃ %	MS
1	2.04	0.740 (c)	1.3	0.8	0.2	-0.003
2	1.28	0.241 (f)	1.4	0.6	0.1	-0.004
3	0.92	0.269 (m)	1.6	0.6	0.0	0.005
4	0.70	0.323 (m)	1.3	0.5	0.0	-0.003
5	1.22	0.323 (m)	1.3	0.5	0.0	-0.001
6	1.98	0.293 (m)	2.1	0.7	0.0	-0.013
7	2.20	0.242 (f)	1.4	0.8	0.2	-0.011
8	1.28	0.274 (m)	1.3	0.6	0.2	-0.019
9	0.73	0.261 (m)	1.3	0.7	0.0	-0.007
10	0.70	0.307 (m)	1.6	0.5	0.2	0.006
11	1.68	0.314 (m)	2.0	0.7	0.0	-0.001
12	2.35	0.234 (f)	1.6	1.0	0.2	-0.008
13	3.17	0.085 (vf)	2.3	8.7	2.8	-0.033
14	3.22	0.091 (vf)	2.1	10.2	2.9	0.028

Note: slt = silt; vf = very fine sand; f = fine sand; m = medium sand; c = coarse sand. MS is $*10^{-6}$.

5.1.5 Erosion pins

Figure 5.21 displays the field measurements of erosion pin exposure at Bon

Secour Bay. The purpose of erosion pins was to measure short-term (less than two years)

erosion at the shoreline. Erosion pins were installed at the BSB site only. The pins were

installed on May 2018 and measured at each field visit, for a total of four measurements.

Erosion pins 1 and 2 are at the first BSB site, and pins 3 and 4 are at the second BSB site. Measurements of all four pins show periods of erosion and deposition at each installation. From May 2018 to November 2018 erosion pin 1 recorded 3 cm of erosion. When visiting the site in November 2019 the erosion pin could not be located and is assumed to have washed away. Erosion pin 1 was located next to a channel cut from storm drainage after installation (See Figure 5.22). Erosion pin 2 recorded minimal changes with an overall 2 cm of deposition from May 2018 to November 2019. Erosion pin 3 recorded the most erosion (other than pin 1) with a net value of 14.5 cm from May 2018 to November 2019. Erosion pin 4 recorded slight overall deposition of 1 cm during the monitored time frame.
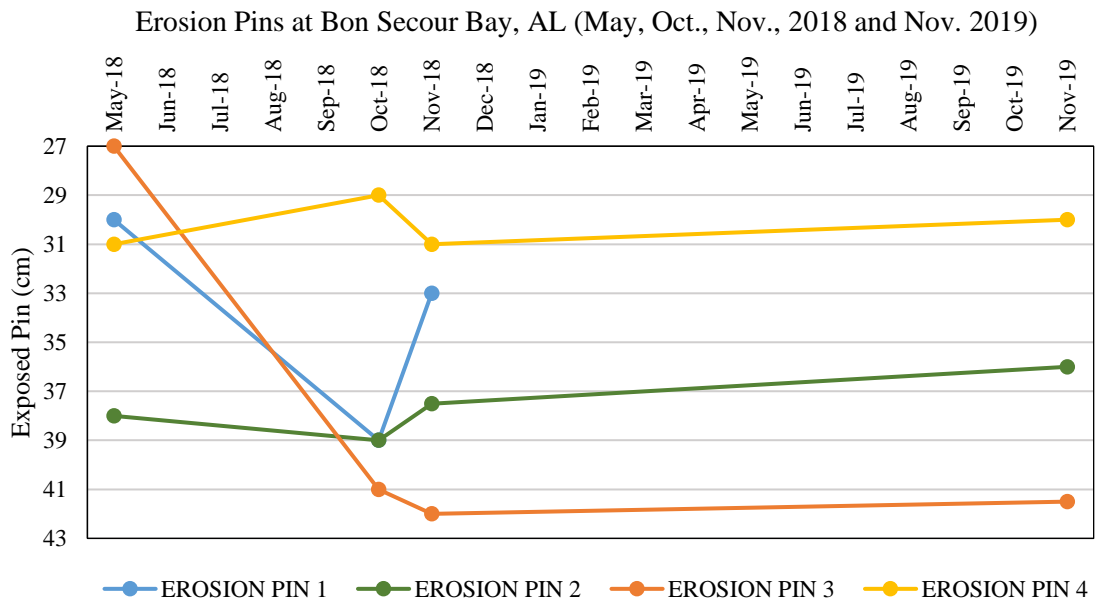
Figure 5.21 Erosion pin exposure measurements.

Note: Erosion pin 1 located at BSB berm. Erosion pin 2 located at BSB shoreline. Erosion pin 3 located near BSB piezometer 2 (east). Erosion pin 4 located near BSB piezometer 2 (west).

Figure 5.22 A) Erosion pin 1 in May 2018. B) Erosion pin 1 (circled in red) in November 2018.

5.2 Statistical Results

The purpose of statistical analyses was to test for similarities or differences of sedimentary variables between the five nearshore cores and amongst samples within individual cores. Data used in statistical testing are the results from laboratory analysis. Nine variables are used including the various particle-size percentiles Dx (10), Dx (16), Dx (25), Dx (50), Dx (75), Dx (84), Dx (90); OM %; and $CaCO_3$ %. Magnetic susceptibility is excluded because the laboratory results are for composites of 5-cm increments and would thus skew the statistical test results. First, inter-core discriminant analysis was done using IBM SPSS 26 statistics software. Discriminant analysis is used to determine the probability of group membership based on the mean values of predictor variables. In other words, which cores, if any, are similar and to what degree based on the tested sedimentary variables.

For discriminant analysis, it is best to have at least five times as many observations as predictor variables. This is possible for the nearshore cores (414 total observations), however there are too few bottom sediment samples and piezometer borehole sediment samples (30 and 33 observations, respectively) for adequate discriminant analysis. An attempt at discriminant analysis was done with the 63 bottom sediment and borehole sediment observations, however the results were not conclusive or sensibly comparable to results for the nearshore cores. Because of this, statistical and laboratory results of the nearshore sediment cores will be compared with only laboratory results of bottom sediment samples and borehole sediment samples to infer if correlations exist. Several output options are available for selection in SPSS; for this analysis, those included are group statistics, eigenvalues, predicted group results, function structure

matrix, and function centroid plots. After completion of discriminant analysis, several *t*-tests were used to identify significance between two cores using the means of their shared variables.

5.2.1 Inter-core discriminant analysis

The null hypothesis states that if there is no significance, *p* values will be less than 0.05 meaning there is less than 5% probability that a relationship exists between specific variables from different groups (cores). To test this hypothesis, discriminant analysis was done to determine if there is a relationship between predictor variables and, thus, reveal similarities and differences between nearshore sediment cores. An overview of group statistics for each core is presented in Table 5.4.

Table 5.4 Group statistics for sediment cores.

Core		Mean	Std. Deviation	N
1	Dx (10)avg	204	135	78
	Dx (16)avg	246	141	78
	Dx (25)avg	298	152	78
	Dx (50)avg	443	189	78
	Dx (75)avg	687	283	78
	Dx (84)avg	833	355	78
	Dx (90)avg	975	425	78
	OM LOI % by weight (g)	0.9	1.2	78
	CaCO3 LOI % by weight (g)	0.3	0.7	78
2	Dx (10)avg	111	80	87
	Dx (16)avg	150	83	87
	Dx (25)avg	193	86	87
	Dx (50)avg	307	113	87
	Dx (75)avg	537	294	87
	Dx (84)avg	665	378	87
	Dx (90)avg	810	488	87
	OM LOI % by weight (g)	0.8	0.2	87
	CaCO3 LOI % by weight (g)	0.2	0.1	87
3	Dx (10)avg	47	39	76

	Dx (16)avg	70	54	76
	Dx (25)avg	100	67	76
	Dx (50)avg	192	97	76
	Dx (75)avg	343	197	76
	Dx (84)avg	464	299	76
	Dx (90)avg	581	398	76
	OM LOI % by weight (g)	1.3	.5	76
	CaCO3 LOI % by weight (g)	0.3	0.2	76
4	Dx (10)avg	161	45	95
	Dx (16)avg	188	43	95
	Dx (25)avg	223	51	95
	Dx (50)avg	324	94	95
	Dx (75)avg	560	323	95
	Dx (84)avg	733	418	95
	Dx (90)avg	883	503	95
	OM LOI % by weight (g)	0.4	0.2	95
	CaCO3 LOI % by weight (g)	0.1	0.2	95
5	Dx (10)avg	163	45	78
	Dx (16)avg	190	44	78
	Dx (25)avg	223	45	78
	Dx (50)avg	310	57	78
	Dx (75)avg	463	168	78
	Dx (84)avg	576	251	78
	Dx (90)avg	690	331	78
	OM LOI % by weight (g)	0.5	0.2	78
	CaCO3 LOI % by weight (g)	0.3	0.3	78
Total	Dx (10)avg	138	93	414
	Dx (16)avg	170	98	414
	Dx (25)avg	208	107	414
	Dx (50)avg	316	140	414
	Dx (75)avg	521	285	414
	Dx (84)avg	659	369	414
	Dx (90)avg	793	457	414
	OM LOI % by weight (g)	0.8	0.6	414
	CaCO3 LOI % by weight (g)	0.2	0.4	414

Note: Core 1 is BSB-C-01-1; Core 2 is BSB-C-01-2; Core 3 is BSB-C-01-3; Core 4 is PB-C-02-1; Core 5 is PB-C-02-2. Particle size

percentile values are in microns. N = number of observations.

5.2.1.2 Classification results

The classification results generated by SPSS are displayed in Table 5.5. Testing reveals 56.3% of original group cases were correctly classified, or stated differently, that 56.3% of the time the correct core was predicted as itself at each observation iteration throughout the core. Line one can be read as Core 1 (BSB-C-01-1) being correctly predicted as Core 1 thirty-six times, however at nine of the core's observations it was incorrectly classified as Core 2, ten times as Core 3 , twenty-one times as Core 4, and two times as Core 5 (n= 78). This is also expressed as a percentage with Core 1 correctly being predicted as Core 1 for 46.2% of its observations. Core 4 (PB-C-02-1) had the highest rate of correct classification at 74.7%. Core 5 (PB-C-02-2) had the lowest rate of correct classification at 39.7%. This information reveals that the cores are not completely unique and differentiable given their sedimentary variables at each 1-cm increment. This is anticipated because of the test's assumption for homogeneity of each core using the mean of the predictor variables. The correctly classified percentages among Cores 1, 2, and 3 from Bon Secour Bay indicate stronger correlation with one another than to Cores 4 and 5 from Perdido Bay. Similarly, correlation is evident between PB Cores 4 and 5 and they can be differentiated from the BSB cores. The lowest percent between two cores is 0% for Cores 5 and 1, indicating the cores are dissimilar and not likely to be identified as the other given their characteristics. The standard for what is considered a "good" or acceptable classification percentage relies upon the interpreter. The result of 56.3% overall correct classification among all cores in this study implies core to core similarity which is understandable being that the cores are from the same depositional environment

and the statistical tests assess the cores as five bulks and does not discern the cores by depth increments where significant differences may be more apparent.

Table 5.5 Classification results for nearshore cores.

		Predicted Group Membership					
	Core	1	2	3	4	5	Total
Count	1	36	9	10	21	2	78
	2	13	44	15	7	8	87
	3	1	18	51	3	3	76
	4	3	5	0	71	16	95
	5	0	12	2	33	31	78
%	1	46.2	11.5	12.8	26.9	2.6	100.0
	2	14.9	50.6	17.2	8.0	9.2	100.0
	3	1.3	23.7	67.1	3.9	3.9	100.0
	4	3.2	5.3	0	74.7	16.8	100.0
	5	0	15.4	2.6	42.3	39.7	100.0

5.2.1.3 Eigenvalues

Eigenvalues and canonical functions are used to determine where the results for discriminant analysis are weighted. The larger the eigenvalue, the more variance the function explains in the outcome. A function was formulated based on the best predictors for a certain outcome. Referring to the eigenvalues in Table 5.6, Functions 1 and 2 carry most of the weight relative to Functions 3 and 4. This is also true with the percent of variance for Functions 1 and 2, which together comprise 87.3% of the percent variance. Functions 1 and 2 consist of variable predictors reported in the structure matrix in Table 5.7.

Table 5.6 Eigenvalues for nearshore cores.

Eigenvalues				
Function	Eigenvalue	% of Variance	Cumulative %	Canonical Correlation
1	.664	55.8	55.8	.632
2	.375	31.5	87.3	.522
3	.107	8.9	96.3	.310
4	.044	3.7	100.0	.206

5.2.1.4 Function structure matrix

Predictors in each function are considered by absolute size of correlation within the function. As displayed in the structure matrix in Table 5.7, the best predictors in Function 1 are Dx (10), Dx (16), Dx (25), OM %, and Dx (50) in that order. The best predictors in Function 2 are Dx (50), Dx (25), and Dx (16) in that order. If a predictor variable has a coefficient less than .500, it is not considered as a best predictor for the function. The number of functions is determined by the number of outcomes, less one. There are five outcomes possible because the significance of five cores is tested, so there are four functions. Function coefficients are comparable to coefficients used in a linear regression analysis.

Table 5.7 Structure matrix for functions.

Predictor	Function			
	1	2	3	4
Dx (10)avg	-.758[*]	.443	.377	-.087
Dx (16)avg	-.742[*]	.556	.247	-.092
Dx (25)avg	-.713[*]	.646	.182	-.018
OM LOI % by weight (g)	.600[*]	.272	.277	.313
Dx (50)avg	-.578	.745[*]	.106	.245
Dx (84)avg	-.309	.333	-.141	.648[*]
Dx (90)avg	-.266	.281	-.172	.624[*]
Dx (75)avg	-.353	.453	-.169	.532[*]
CaCO$_3$ LOI % by weight (g)	.208	.183	.286	-.528[*]

Note: Variables ordered by absolute size of correlation within function. * = Largest absolute correlation between each variable and any discriminant function.

Figure 5.23 is a plot of Functions 1 and 2 for all five cores. Core 1 has the uppermost

centroid on the plot. Clockwise from the Core 1 centroid is Core 2, Core 3, and

overlapping Cores 4 and 5. All centroids are in relatively close proximity to each other

with little spread within the plot. Based on this plot, the centroid overlap of Cores 4 and 5

indicates they are the most similar compared to other cores. This is as also supported by

the classification results of predicted group members in Table 5.5. Cores 1 and 3 are

arguably the most different because of the distance between their centroids along both

Function 1 and Function 2. Along Function 1, Cores 3 and 4 are the most different, and

along Function 2, Cores 1 and 4 are the most different. Core 1 has the largest spread

compared the other four cores, indicating the largest variance within its group.
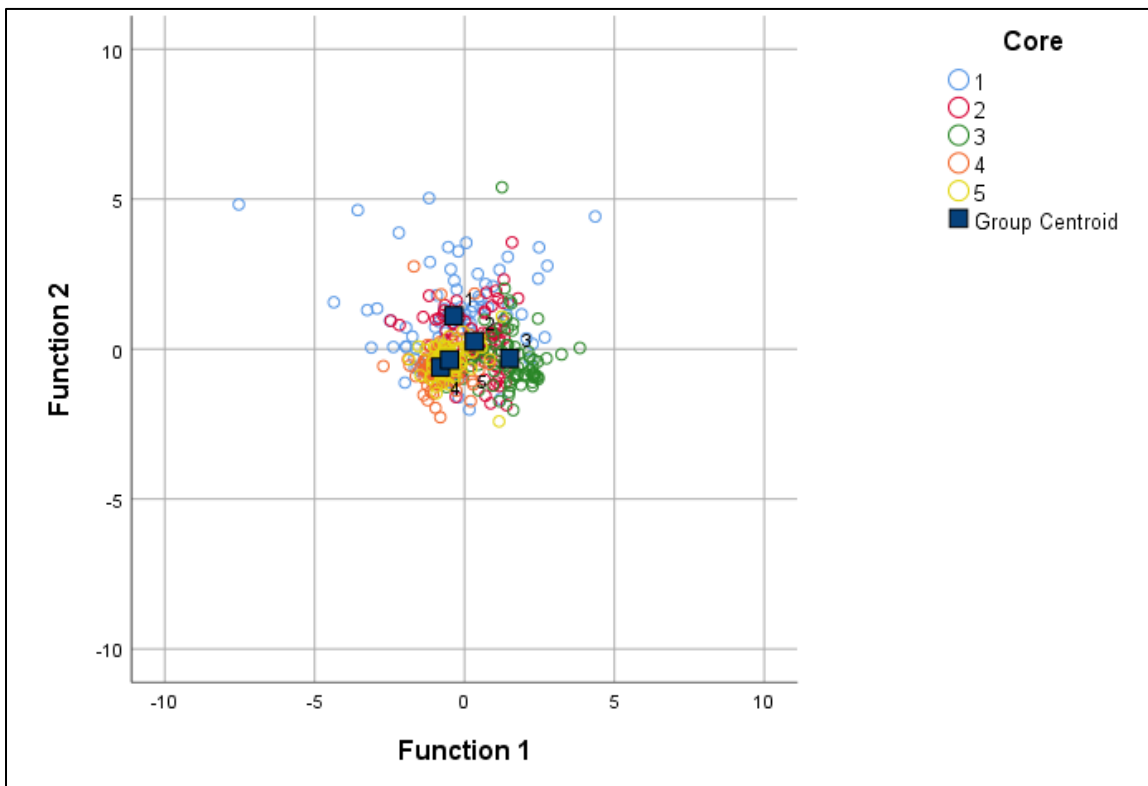
Figure 5.23 Discriminant function plot of nearshore sediment cores.

5.2.2 Inter-core *t*-tests

 T-tests were used to further explain the discriminant function results. Independent

sample *t*-tests discern differences between two groups (cores). As previously revealed,

Cores 4 and 5 are statistically similar, and a *t*-test with the predictors from Core 4 and

Core 5 indicates how (i.e., sedimentary variables) they are similar. *T*-test results for Cores

4 and 5 are reported in Table 5.12. The significance value from Levene's Test for

Equality of Variances was used to test the null hypothesis and determine if group

variances are equal. If Levene's test is less than 0.05, then the null hypothesis is rejected

and equal variances are not assumed. A *t*-test significance value is then selected when

assumed equal variance has been determined. If equal variance is assumed for a predictor

variable, then the top value of 2-tailed significance is used. If equal variance is not

assumed, then the bottom value is used. Between Cores 4 and 5, the differences are in the

coarser fraction particle percentiles and $CaCO_3$ content. Table 5.9 reports the *t*-test results

for Cores 1 and 4. These two cores are significantly different for all predictor variables,

except Dx (84) and Dx (90) where results of the *t*-test fail to reject the null hypothesis.

Table 5.8 reports *t*-test results for Cores 1 and 3. $CaCO_3$ content is the only predictor

variable where results of the test fail to reject the null hypothesis. All other predictor

variables are not statistically similar. This is supported in the function plot in Figure 5.22

where the cores' function centroids are farthest apart. Table 5.10 reports *t*-test results for

Cores 2 and 4. These cores have significance values below 0.05 for Dx (10), Dx (16), Dx

(25), OM content, and $CaCO_3$ content, therefore, there is no statistical similarity in those

predictor variables and the null hypothesis is rejected. Table 5.11 reports *t*-test results for

Cores 3 and 5. These two cores are statistically different for every predictor variable

except Dx (90) and calcium carbonate.

Table 5.8 Independent sample *t*-tests for Cores 1 and 3.

		Levene's Test for Equality of Variances	t-test for Equality of Means	
		Sig.	t	Sig. (2-tailed)
Dx (10)avg	Equal variances assumed	0	9.777	0
	Equal variances not assumed		9.886	0
Dx (16)avg	Equal variances assumed	0	10.163	0
	Equal variances not assumed		10.262	0
Dx (25)avg	Equal variances assumed	0.001	10.381	0
	Equal variances not assumed		10.473	0
Dx (50)avg	Equal variances assumed	0.001	10.349	0
	Equal variances not assumed		10.428	0
Dx (75)avg	Equal variances assumed	0	8.75	0
	Equal variances not assumed		8.789	0
Dx (84)avg	Equal variances assumed	0.031	6.956	0
	Equal variances not assumed		6.971	0
Dx (90)avg	Equal variances assumed	0.315	5.925	0
	Equal variances not assumed		5.93	0
OM LOI % by weight (g)	Equal variances assumed	0	-2.84	0.005
	Equal variances not assumed		-2.866	0.005
$CaCO_3$ LOI % by weight (g)	Equal variances assumed	0	-0.573	0.567
	Equal variances not assumed		-0.58	0.563

Table 5.9 Independent sample *t*-tests for Cores 1 and 4.

		Levene's Test for Equality of Variances	t-test for Equality of Means	
		Sig.	t	Sig. (2-tailed)
Dx (10)avg	Equal variances assumed	0	2.89	0.004
	Equal variances not assumed		2.67	0.009
Dx (16)avg	Equal variances assumed	0	3.791	0
	Equal variances not assumed		3.493	0.001
Dx (25)avg	Equal variances assumed	0	4.502	0
	Equal variances not assumed		4.158	0
Dx (50)avg	Equal variances assumed	0	5.38	0
	Equal variances not assumed		5.069	0
Dx (75)avg	Equal variances assumed	0.878	2.73	0.007
	Equal variances not assumed		2.767	0.006
Dx (84)avg	Equal variances assumed	0.609	1.672	0.096
	Equal variances not assumed		1.699	0.091
Dx (90)avg	Equal variances assumed	0.481	1.283	0.201
	Equal variances not assumed		1.304	0.194
OM LOI % by weight (g)	Equal variances assumed	0	3.546	0.001
	Equal variances not assumed		3.224	0.002
$CaCO_3$ LOI % by weight (g)	Equal variances assumed	0	2.769	0.006
	Equal variances not assumed		2.559	0.012

Table 5.10 Independent sample *t*-test for Cores 2 and 4.

		Levene's Test for Equality of Variances	t-test for Equality of Means	
		Sig.	t	Sig. (2-tailed)
Dx (10)avg	Equal variances assumed	0	-5.22	0
	Equal variances not assumed		-5.104	0
Dx (16)avg	Equal variances assumed	0	-3.827	0
	Equal variances not assumed		-3.731	0
Dx (25)avg	Equal variances assumed	0	-2.867	0.005
	Equal variances not assumed		-2.806	0.006
Dx (50)avg	Equal variances assumed	0.017	-1.112	0.267
	Equal variances not assumed		-1.103	0.271
Dx (75)avg	Equal variances assumed	0.887	-0.497	0.62
	Equal variances not assumed		-0.499	0.618
Dx (84)avg	Equal variances assumed	0.692	-1.143	0.254
	Equal variances not assumed		-1.148	0.252
Dx (90)avg	Equal variances assumed	0.634	-0.985	0.326
	Equal variances not assumed		-0.987	0.325
OM LOI % by weight (g)	Equal variances assumed	0.202	14.448	0
	Equal variances not assumed		14.393	0
$CaCO_3$ LOI % by weight (g)	Equal variances assumed	0.713	5.157	0
	Equal variances not assumed		5.273	0

Table 5.11 Independent sample *t*-test for Cores 3 and 5.

		Levene's Test for Equality of Variances	t-test for Equality of Means	
		Sig.	t	Sig. (2-tailed)
Dx (10)avg	Equal variances assumed	0.048	-16.617	0
	Equal variances not assumed		-16.783	0
Dx (16)avg	Equal variances assumed	0.099	-14.859	0
	Equal variances not assumed		-14.741	0
Dx (25)avg	Equal variances assumed	0	-13.167	0
	Equal variances not assumed		-12.945	0
Dx (50)avg	Equal variances assumed	0	-9.247	0
	Equal variances not assumed		-9.032	0
Dx (75)avg	Equal variances assumed	0.137	-3.96	0
	Equal variances not assumed		-3.924	0
Dx (84)avg	Equal variances assumed	0.073	-2.342	0.02
	Equal variances not assumed		-2.32	0.022
Dx (90)avg	Equal variances assumed	0.054	-1.64	0.103
	Equal variances not assumed		-1.623	0.107
OM LOI % by weight (g)	Equal variances assumed	0	13.576	0
	Equal variances not assumed		13.081	0
$CaCO_3$ LOI % by weight (g)	Equal variances assumed	0	1.727	0.086
	Equal variances not assumed		1.738	0.085

Table 5.12 Independent sample *t*-tests for Cores 4 and 5.

		Levene's Test for Equality of Variances	t-test for Equality of Means	
		Sig.	t	Sig. (2-tailed)
Dx (10)avg	Equal variances assumed	0.697	0.057	0.955
	Equal variances not assumed		0.057	0.955
Dx (16)avg	Equal variances assumed	0.775	0.015	0.988
	Equal variances not assumed		0.015	0.988
Dx (25)avg	Equal variances assumed	0.852	0.367	0.714
	Equal variances not assumed		0.368	0.713
Dx (50)avg	Equal variances assumed	0.051	1.423	0.157
	Equal variances not assumed		1.463	0.146
Dx (75)avg	Equal variances assumed	0	2.653	0.009
	Equal variances not assumed		2.751	0.007
Dx (84)avg	Equal variances assumed	0	3.214	0.002
	Equal variances not assumed		3.312	0.001
Dx (90)avg	Equal variances assumed	0.001	3.243	0.001
	Equal variances not assumed		3.326	0.001
OM LOI % by weight (g)	Equal variances assumed	0.045	-1.974	0.05
	Equal variances not assumed		-1.957	0.052
$CaCO_3$ LOI % by weight (g)	Equal variances assumed	0	-4.369	0
	Equal variances not assumed		-4.241	0

CHAPTER VI – DISCUSSION

6.1 Transgressive estuarine nearshore sedimentary profile

The primary objective of this study is to determine if there is an identifiable

clastic sedimentary profile for actively eroding microtidal estuarine shorelines along the

transgressing Gulf Coastal Plain. To answer this question, nearshore sediment layers

from cores are compared to onshore borehole sediment samples to test one hypothesis of

the study that postulates the source of nearshore sediment is from the adjacent eroding

shoreline sand. Additionally, sediment from subaqueous bottom samples are analyzed

with nearshore sediment layers from cores to develop other possible correlations.

6.1.1 Bon Secour Bay sediment sample correlations

Statistically, Dx (50) particle size and OM content are two predictor variables that

control the discriminant analysis functions presented in Section 5.2. The Dx (50) curve

for BSB-C-01-1 in Figure 5.4 exhibits a semi-homogenous particle size throughout the

core, ranging from medium to coarse sand with infrequent occasions of very fine and

very coarse sand. BSB-C-01-1 contains less than 2% organic matter on average. Onshore

borehole samples from BSB-PZ-01-1, which is the nearest to the BSB-C-01-1 core

location, are coarse sand for the top 52 cm and contain less than 2% organic matter on

average. Based on these two parameters (Dx (50) and OM content), it is hypothesized

that proximal shoreline sediment is being eroded at this location and deposited into the

nearshore zone.

Nearshore sediment core BSB-C-01-2 is in deeper water further offshore from

BSB-C-01-1. The Dx (50) particle size for the more distal core is finer compared to BSB-

C-01-1 and the sandy top portion of BSB-PZ-01-1. This is to be expected as the second

core location is closer to the muddy central basin than the first. Organic content for BSB-C-01-2 is around 1% on average. Examining bottom sediment samples, Sample #16 is at a water depth of 0.86 m and is closest to BSB-C-01-2. Sample #16 has a medium sand Dx (50) and organic content of 0.7%, which is a closer sedimentological match to the entire core of BSB-C-01-2 than BSB-PZ-01-1 sediment is to the core. BSB-C-01-2 sediment is nevertheless comparable to the onshore borehole sediments, and the fining is attributed to transport from a high energy coastline to a lower energy basin environment.

Core BSB-C-01-3 (Fig. 5.5) and onshore borehole BSB-PZ-01-2 (Fig. 5.11) are closely positioned. When comparing their Dx (50), the onshore sediments are coarser than core sediments. BSB-C-01-3 Dx (50) is mostly fine sand throughout, whereas the borehole sediment is medium to coarse until a depth of around 80 cm. OM is approximately 1.5% on average for BSB-C-01-3 and 1% for BSB-PZ-01-2 until the sharp sand-OM contact at 82 cm. As with the previous cores, sediment fining is expected along the higher-to lower-energy gradient. However, a direct correlation between onshore borehole sediment to core sediment at this location is not well supported by the data. The closest sedimentological match for BSB-C-01-3 would be bottom Sample #2 from a water depth of 0.94 m that has a fine sand Dx (50) and OM content of 0.9%. Similar particle-size characteristics are shared with bottom samples collected further from shore (i.e. #4 and #13), but OM content is greater in these deeper samples. The borehole located in the forested swamp area, BSB-PZ-01-3, is not considered as a possible direct sediment source and is therefore not included here.

6.1.2 Perdido Bay sediment sample correlations

Statistical tests reveal that the Perdido Bay nearshore sediment cores (Cores 4 and 5) are the most similar of all five cores. One onshore borehole at Perdido Bay is used with Perdido Bay bottom sediment samples to compare Dx (50) and OM results with PB-C-02-1 and PB-C-02-2. PB-C-02-1 is dominantly medium sand throughout with sporadic increments of fine and coarse sand. PB-C-02-2 is also dominantly medium sand throughout with few very fine sand layers. Both cores have less than 1% OM on average. The Dx (50) for onshore borehole PB-PZ-02-1 is comprised of medium to coarse sand with some very fine sand around 50 cm depth. Organic content in PB-PZ-02-1 is less than 1% in the top 30 cm followed by a spike to 18.1% at 47 cm, and then returns to below 5% for the remaining depth of the borehole. Between the cores and the onshore borehole, the Dx (50) particle size indicates that onshore sand is likely the source of nearshore sand in the cores. This is further supported because the first 30 cm lacks any appreciable amounts of organic matter, and therefore not sourced from the deeper estuary basin. Bottom sediment samples in PB are similarly fine to medium, well to normally sorted sand with few very fine and coarse occurrences as seen nearshore core sediment. Save for the deepest bottom samples collected at the basin shelf margin, OM and calcium carbonate content in bottom samples is at or below 1%, which is similar to the abundance found in nearshore core sediment.

6.2 Down-core trends

When analyzing for down-core trends, BSB-C-01-1 and BSB-C-01-3 show sedimentological evidence of a possible ravinement surface toward the bottom of each core. These two cores are both approximately 60 m offshore in less than one meter of

water. As previously stated, there was difficulty in physically maneuvering the coring device through the sediment, so encountering a surface that is characteristically coarse-grained and contains hard organic matter hash would explain the relatively shallow depths for each core (78 and 76 cm, respectively). The presence of medium to coarse sand, shell and wood fragments, and coal-peat like matter (especially abundant in BSB-C-01-3) at the base of these two cores suggests a once high-energy subaerial environment that has been buried during a transgressive cycle.

BSB-C-01-2 exhibits coarsening with depth (or fining upwards) and a decrease in sorting quality in the last ~15 cm which could possibly be indicative of a facies change from higher energy to lower energy, however the core lacks organic and shell matter in the bottom portion that was present in the previous two cores. This does not preclude the existence of a ravinement surface in BSB-C-01-2, but it is not as strongly supported as the other BSB cores.

PB-C-02-1 core changes very little sedimentologically with depth. This was the deepest core, and perhaps the lack of coarse particles and accessories in the core made the high recovery amount possible.

PB-C-02-2 is well sorted with a Dx (50) that stays between fine to medium size sand throughout the depth of the core and has an occurrence of shell and wood material at the base of the core around 75 cm. The lack of coarse particles at the bottom of the core with the presence of the organic material does not strongly represent or suggest a facies change, but does not eliminate the possibility. The same is true for the absence of a trend towards finer grain or any other trend change with depth for the sedimentological parameters analyzed.

110

6.3 Sedimentological variability of eroding microtidal estuarine shorelines

Sedimentological variability of nearshore sediment cores from Bon Secour Bay and Perdido Bay could indicate the influence of basin size (i.e., fetch) and fluvial inputs. However, after statistical analysis, the strongest longitudinal variation occurs within cores from the same estuary (Figure 5.23), not between estuaries as predicted. In Bon Secour Bay, cores BSB-C-01-1 and BSB-C-01-3 share no significant similarities, except $CaCO_3$ content which is not a strong predictor variable as defined by canonical functions (Table 5.7). Both cores are located equidistant from the shoreline and are 1.2 km apart. BSB-C-01-1 is coarser by one degree of magnitude and contains 0.5% less OM than BSB-C-01-3. Nearshore sediment reworking and mixing from storm events could be a possible explanation for the variation. Also, the cores are only local samples of a larger body, and they are not complete representations of the sedimentology along the dynamic shoreline.

There is less extreme, but nevertheless significant variation between the Perdido Bay and Bon Secour Bay cores as two separate groups. According to the functions plot in Figure 5.23, sedimentological variation of PB cores and BSB cores is strongest with predictor variables Dx (10), Dx (16), Dx (25), Dx (50), and OM %. Bon Secour Bay cores are overall coarser and contain slightly more organic matter content than the PB cores. The greater estuarine size and therefore more energetic conditions can be the reason for coarser-grained particles in BSB cores. The increased organic matter content could be attributed to the larger fluvial input to the Mobile Bay estuary. Cores from BSB have layers of silt and Dx (50) for PB cores does not go below very fine sand, which does not support the earlier stated hypothesis that expects a similar sand to mud abundance between the cores. Again, the reason for this could be the greater amount of fluvial

influence to Mobile Bay transporting more silt than the streams contributing to Perdido

Bay. The sandier beach environment of Perdido Bay produces coarser core sediment due

to the regional geology lacking fine-grained strata as compared to Bon Secour Bay.

6.4 Hydrologic response and erosional contribution of shallow groundwater tables

Piezometer sensors that monitored shallow groundwater table fluctuation indicate

that levels respond readily to precipitation events. Daily average plots display rapid

increases in groundwater levels followed by a less rapid recession. In context with the

sandy shoreline environments, erosion has occurred at BSB-PZ-1-1 (Figure 5.22). Figure

5.22 A and B were at the same location six months apart. During a precipitation event,

enough rainfall had infiltrated and caused a rapid water table rise, followed by a slow

recession even though bank sediments are highly permeable. The drainage channel

incision likely formed around the same time of this precipitation event. The proximity of

sea level inhibits percolation, therefore a likely reason for the slow recession of

groundwater. This supports the hypothesis that coastal erosion is exacerbated when

groundwater tables rise in a sandy environment. The slope of a bank influences its

tendency to erode. The shoreline at Perdido Bay is a slightly lower slope than Bon Secour

Bay and has not experienced the same erosion with fluctuating groundwater tables. Also,

groundwater response at PB spans a smaller range in level compared to BSB which could

also be a reason for the slower erosion rates observed at Perdido Bay.

6.5 Shoreline erosion rate

Short-term (~1 year) erosion rates along Bon Secour Bay are highly variable

based on erosion pin measurements (Figure 5.21). All four pins experienced episodes of

erosion and deposition. Observations from May 2018 to November 2019 indicate net

erosion occurred only at pin 3 with a rate of -0.8 cm/month (-9.7 cm yr^{-1}). From May 2018 to November 2019 net deposition occurred at pin 2 at a rate of 0.1 cm/month (1.3 cm yr^{-1}), and at pin 4 at a rate of 0.06 cm/month (0.7 cm yr^{-1}). Erosion pin 1 washed away, but data available from May 2018 to November 2018 indicate an erosion rate of -0.5 cm/month (-6 cm yr^{-1}). These results are supported by previous work that finds erosion does not occur at every point along a coastline (Bache et al., 2014). Short-term erosion rates are much slower when compared with long-term rates determined by aerial imagery. A plausible reason for this is because erosion rates determined from historical aerial imagery were measured using only the high-tide water line in planform as a proxy for erosion where the erosion pins measured a vertical change in shoreline. It is a combination of erosion and rising sea level that results in the faster shoreline retreat rate when examining long-term changes. Additionally, long-term rates capture more events and larger events that result in the faster rate of erosion than a shorter period that did not capture any significant storm and erosion events. The erosion to shoreline retreat rate is not one-to-one. Presumably a shoreline can retreat one meter in planform, while only having a few centimeters in vertical erosion. Erosion pins are useful to measure local erosion and deposition but fail to include rising sea level that also attributes to land loss.

CHAPTER VII – CONCLUSION

Results from this study have found that eroded shoreline sediments can be identified in the adjacent nearshore zone of microtidal, clastic estuaries. Nearshore sediment core variables closely compare with beach surface sediment statistically and experimentally. Therefore, identifying a sedimentary signature of an eroding estuarine shoreline is possible, however deeper coring depths (>1 m) are required to constrain the boundary. Nearshore facies are a range of sediment types with varying proportions of sand and silt representative of the transitional environment between the central estuarine basin and the beach. Sand-sized particles are from the proximal eroding shoreline and winnowing of finer grained material occurs by wave activity.

All cores in this study were less than one meter in sediment depth and are comprised of nearshore facies as described by Hummell (1996). Two cores: BSB-C-01-1 and BSB-C-01-3 show the strongest sedimentological evidence of possible ravinement surfaces toward the bottom of each core. Two cores: BSB-C-01-2 and PB-C-02-2, primarily homogenous throughout, however might suggest a facies change with a ravinement surface at the bottom of each core given the sedimentology. Finally, core PB-C-02-1 is sedimentologically uniform and does not show any trends that would suggest a change in facies with depth.

Nearshore sediments from Perdido Bay and Bon Secour Bay are distinctively different based on predictor variables Dx (10), Dx (16), Dx (25), Dx (50), and OM %. Bon Secour Bay cores are overall coarser and contain more organic matter content than the Perdido Bay cores, which is likely because of energy associated with the greater size (i.e., fetch) of Bon Secour Bay and inputs of organic matter from its large fluvial system.

114

Shallow groundwater levels responded rapidly during precipitation events and likely contribute to sandy shoreline destabilization and erosion as observed at Bon Secour Bay. Further monitoring of groundwater levels and short-term erosion is necessary for more conclusive evidence.

Short-term erosion pins measurements indicated episodes of local erosion and deposition, are highly variable from month to month, and do not account for longer-term sea level rise. Erosion pins as indicators of long-term erosion rates only account for one portion of the land-loss equation and reflect slower erosion rates (< 10 cm yr^{-1}) than long-term rates determined from aerial imagery (> 50 cm yr^{-1}).

Future expansion on this research would benefit to include making additional nearshore cores in the Bon Secour Bay and Perdido Bay to further investigate and map a shallow unlithified ravinement surface. Cores that reach one meter or more in depth would be ideal for capturing deep enough sediment for this analysis. Radiometric dating of organic material found in nearshore core sediment could aid in constraining the time of deposition of the postulated ravinement surface, but may be unlikely due to the amount of available oxygen in the sediment. Also, examining for microscopic and macroscopic fossils or biologic material could help identify a specific environment and timing of deposition.

APPENDIX A – Sediment Analyses Tables

Table A.1 Sedimentary analysis results for BSB-C-01-1.

Depth (cm)	Dx (10)	Dx (16)	Dx (25)	Dx (50)	Dx (75)	Dx (84)	Dx (90)	OM LOI %	CaCO₃ LOI %	MS
1	89	126	163	248	354	411	465	0.0	1.9	0.14
2	194	220	255	349	483	567	678	0.0	0.0	0.14
3	203	231	268	366	497	569	638	0.0	0.0	0.14
4	136	209	287	421	571	649	720	0.0	0.0	0.14
5	18	29	50	153	293	368	439	0.0	0.0	0.14
6	24	37	63	168	302	372	438	1.9	0.0	0.42
7	125	169	216	328	474	556	635	0.0	0.0	0.42
8	10	16	26	78	196	316	462	0.0	1.4	0.42
9	195	230	271	373	503	573	638	0.0	2.2	0.42
10	100	141	185	297	457	556	663	0.0	0.0	0.42
11	129	157	193	289	440	544	672	0.0	0.0	0.47
12	128	187	247	506	1084	1393	1642	0.0	0.0	0.47
13	27	52	90	155	214	242	266	2.4	0.0	0.47
14	85	114	147	229	338	399	458	0.0	0.0	0.47
15	41	116	181	306	486	622	766	2.1	0.0	0.47
16	93	165	241	444	874	1156	1433	0.0	2.1	0.09
17	20	41	93	214	487	664	819	2.2	0.0	0.09
18	28	52	107	275	575	804	1013	1.9	0.0	0.09
19	150	210	251	337	434	483	527	0.0	0.0	0.09
20	129	161	204	337	842	1045	1219	2.6	0.0	0.09
21	53	77	103	160	245	295	339	0.0	0.0	0.47
22	172	205	252	389	584	717	920	0.0	0.0	0.47
23	224	279	359	603	1075	1357	1648	1.3	0.0	0.47
24	200	232	274	394	569	683	809	1.2	0.0	0.47
25	179	207	247	408	1088	1481	1881	0.0	0.0	0.47
26	226	274	344	553	851	1032	1219	1.2	0.0	0.75
27	578	648	743	1002	1355	1549	1738	1.1	0.0	0.75
28	300	342	397	546	741	847	948	1.4	0.0	0.75
29	245	319	422	700	1072	1297	1519	1.0	0.0	0.75
30	95	126	165	260	373	431	484	0.0	0.0	0.75
31	254	323	407	620	896	1055	1212	1.0	1.0	0.16
32	218	262	321	502	940	1357	1639	0.0	0.0	0.16
33	309	403	531	891	1432	1764	2081	0.0	1.2	0.16
34	364	412	474	637	841	952	1059	0.0	0.0	0.16
35	280	305	338	423	525	577	623	6.2	0.0	0.16
36	323	357	400	531	1002	1165	1301	0.0	0.0	0.22
37	869	940	1027	1259	1552	1714	1860	0.0	0.0	0.22
38	308	353	416	606	926	1152	1401	0.0	0.0	0.22
39	310	350	403	551	750	862	967	0.0	2.6	0.22
40	178	217	269	429	907	1287	1603	4.2	0.0	0.22
41	294	327	372	494	675	802	993	0.0	0.0	0.26

Depth (cm)	Dx (10)	Dx (16)	Dx (25)	Dx (50)	Dx (75)	Dx (84)	Dx (90)	OM LOI %	CaCO₃ LOI %	MS
42	258	300	360	533	777	915	1045	0.0	0.0	0.26
43	250	284	331	468	666	784	912	0.0	0.0	0.26
44	154	185	224	339	522	640	762	0.0	0.0	0.26
45	236	279	340	570	1212	1538	1881	3.4	0.0	0.26
46	174	212	258	376	531	619	706	0.0	1.8	0.39
47	196	225	264	370	517	603	689	1.5	0.0	0.39
48	221	254	303	463	763	965	1177	1.3	0.0	0.39
49	218	255	310	504	842	1061	1290	1.4	0.0	0.39
50	215	251	299	430	612	716	815	0.0	0.0	0.39
51	216	247	288	404	573	675	776	0.0	0.0	0.17
52	192	225	268	386	550	649	756	1.5	0.0	0.17
53	196	237	295	462	670	781	884	2.1	0.0	0.17
54	224	265	317	457	644	748	847	1.0	0.0	0.17
55	510	551	607	747	920	1017	1105	0.0	0.0	0.17
56	213	240	275	369	498	577	671	0.0	0.0	0.56
57	208	238	277	378	511	584	653	0.0	2.7	0.56
58	162	190	223	312	429	494	555	2.3	0.0	0.56
59	199	227	263	360	489	563	635	0.0	2.0	0.56
60	134	163	197	286	402	468	532	2.6	0.0	0.56
61	427	467	520	653	815	899	979	2.3	0.0	1.13
62	234	275	328	476	676	786	890	0.0	0.0	1.13
63	225	268	325	486	726	882	1055	2.2	0.0	1.13
64	396	440	498	655	859	970	1076	0.0	0.0	1.13
65	239	289	352	520	746	872	992	2.0	0.0	1.13
66	208	284	387	646	1163	1499	1762	0.9	0.5	0.70
67	159	204	256	393	609	784	996	1.6	0.2	0.70
68	182	231	287	434	627	735	839	0.0	0.3	0.70
69	171	214	263	387	551	648	756	1.3	0.5	0.70
70	515	572	635	797	1008	1130	1256	1.8	0.2	0.70
71	180	223	274	406	592	707	855	0.6	0.0	0.48
72	132	189	259	447	1080	1392	1644	2.6	1.3	0.48
73	214	253	302	437	624	729	827	1.5	0.5	0.48
74	190	239	293	422	579	663	738	0.0	1.1	0.48
75	132	189	252	453	969	1334	1668	1.0	0.0	0.48
76	84	153	205	324	483	576	667	0.0	0.0	1.71
77	71	131	183	333	711	891	1062	1.7	0.0	1.71
78	53	85	131	238	351	407	457	0.0	0.0	1.71

Note: Percentiles are in microns. OM and CaCO₃ percentages are from weight. Magnetic susceptibility (MS) is $* 10^8$ m^3 kg^{-1}.

Table A.2 Sedimentary analysis results for BSB-C-01-2.

Depth (cm)	Dx (10)	Dx (16)	Dx (25)	Dx (50)	Dx (75)	Dx (84)	Dx (90)	OM LOI %	CaCO₃ LOI %	MS
1	113	142	179	277	402	478	579	1.2	0.3	0.85
2	63	96	131	201	276	314	348	0.8	0.0	0.85
3	37	62	104	175	244	277	307	0.7	0.4	0.85
4	82	115	149	221	304	346	384	1.1	0.0	0.85
5	124	147	173	234	306	341	374	0.7	0.0	0.85
6	149	167	191	251	324	360	393	0.9	0.0	0.31
7	152	179	210	289	383	431	475	0.7	0.2	0.31
8	139	169	204	293	414	497	704	0.8	0.2	0.31
9	176	219	271	414	956	1316	1593	0.5	0.2	0.31
10	123	147	177	249	335	379	420	0.7	0.4	0.31
11	140	169	201	279	372	420	465	1.0	0.2	0.30
12	217	245	282	379	505	572	635	0.8	0.3	0.30
13	237	279	326	439	575	646	709	0.6	0.4	0.30
14	196	253	319	470	651	748	844	0.4	0.2	0.30
15	125	161	199	288	397	455	508	0.7	0.2	0.30
16	84	136	193	398	671	794	903	0.5	0.5	0.25
17	150	177	210	291	389	441	489	0.4	0.4	0.25
18	71	110	150	236	326	372	414	0.7	0.2	0.25
19	71	116	161	252	361	423	488	0.6	0.3	0.25
20	55	104	157	246	342	391	435	0.7	0.4	0.25
21	204	248	300	521	737	853	974	0.7	0.2	0.29
22	68	119	164	254	368	435	503	0.9	0.2	0.29
23	94	136	164	221	283	314	342	0.6	0.3	0.29
24	157	183	214	291	384	433	487	0.7	0.2	0.29
25	29	49	92	194	303	359	412	0.5	0.0	0.29
26	57	102	154	259	393	472	562	0.8	0.4	0.53
27	50	142	237	388	646	901	1378	0.8	0.4	0.53
28	23	38	64	140	665	823	1159	0.9	0.4	0.53
29	22	34	61	175	559	743	905	0.9	0.4	0.53
30	240	297	353	499	1058	1315	1741	0.7	0.2	0.53
31	44	103	145	216	286	326	361	0.7	0.2	0.26
32	94	157	204	324	455	529	593	0.6	0.3	0.26
33	48	78	141	281	414	486	566	0.8	0.4	0.26
34	60	144	208	322	468	546	607	0.6	0.4	0.26
35	177	208	239	324	453	845	1140	0.7	0.4	0.26
36	136	165	195	265	349	392	432	0.8	0.2	0.37
37	24	41	85	218	1381	1741	2076	0.8	0.4	0.37
38	127	162	197	277	374	427	480	0.9	0.2	0.37
39	139	176	211	291	387	439	489	0.8	0.4	0.37
40	78	152	201	297	408	465	517	0.9	0.2	0.37
41	45	98	149	214	280	312	347	1.1	0.2	0.20
42	39	62	100	199	564	828	992	1.2	0.4	0.20
43	55	96	144	254	573	770	1125	1.1	0.4	0.20

Depth (cm)	Dx (10)	Dx (16)	Dx (25)	Dx (50)	Dx (75)	Dx (84)	Dx (90)	OM LOI %	CaCO₃ LOI %	MS
44	86	149	207	330	518	667	889	1.2	0.4	0.20
45	314	358	410	547	729	839	963	0.9	0.4	0.20
46	230	265	312	490	1025	1192	1345	0.8	0.4	0.25
47	143	180	222	431	1236	1513	1790	1.0	0.2	0.25
48	96	142	180	269	391	469	563	0.8	0.5	0.25
49	96	141	182	282	452	844	1099	0.9	0.2	0.25
50	159	187	217	300	484	899	1452	0.7	0.4	0.25
51	114	150	185	273	396	650	870	0.8	0.3	0.18
52	65	114	167	308	1162	1463	1917	0.9	0.4	0.18
53	61	119	168	271	698	917	1090	0.8	0.3	0.18
54	46	80	139	247	353	408	459	1.0	0.4	0.18
55	30	48	83	177	272	321	367	1.1	0.2	0.18
56	215	252	293	396	518	584	644	0.8	0.2	0.15
57	14	21	36	106	182	224	270	0.5	0.2	0.15
58	25	40	74	160	244	283	326	0.9	0.2	0.15
59	175	215	248	329	427	485	539	0.6	0.2	0.15
60	22	37	62	163	272	326	376	0.7	0.2	0.15
61	25	50	91	245	447	616	821	0.7	0.3	0.02
62	156	212	249	331	428	477	522	0.8	0.2	0.02
63	133	168	197	283	599	864	1074	0.7	0.2	0.02
64	239	285	326	434	564	636	715	0.9	0.2	0.02
65	187	233	281	404	556	643	734	0.8	0.0	0.02
66	246	288	343	466	625	708	789	1.1	0.0	0.10
67	10	14	20	35	52	60	68	1.1	0.2	0.10
68	20	29	61	151	221	255	286	1.0	0.0	0.10
69	118	157	182	237	305	339	370	0.8	0.2	0.10
70	29	77	179	251	321	355	386	0.9	0.2	0.10
71	197	221	251	329	423	473	520	1.0	0.2	0.09
72	37	85	150	274	755	943	1114	0.9	0.4	0.09
73	118	195	243	335	436	490	541	0.9	0.4	0.09
74	33	72	131	262	746	959	1168	1.0	0.2	0.09
75	111	150	185	280	455	623	929	0.8	0.2	0.09
76	55	118	177	332	1153	1473	1733	1.0	0.2	0.32
77	185	208	244	352	921	1272	1545	0.8	0.2	0.32
78	81	170	228	340	515	682	1894	1.4	0.0	0.32
79	16	25	41	174	249	284	315	0.9	0.0	0.32
80	226	263	308	429	577	658	734	0.9	0.3	0.32
81	81	154	207	321	449	532	618	1.0	0.2	0.14
82	38	69	160	302	855	1264	1582	0.9	0.5	0.14
83	340	372	415	537	948	1136	1288	0.9	0.2	0.14
84	21	30	64	583	1677	1981	2268	0.9	0.2	0.14
85	385	417	458	570	729	841	1010	0.6	0.2	0.14
86	153	216	261	387	666	875	1071	0.7	0.2	0.20
87.5	54	129	186	676	1360	1591	1798	0.7	0.2	0.20

Note: Percentiles are in microns. OM and CaCO₃ percentages are from weight. Magnetic susceptibility (MS) is $* 10^8 \, m^3 \, kg^{-1}$.

Table A.3 Sedimentary analysis results for BSB-C-01-3.

Depth (cm)	Dx (10)	Dx (16)	Dx (25)	Dx (50)	Dx (75)	Dx (84)	Dx (90)	OM LOI %	CaCO₃ LOI %	MS
1	147	169	197	271	387	649	886	1.2	0.2	0.41
2	166	188	216	293	616	1225	1571	1.1	0.0	0.41
3	157	180	208	287	410	551	1383	0.6	0.2	0.41
4	150	172	200	278	389	450	510	0.7	0.2	0.41
5	54	94	127	186	248	279	306	1.4	0.0	0.41
6	45	76	118	197	282	325	365	0.9	0.3	0.11
7	34	53	84	164	241	278	312	1.8	0.2	0.11
8	48	77	108	175	255	298	337	0.8	0.3	0.11
9	95	125	153	216	289	326	360	1.1	0.0	0.11
10	39	63	94	172	331	719	921	1.1	0.0	0.11
11	80	110	140	209	293	337	377	0.7	0.1	0.01
12	89	123	157	231	319	365	408	0.3	0.6	0.01
13	50	86	139	227	320	369	414	0.9	0.0	0.01
14	116	140	169	240	332	385	441	0.2	0.4	0.01
15	78	119	161	241	342	395	448	0.7	0.4	0.01
16	59	102	147	229	319	365	407	0.5	0.3	-0.04
17	53	103	169	543	1066	1342	1591	0.7	0.3	-0.04
18	34	53	86	165	249	291	338	1.1	0.5	-0.04
19	32	50	79	163	269	373	556	1.0	0.5	-0.04
20	111	163	209	319	477	578	682	0.8	0.5	-0.04
21	56	136	175	250	333	376	427	1.3	0.0	0.34
22	47	82	153	256	351	397	437	1.6	0.0	0.34
23	75	123	167	255	358	421	479	0.6	0.6	0.34
24	45	74	122	215	320	375	425	1.0	0.3	0.34
25	58	103	155	245	348	400	450	0.8	0.3	0.34
26	102	149	193	292	522	1174	1500	0.9	0.3	0.77
27	82	132	172	257	366	433	537	1.4	0.0	0.77
28	32	47	75	167	260	305	345	1.1	0.4	0.77
29	48	78	126	209	290	329	364	1.1	0.5	0.77
30	34	51	87	196	294	340	382	1.3	0.5	0.77
31	21	33	63	175	267	309	354	1.3	0.2	0.43
32	22	31	48	126	210	246	279	1.2	0.2	0.43
33	23	33	51	123	196	231	261	1.2	0.3	0.43
34	56	99	210	334	451	520	581	1.2	0.5	0.43
35	26	38	60	163	293	353	410	1.5	0.7	0.43
36	55	98	159	308	511	768	1079	1.2	0.5	-0.03
37	26	37	55	121	214	261	304	1.1	0.6	-0.03
38	18	26	38	94	449	650	812	1.4	0.5	-0.03
39	37	58	102	237	381	455	524	1.3	0.3	-0.03
40	24	35	52	118	305	758	933	1.1	0.5	-0.03
41	37	80	145	260	374	432	484	1.1	0.2	0.25
42	23	32	46	102	193	251	596	1.1	0.2	0.25
43	31	50	87	216	331	395	449	1.0	0.3	0.25

Depth (cm)	Dx (10)	Dx (16)	Dx (25)	Dx (50)	Dx (75)	Dx (84)	Dx (90)	OM LOI %	CaCO$_3$ LOI %	MS
44	26	37	58	177	1215	1466	1672	1.4	0.3	0.25
45	21	29	44	110	182	215	243	1.2	0.2	0.25
46	46	72	125	246	381	453	521	1.3	0.2	0.37
47	58	103	184	380	922	1313	1801	1.5	0.3	0.37
48	137	299	364	483	611	674	731	1.1	0.3	0.37
49	40	61	111	231	363	645	928	1.1	0.3	0.37
50	128	142	163	275	381	429	474	1.2	0.3	0.37
51	32	49	89	279	833	1297	1599	1.0	0.5	0.18
52	23	31	43	112	190	224	253	1.6	0.3	0.18
53	23	31	46	138	244	287	327	1.2	0.5	0.18
54	19	26	36	89	232	875	1198	1.5	0.5	0.18
55	19	26	36	76	163	473	665	1.9	0.5	0.18
56	20	28	40	195	523	711	1131	2.2	0.3	1.26
57	18	24	35	97	244	334	422	1.8	0.5	1.26
58	23	29	37	66	126	167	209	1.8	0.6	1.26
59	24	38	116	387	709	1014	1234	1.7	0.5	1.26
60	18	24	34	84	176	221	260	2.7	0.4	1.26
61	15	20	27	58	122	163	203	3.4	0.2	1.27
62	16	21	30	77	243	318	395	2.0	0.4	1.27
63	11	15	20	45	122	171	218	1.8	0.7	1.27
64	12	17	24	54	136	185	230	1.8	0.5	1.27
65	11	15	22	61	183	241	289	1.9	0.5	1.27
66	13	19	28	96	238	304	387	1.4	0.4	1.36
67	12	16	24	62	158	209	251	1.7	0.7	1.36
68	12	17	28	101	230	287	335	1.6	0.5	1.36
69	13	19	29	97	247	309	363	1.9	0.3	1.36
70	15	23	36	144	261	310	354	1.7	0.5	1.36
71	17	25	39	129	245	297	343	1.6	0.5	0.99
72	20	29	45	138	285	367	645	1.3	0.5	0.99
73	22	31	48	160	266	313	354	1.7	0.3	0.99
74	18	26	39	119	247	307	366	1.6	0.5	0.99
75	22	32	50	140	264	327	386	1.4	0.2	0.99
76	30	41	65	160	257	307	359	1.4	0.4	0.65

Note: Percentiles are in microns. OM and CaCO$_3$ percentages are from weight. Magnetic susceptibility (MS) is $* 10^8$ m^3 kg^{-1}.

Table A.4 Sedimentary analysis results for PB-C-02-1.

Depth (cm)	Dx (10)	Dx (16)	Dx (25)	Dx (50)	Dx (75)	Dx (84)	Dx (90)	OM LOI %	CaCO₃ LOI %	MS
1	112	144	175	247	334	381	422	0.3	0.1	-0.35
2	170	202	244	378	587	686	777	0.3	0.0	-0.35
3	166	192	221	295	397	682	923	0.3	0.2	-0.35
4	172	192	218	283	364	406	443	0.3	0.4	-0.35
5	160	185	215	290	393	464	755	0.5	0.0	-0.35
6	158	182	212	285	391	657	884	0.3	0.0	-0.41
7	157	181	212	300	485	1148	1451	0.2	0.2	-0.41
8	188	212	242	320	421	474	523	0.2	0.3	-0.41
9	143	171	204	290	587	887	1044	0.3	0.0	-0.41
10	137	171	215	392	1102	1319	1511	0.6	0.0	-0.41
11	188	222	265	385	556	659	765	0.4	0.0	-0.04
12	142	171	204	290	424	874	1043	0.5	0.0	-0.04
13	214	243	286	476	1804	2136	2420	0.5	0.0	-0.04
14	51	78	113	197	333	779	1291	0.3	0.2	-0.04
15	130	164	205	339	1433	1890	2233	1.0	0.0	-0.04
16	138	158	182	246	327	372	414	0.4	0.0	-0.89
17	93	127	168	472	1158	1425	1770	0.4	0.0	-0.89
18	98	149	197	320	1144	1448	1692	0.3	0.1	-0.89
19	153	176	203	274	398	793	945	0.3	0.0	-0.89
20	136	168	200	276	368	416	461	0.4	0.0	-0.89
21	148	182	224	405	771	950	1142	0.3	0.0	-0.38
22	196	219	247	318	405	450	490	0.3	0.0	-0.38
23	139	161	187	257	607	775	910	0.3	0.0	-0.38
24	216	253	474	824	1515	1773	2018	0.3	0.1	-0.38
25	149	167	192	264	682	853	990	0.1	0.1	-0.38
26	151	170	198	281	680	851	990	0.4	0.1	0.00
27	86	123	147	208	303	464	556	0.3	0.0	0.00
28	45	87	217	337	518	601	672	0.3	0.1	0.00
29	86	133	181	290	496	822	994	0.3	0.0	0.00
30	232	254	281	352	440	487	531	0.5	0.0	0.00
31	222	247	279	363	471	530	584	0.4	0.0	0.06
32	203	230	266	370	528	678	998	0.3	0.0	0.06
33	185	207	237	321	486	887	1050	0.4	0.0	0.06
34	205	229	262	352	508	717	900	0.5	0.0	0.06
35	197	221	253	347	761	940	1082	0.6	0.0	0.06
36	183	207	238	326	664	876	1032	0.3	0.1	0.12
37	150	178	213	305	447	607	883	0.6	0.0	0.12
38	110	140	186	706	1620	1939	2201	0.6	0.0	0.12
39	191	213	243	326	454	554	942	0.6	0.0	0.12
40	92	117	145	223	677	1329	1878	0.4	0.0	0.12
41	207	229	258	332	424	471	516	0.4	0.1	-0.40
42	133	161	200	536	1723	2063	2350	0.3	0.1	-0.40
43	185	208	237	313	409	460	509	0.5	0.0	-0.40

Depth (cm)	Dx (10)	Dx (16)	Dx (25)	Dx (50)	Dx (75)	Dx (84)	Dx (90)	OM LOI %	CaCO₃ LOI %	MS
44	203	227	257	338	454	531	847	0.5	0.0	-0.40
45	171	194	223	305	429	640	898	0.3	0.1	-0.40
46	209	232	261	338	434	484	531	0.6	0.0	0.69
47	194	216	246	330	462	570	720	0.5	0.0	0.69
48	201	224	256	348	659	870	1020	0.6	0.0	0.69
49	155	179	208	287	403	721	925	0.4	0.1	0.69
50	92	121	154	248	844	1487	1911	0.4	0.0	0.69
51	228	251	282	365	471	527	578	0.4	0.0	0.13
52	222	246	278	364	480	549	619	0.4	0.0	0.13
53	185	210	247	350	899	1123	1347	0.3	0.1	0.13
54	179	200	229	309	419	484	555	0.3	0.2	0.13
55	170	193	224	303	408	469	536	0.5	0.3	0.13
56	153	179	209	284	373	419	461	0.6	0.0	-0.40
57	196	224	263	374	510	579	641	0.4	0.1	-0.40
58	184	207	237	313	408	457	502	0.5	0.2	-0.40
59	105	131	159	227	343	744	908	0.6	0.0	-0.40
60	158	179	207	288	433	626	789	0.6	0.0	-0.40
61	166	189	218	293	388	440	488	0.5	0.0	-0.37
62	191	216	249	344	487	878	1084	0.4	0.1	-0.37
63	213	237	268	353	468	539	632	0.6	0.0	-0.37
64	149	178	211	294	411	511	804	0.4	0.0	-0.37
65	261	285	314	394	648	908	1048	0.5	0.2	-0.37
66	201	223	252	329	437	524	962	0.5	0.0	-0.08
67	165	186	212	276	354	393	429	0.3	0.1	-0.08
68	209	231	260	340	445	503	557	0.4	0.0	-0.08
69	199	237	286	459	1351	1893	2232	0.6	0.0	-0.08
70	176	196	223	290	373	416	455	0.6	0.0	-0.08
71	163	184	211	278	360	402	439	0.5	0.0	-0.61
72	144	166	191	256	336	377	414	0.6	0.2	-0.61
73	67	90	118	186	261	299	333	0.4	0.1	-0.61
74	131	149	171	227	293	326	357	0.6	0.0	-0.61
75	117	143	171	235	308	345	378	0.4	0.1	-0.61
76	234	257	288	365	465	516	564	0.6	0.0	-0.35
77	181	202	230	304	395	444	488	0.3	0.0	-0.35
78	172	191	217	285	372	419	462	0.5	0.0	-0.35
79	99	144	183	264	353	399	442	0.5	0.2	-0.35
80	151	175	204	286	488	728	883	0.3	0.3	-0.35
81	176	195	220	287	369	413	462	0.5	0.0	0.21
82	57	79	109	178	258	300	338	0.5	0	0.21
83	194	214	239	302	380	420	454	0.4	0	0.21
84	166	188	215	284	370	415	457	0.9	0	0.21
85	185	204	228	290	366	406	443	0.4	1.6	0.21
86	155	184	216	295	391	441	486	0.4	0	-0.31
87	197	221	255	358	750	955	1208	0.4	0.1	-0.31
88	167	192	220	291	377	420	459	0.3	0.2	-0.31

Depth (cm)	Dx (10)	Dx (16)	Dx (25)	Dx (50)	Dx (75)	Dx (84)	Dx (90)	OM LOI %	CaCO$_3$ LOI %	MS
89	221	266	355	586	846	979	1097	0.7	0.0	-0.31
90	196	229	273	408	670	839	998	0.6	0.2	-0.31
91	104	140	183	324	894	1242	1479	0.6	0.3	-0.03
92	57	91	118	176	243	278	311	0.9	0.0	-0.03
93	151	179	210	288	402	693	882	0.4	0.4	-0.03
94	86	117	153	243	389	795	989	1.0	0.0	-0.03
95	185	210	247	336	457	523	587	0.0	1.4	-0.03

Note: Percentiles are in microns. OM and CaCO$_3$ percentages are from weight. Magnetic susceptibility (MS) is $* 10^8 \ m^3 \ kg^{-1}$.

Table A.5 Sedimentary analysis results for PB-C-02-2.

Depth (cm)	Dx (10)	Dx (16)	Dx (25)	Dx (50)	Dx (75)	Dx (84)	Dx (90)	OM LOI %	CaCO₃ LOI %	MS
1	196	220	251	336	456	524	596	0.9	0.0	-0.44
2	177	201	230	306	401	451	497	0.8	0.0	-0.44
3	129	163	201	294	422	676	912	0.5	0.0	-0.44
4	159	182	209	278	363	407	447	0.5	0.5	-0.44
5	201	224	253	331	432	486	536	0.5	0.4	-0.44
6	210	236	275	378	568	736	944	0.4	0.7	-0.15
7	157	187	222	314	434	502	569	0.7	0.2	-0.15
8	86	114	145	214	291	329	364	0.4	0.3	-0.15
9	181	207	242	343	512	642	781	0.3	0.0	-0.15
10	136	178	227	385	1321	1605	1839	0.6	0.4	-0.15
11	159	183	212	287	385	447	744	0.1	0.4	-0.23
12	113	164	217	340	537	1100	1436	0.5	0.0	-0.23
13	121	160	203	312	480	609	1011	0.4	0.9	-0.23
14	170	203	246	383	648	843	1191	0.5	0.0	-0.23
15	206	227	254	325	419	467	513	0.2	0.0	-0.23
16	168	198	240	350	1041	1406	1688	0.5	0.7	-0.07
17	272	298	327	402	498	550	597	0.3	0.5	-0.07
18	-	-	-	-	-	-	-	0.8	0.2	-0.07
19	151	185	221	305	426	515	613	0.7	0.2	-0.07
20	119	141	165	223	291	326	358	0.3	0.0	-0.07
21	181	206	238	319	436	717	927	0.5	0.5	-0.07
22	140	174	217	355	938	1457	1874	0.4	0.0	-0.07
23	200	222	251	326	424	478	531	0.3	0.8	-0.07
24	82	118	160	248	347	397	443	0.5	0.5	-0.07
25	140	173	210	298	403	458	508	0.6	0.4	-0.07
26	113	152	192	288	430	756	950	0.6	0.5	-0.24
27	108	140	174	255	372	685	852	0.3	0.2	-0.24
28	226	250	281	368	482	547	611	0.4	1.0	-0.24
29	218	241	271	348	445	496	544	0.5	0.7	-0.24
30	156	172	194	250	314	348	379	0.4	0.0	-0.24
31	180	197	219	275	346	382	415	0.3	0.4	-0.07
32	127	163	197	272	358	402	442	0.3	0.0	-0.07
33	101	135	172	256	352	401	445	0.3	0.6	-0.07
34	120	150	181	251	330	370	405	0.6	0.0	-0.07
35	242	267	300	389	499	558	616	0.3	0.4	-0.07
36	85	122	167	275	423	530	741	0.3	0.8	-0.43
37	165	189	219	299	397	450	500	0.3	0.0	-0.43
38	191	217	250	339	458	524	588	0.8	0.2	-0.43
39	230	256	289	382	498	562	637	0.5	0.4	-0.43
40	188	210	238	318	428	492	557	0.6	0.0	-0.43
41	178	201	232	319	432	496	558	0.8	0.4	-0.44
42	187	214	252	374	695	872	1035	0.8	0.3	-0.44
43	181	211	249	346	469	534	594	0.4	0.0	-0.44

Depth (cm)	Dx (10)	Dx (16)	Dx (25)	Dx (50)	Dx (75)	Dx (84)	Dx (90)	OM LOI %	CaCO₃ LOI %	MS
44	129	154	184	262	370	444	705	0.4	0.0	-0.44
45	67	95	132	216	318	380	455	0.9	0.2	-0.44
46	182	205	236	324	462	557	656	0.6	0.3	-0.11
47	159	185	217	303	426	506	614	0.4	0.3	-0.11
48	194	221	257	359	508	597	687	0.6	1.0	-0.11
49	154	177	207	290	404	471	541	0.6	0.2	-0.11
50	150	178	212	305	429	508	777	0.3	0.0	-0.11
51	192	216	247	330	439	498	556	0.4	0.2	-0.07
52	198	220	250	337	457	545	654	0.4	0.3	-0.07
53	182	206	237	318	427	492	573	0.7	0.0	-0.07
54	191	213	244	317	412	469	520	0.7	0.6	-0.07
55	203	227	259	344	454	513	568	0.8	0.0	-0.07
56	191	215	247	333	451	516	581	0.6	0.4	-0.17
57	212	235	265	349	462	524	584	0.7	0.2	-0.17
58	201	226	260	353	487	570	658	0.5	0.0	-0.17
59	120	150	182	265	698	876	1018	0.5	0.2	-0.17
60	187	214	249	340	462	526	587	0.5	0.2	-0.17
61	152	180	212	293	396	451	502	0.5	0.0	-0.21
62	166	187	216	293	410	767	948	0.4	0.0	-0.21
63	264	288	318	400	504	559	612	0.3	0.0	-0.21
64	194	215	243	318	419	483	591	0.6	0.6	-0.21
65	215	246	290	429	734	988	1397	0.6	0.3	-0.21
66	190	212	239	313	409	462	512	0.6	0.0	-0.55
67	176	199	230	310	415	473	528	0.5	0.0	-0.55
68	183	204	231	302	392	446	492	0.3	0.0	-0.55
69	163	182	207	272	355	398	440	0.4	0.1	-0.55
70	149	176	210	302	466	1090	1439	0.3	0.1	-0.55
71	130	154	182	257	353	407	460	0.4	0.2	-0.41
72	195	222	258	366	517	603	690	0.4	0.5	-0.41
73	139	166	200	286	393	450	503	0.6	0.0	-0.41
74	122	149	182	278	786	880	963	0.8	0.4	-0.41
75	188	212	243	325	430	486	537	0.9	0.0	-0.41
76	126	159	196	285	394	452	507	0.7	1.6	-0.40
77	55	78	110	194	302	360	416	0.8	-	-0.40
78	119	143	172	246	338	387	432	0.6	-	-0.40
79	112	144	181	271	380	437	489	0.5	0.0	-0.40
80	123	157	197	305	469	562	651	0.7	0.4	-0.40
81	229	254	287	375	490	555	617	0.2	-	-0.35
82	149	177	211	299	410	469	524	0.0	-	-0.35
83	77	106	138	213	303	350	395	0.0	-	-0.35
84.5	124	153	186	270	378	444	529	0.2	-	-0.35

Note: Percentiles are in microns. OM and CaCO₃ percentages are from weight. Magnetic susceptibility (MS) is $* 10^8$ m³ kg^{-1}. No particle size or sorting data for 18 cm. No CaCO₃ data for 77, 78, 81-84.5 cm.

Table A.6 Sedimentary analysis results for piezometer samples.

Sample	Dx (10)	Dx (16)	Dx (25)	Dx (50)	Dx (75)	Dx (84)	Dx (90)	OM LOI %	CaCO$_3$ LOI %	MS
1	381	413	456	576	733	820	932	0.5	0.0	0.38
2	81	301	390	623	965	1126	1273	1.6	0.3	0.51
3	9	13	19	52	147	195	237	1.6	0.3	1.41
4	9	12	18	45	151	216	278	1.4	0.0	0.35
5	10	14	20	60	195	243	283	0.8	0.0	0.26
6	9	13	19	78	228	283	330	0.5	0.0	-0.30
7	9	12	17	41	152	211	285	0.8	0.3	0.12
8	115	134	200	505	1297	1938	2802	0.9	0.0	0.93
9	822	911	1028	1271	1698	1951	2220	1.2	0.0	0.71
10	728	1072	1274	1689	2231	2565	2887	0.6	0.0	-0.71
11	476	552	658	925	1356	1747	2156	0.8	0.0	0.26
12	12	17	24	53	113	160	212	12.7	1.4	1.04
13	12	17	26	65	165	220	270	7.1	1.0	0.41
14	20	31	52	202	495	662	828	6.5	0.4	0.95
15	41	90	187	393	565	650	727	1.9	0.0	0.08
16	14	23	38	203	352	426	541	1.6	0.0	0.68
17	35	55	98	389	613	745	930	9.1	1.2	0.81
18	12	16	22	47	103	139	172	1.7	0.2	0.74
19	10	14	20	38	83	126	178	2.4	0.0	0.75
20	9	13	18	35	75	116	159	1.2	0.4	0.35
21	24	42	143	288	431	516	629	0.4	0.6	1.06
22	475	515	565	693	850	934	1018	1.2	0.0	-0.77
23	161	227	328	804	1239	1481	1720	0.0	0.0	0.55
24	121	190	249	369	556	706	1073	18.1	0.0	0.72
25	28	40	58	111	410	662	826	3.5	0.3	-0.12
26	280	326	388	570	798	945	1091	2.6	1.3	0.22
27	58	99	150	270	405	482	580	3.3	0.0	-0.80
28	397	487	607	957	1459	1809	2140	2.7	0.2	-0.68
29	132	179	212	327	440	504	564	2.3	0.0	-0.98
30	376	422	477	643	989	1350	1702	3.6	0.3	0.18
31	307	368	432	588	778	877	972	6.1	0.3	-0.45
32	366	413	467	615	812	934	1049	3.6	0.3	-0.13
33	200	256	316	451	622	734	840	2.3	0.2	-0.41

Note: Percentiles are in microns. OM and CaCO$_3$ percentages are from weight. Magnetic susceptibility (MS) is $* 10^8$ m^3 kg^{-1}.

Table A.7 Sedimentary analysis results for Bon Secour Bay grab samples.

Sample	Dx (10)	Dx (16)	Dx (25)	Dx (50)	Dx (75)	Dx (84)	Dx (90)	OM LOI %	CaCO$_3$ LOI %	MS
1	15	20	28	60	127	169	209	10.6	3.0	7.75
2	122	143	167	224	292	326	356	0.9	0.2	0.10
3	150	169	192	253	328	367	402	0.8	0.2	-0.24
4	34	51	81	171	268	316	360	4.1	1.8	3.60
5	59	91	134	253	638	874	1047	2.7	0.7	1.25
6	164	181	203	260	330	366	399	0.7	0.2	0.40
7	141	163	189	257	342	388	429	0.8	0.3	0.63
8	143	164	191	259	344	390	433	1.1	0.2	0.52
9	196	221	253	335	440	498	552	0.7	0.2	-0.26
10	113	137	164	228	305	344	380	1.2	0.2	-0.21
11	186	232	265	342	434	481	523	1.1	0.0	0.25
12	179	200	225	286	360	398	433	1.0	0.3	0.60
13	10	14	20	45	103	142	179	10.1	4.2	7.71
14	43	60	87	183	312	375	431	3.3	1.1	2.68
15	131	151	177	243	329	374	417	1.3	0.2	0.09
16	154	181	216	305	428	503	593	0.7	0.5	-0.10

Note: Percentiles are in microns. OM and CaCO$_3$ percentages are from weight. Magnetic susceptibility (MS) is * 10^8 m^3 kg^{-1}.

Table A.8 Sedimentary analysis results for Perdido Bay grab samples.

Sample	Dx (10)	Dx (16)	Dx (25)	Dx (50)	Dx (75)	Dx (84)	Dx (90)	OM LOI %	CaCO$_3$ LOI %	MS
1	417	485	561	740	951	1060	1159	0.8	0.2	-0.31
2	76	127	166	241	321	361	396	0.6	0.1	-0.38
3	63	93	142	269	380	433	481	0.6	0.0	0.46
4	206	226	253	323	406	449	490	0.5	0.0	-0.34
5	152	198	237	323	424	475	522	0.5	0.0	-0.14
6	87	134	178	293	803	938	1055	0.7	0.0	-1.30
7	121	145	174	242	326	371	413	0.8	0.2	-1.15
8	144	172	202	274	361	406	447	0.6	0.2	-1.95
9	146	168	195	261	343	385	425	0.7	0.0	-0.65
10	131	172	211	307	562	849	1012	0.5	0.2	0.61
11	117	156	199	314	809	1319	1590	0.7	0.0	-0.07
12	76	106	142	234	373	559	780	1.0	0.2	-0.78
13	17	24	35	85	189	240	285	8.7	2.8	-3.26
14	20	28	40	91	179	222	260	10.2	2.9	2.82

Note: Percentiles are in microns. OM and CaCO$_3$ percentages are from weight. Magnetic susceptibility (MS) is * 10^8 m^3 kg^{-1}.
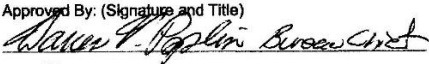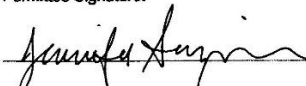
APPENDIX B – FDEP Permit Approval

Permit Number
18110912

Florida Department of Environmental Protection
Division of Recreation and Parks
Florida Park Service

SCIENTIFIC (NON-COMMERCIAL) RESEARCH / COLLECTING PERMIT

Park Visits Must Be Arranged A Minimum Of One Week In Advance. Failure To Make Required Arrangements Will Result In Denial Of Park Entry.
Permit Must Be Carried At All Times While Working In State Parks.

Permittee:	Address, Phone, Email:	Issue Date:
Jennifer Simpson	Department of Geography and Geology	**November 9, 2018**
	Chain Technology Bldg. (TEC) 103	
Representing:	118 College Drive, Box 5018	**Expiration Date:**
University of Southern Mississippi	Hattiesburg, MS 39406	**March 31, 2019**
	904-412-1346; Jennifer.simpson@usm.edu	

Additional Authorized Researchers: Franklin Heitmuller	Subject: Analysis of estuarine shoreline erosion in microtidal zones Permitted Activity: The researchers are studying the sedimentology and geomorphology of two SW-facing estuarine peninsulas in the context of long-term change at these coastlines and a possible connection to sea level rise; the peninsula at the westernmost extension of the park is one focal site (the other along Bon Secour Bay, Alabama). Using a boat for access to the site, they will select two locations along the shoreline from which to perform the following tasks: (1) initial collection of substrate cores from terrestrial habitat using a soil auger inserted down to the water table [at 10m and 50m from shoreline; bagged at increments], (2) subsequent installation of 6-ft. PVC pipes for groundwater pressure logging device to record groundwater fluctuation, (3) a few months later, several shallow subaqueous samples will be collected in the nearshore area (>/= 50m from shoreline). When selecting coring sites, avoid any large-leaf jointweed plants (*Polygonella macrophylla*; Florida-threatened species) encountered.
In the Following Park(s): Tarkiln Bayou Preserve State Park	Permitted Collection: Sediment cores (2 inch diameter) as indicated above. Coordinate potential collecting sites with the park manager or designee in order to avoid any known cultural sites.

*** Note characteristic features of large-leaf jointweed at this website:

http://florida.plantatlas.usf.edu/Plant.aspx?id=2559&syn_name=Polygonella+macrophylla

Researchers shall take care to minimize the area and depth of ground disturbing activities and shall consult with the park manager at each location to determine the best locations for sampling away from any known cultural resources. If prehistoric or historic artifacts, such as pottery or ceramics, projectile points, dugout canoes, metal implements, historic building materials, or any other physical remains that could be associated with Native American, early European, or American settlement are encountered at any time within the project site area, the permitted project shall cease all activities involving subsurface disturbance in the immediate vicinity of the discovery and contact the Park Manager and the Florida Department of State, Division of Historical Resources, Compliance Review Section at (850)-245-6333. Project activities shall not resume without verbal and/or written authorization. In the event that unmarked human remains are encountered during permitted activities, all work shall stop immediately, and the proper authorities notified in accordance with Section 872.05, Florida Statutes.

Permit Attachments: Standard Conditions

Permit Not Valid Unless Signed By All Parties

Issuing Office

Approved By: (Signature and Title)

Dawn V. Poslin, Bureau Chief

11-13-2018
Date

District 1 Administration
Division of Recreation and Parks
4620 State Park Lane
Panama City, FL 32408
850-233-5110 (fax: 850-233-5147)

Permittee

I have read this permit and all attachments listed above. I fully understand it, and will abide by all rules and regulations.

Permittee Signature: *Jennifer Simpson*

Date: 11/14/2018

REFERENCES

Anderson, J.B., and Rodriguez, A.B., eds., 2008, Response of Upper Gulf Coast Estuaries
to Holocene Climate Change and Sea-Level Rise: Geological Society of America
Special Paper 443.

Bache, F., Sutherland, R., and King, P.R., 2014, Use of ancient wave-ravinement surfaces
to determine palaeogeography and vertical crustal movements around New
Zealand: New Zealand Journal of Geology and Geophysics, doi:
10.1080/00288306.2014.975254.

Benninger, L. K. and Wells, J. T., 1993, Sources of sediment to the Neuse River estuary,
North Carolina, Marine Chemistry, 43, pp.137–156.

Boyd, R., 2010, Transgressive wave-dominated coasts, in James, N.P., and Dalrymple,
R.W., eds., Facies Models 4: Geological Association of Canada, p. 265–294.

Bruun, P., 1962, Sea level rise as a cause of shore erosion: Journal of Waterways and
Harbors Division, American Society of Civil Engineers, v. 88, no. 1, p. 117–132.

Carter, Ly'Nita, 2019, Tarkiln Bayou Preserve State Park conducts prescribed burn in
Escambia County: https://weartv.com/news/local/tarkiln-bayou-preserve-state-
park-conducts-prescribed-burn (accessed December 2019).

Catuneanu, O., Abreu, V., Bhattacharya, J.P., Blum, M.D., Dalrymple, R.W., Eriksson,
P.G., Fielding, C.R., Fisher, W.L., Galloway, W.E., Gibling, M.R., Giles, K.A.,
Holbrook, J.M., Jordan, R., Kendall, C.G.S.C., et al., 2009, Towards the
standardization of sequence stratigraphy: Earth-Science Reviews, doi:
10.1016/j.earscirev.2008.10.003.

Chandler, R.V., Moore, J.D., Gillett, B., 1985, Ground-water chemistry and salt-water encroachment, southern Baldwin County, Alabama: Geological Survey of Alabama Bulletin 126.

Cowart, L., Walsh, J.P., and Corbet, D.R., 2010, Analyzing estuarine shoreline change: a case study of Cedar Island, North Carolina, Journal of Coastal Research, 26(5), 817-830, West Palm Beach, Florida.

Dalrymple, R.W., Zaitlin, B.A., and Boyd, R., 1992, Estuarine facies models : conceptual basis and stratigraphic implications: Journal of Sedimentary Petrology, doi: 10.1306/D4267A69-2B26-11D7-8648000102C1865D.

Dalrymple, R.W., 2010, Interpreting sedimentary successions: facies, facies analysis and facies models, in James, N.P., and Dalrymple, R.W., eds., Facies Models 4: Geological Association of Canada, p. 3–18.

Dearing, J. A. 1999, Using the Bartington MS2 System. Environmental Magnetic Susceptibility p. 29.

DuBar, J.R., Ewing, T.E., Lundelius, E.L., Jr., Otvos, E.G., and Winkler, C.D., 1991, Quaternary geology of the Gulf of Mexico Coastal Plain, in Morrison, R.B., ed., Quaternary nonglacial geology; Conterminous U.S.: Boulder Colorado, Geological Society of America, The Geology of North America, The Decade of North American Geology (DNAG), v. K-2, p. 583–594.

EPA, 2012, Total Solids, in Water: Monitoring & Assessment, https://archive.epa.gov/water/archive/web/html/vms58.html (accessed January 2020).

Ewing, T. E., 1991, Quaternary geology of the Gulf of Mexico Coastal Plain, in

    Morrison, R.B., ed., Quaternary nonglacial geology; Conterminous U.S.: Boulder

    Colorado, Geological Society of America, The Geology of North America, v. K-

    2,584 p.

Friedman, G.M., 1962, On Sorting, Sorting Coefficients, and the Lognormality of the

    Grain-Size Distribution of Sandstones: The Journal of Geology, doi:

    10.1086/jg.70.6.30066373.

Hardin, J. D., Sapp C. D., Emplaincourt, J. L., and Richter, K. E., 1976, Shoreline and

    bathymetric changes in the coastal area of Alabama: Alabama Geological Survey

    Information Series 50, 125 p.

Halka, J. P., and L. P. Sanford 2014. Contributions Of Shore Erosion And Resuspension

    To Nearshore Turbidity In The Choptank River, MARYLAND, Rep. 83, 64 pp,

    MD Department of Natural Resources, Maryland Geological Survey, Baltimore,

    MD.

Heiri, O., Lotter, A.F., and Lemcke, G., 2001, Loss on ignition as a method for estimating

    organic and carbonate content in sediments: Reproducibility and comparability of

    results: Journal of Paleolimnology, doi: 10.1023/A:1008119611481.

Hollis, R.J., Wallace, D.J., Miner, M.D., Gal, N.S., Dike, C., and Flocks, J.G., 2019, Late

    Quaternary Evolution and Stratigraphic Framework Influence on Coastal Systems

    along the North-Central Gulf of Mexico, USA: Quaternary Science Reviews, v. 223,

    105910. https://doi.org/10.1016/j.quascirev.2019.105910

Hummell, R.L., 1996, Holocene Geologic History of the West Alabama Inner

    Continental Shelf, Alabama: Geological Survey of Alabama Circular 189, p. 131.

Hummell, R.L., and Parker, S.J., 1995, Holocene Geologic History of Mobile Bay, Alabama: Geological Survey of Alabama Circular 186, 97 p.

Isphording, W.C., and Flowers, G.C., 1990, Mobile Bay: Issues, Resources, Status, and Management: Geological and Geochemical Characterization: NOAA Estuary-of-the-Month Seminar Series Number 15, p. 9–25.

Isphording, W.C., and Lamb, G.M., 1971, Age and Origin of the Citronelle Formation in Alabama: Geological Society of America Bulletin, v. 82, p. 775–780.

Kindinger, J.L., Balson, P.S., and Flocks, J.G., 1994, Stratigraphy of the Mississippi-Alabama shelf and the Mobile River incised-valley system, in Dalrymple, R.W., Boyd, R., and Zaitlin, B.A., eds., Incised-Valley Systems: Origin and Sedimentary Sequences: Society for Sedimentary Geology Special Publication 51, p. 83–95.

Kolker, A.S., Allison, M.A., and Hameed, S., 2011, An evaluation of subsidence rates and sea-level variability in the northern Gulf of Mexico: Geophysical Research Letters, vol. 38, no. 21, doi:10.1029/2011GL049458.

Leatherman, S.P., Zhang, L., and Douglas, B.C., 2000, Sea level rise shown to drive coastal erosion: Eos, v. 81, p. 55–57.

Livingstone, D.A., 1955, A Lightweight Piston Sampler for Lake Deposits: Ecology, v. 36, p. 137–139, doi:10.2307/1931439.

Marsh, O.T., 1996, Geology of Escambia and Santa Rosa Counties, Western Florida Panhandle, Florida Geological Survey Bulletin, No. 46, 140 p.

Martin, D.M., Morton, T., Dobrzynski, T., and Valentine, B., 1996, Estuaries on the
Edge: The Vital Link between Land and Sea, Washington, DC: American Oceans
Campaign, 297p.

Matson, G.C., 1916, The Pliocene Citronelle Formation of the Gulf Coastal Plain: U.S.
Geological Survey Professional Paper 98-L, p. 167–192.

McBride, R.A., and Byrnes, M.R., 1995, Surficial Sediments and Morphology of the
Southwestern Alabama/Western Florida Panhandle Coast and Shelf: Gulf Coast
Association of Geological Societies Transactions, v. 45, p. 393–404.

Milliken, K.T., Anderson, J.B., and Rodriguez, A.B., 2008, A new composite Holocene
seal-level curve for the northern Gulf of Mexico, in Anderson, J.B., and
Rodriguez, A.B., eds., 2008, Response of Upper Gulf Coast Estuaries to Holocene
Climate Change and Sea-Level Rise: Geological Society of America Special
Paper 443, p. 1–11, doi: 10.1130/2008.2443(01).

Morton, R.A., Miller, T.L., and Moore, L.J., 2004, National assessment of shoreline
change: Part 1: Historical shoreline changes and associated coastal land loss along
the U.S. Gulf of Mexico: U.S. Geological Survey Open-file Report 2004-1043,
45p.

Nichols, M.M., and Biggs, R.B., 1985, Estuaries, in Davis, R.A., Jr., ed., Coastal
Sedimentary Environments: New York, New York, Springer-Verlag, p.77–186.

NOAA, 2019, National Weather Service, January 2019 Climate Summaries: Mobile,
Alabama and Pensacola, Florida Area:
https://www.weather.gov/mob/january2019climatesummaries (accessed June
2019).

Northwest Florida Water Management District, 2017, Perdido River and Bay Surface

> Water Improvement and Management Plan, Program Development Series 17-07:

> https://www.nwfwater.com/layout/set/print/content/download/15863/110068/versi

> on/1/file/Perdido+River+and+Bay+SWIM+Plan+November+2017.pdf (accessed

> May 2019).

Otvos, E.G., 1991, Northeastern Gulf Coast Quaternary, in DuBar, J.R., and others,

> Quaternary geology of the Gulf of Mexico coastal plain, Chapter 19, of Morrison,

> R.B., ed., Quaternary nonglacial geology; conterminous United States: Geological

> Society of America, The Geology of North America, The Decade of North

> American Geology (DNAG), v. K-2, p. 588-594.

Raymond, D. E., Osborne, W. E., Copeland, C. W., and Neathery, T. L., 1988, Alabama

> stratigraphy: Alabama Geological Survey Circular 140, 97 p.

Reading, H.G., and Collinson, J.D., 1996, Clastic coasts, in Reading, H.G., ed.,

> Sedimentary environments: Processes, Facies and Stratigraphy (third edition):

> Oxford, UK: Blackwell, p. 154–231.

Reinson, G.E., 1992, Transgressive Barrier Island and Estuarine Systems, in Walker,

> R.G., and James, N.P., eds., Facies Models: Response to Sea Level Change:

> Geological Association of Canada, p. 179–194.

Rodriguez, A.B., Greene, D.L., Jr., Anderson, J.B., and Simms, A.R., 2008, Response of

> Mobile Bay and eastern Mississippi Sound, Alabama, to changes in sediment

> accommodation and accumulation, in Anderson, J.B., and Rodriguez, A.B., eds.,

> Response of Upper Gulf Coast Estuaries to Holocene Climate Change and Sea-

Level Rise: Geological Society of America Special Paper 443, p. 13–29, doi: 10.1130/2008.2443(02).

Rodriguez, A.B., Simms, A.R., and Anderson, J.B., 2010, Bay-head deltas across the northern Gulf of Mexico back step in response to the 8.2ka cooling event: Quaternary Science Reviews, doi: 10.1016/j.quascirev.2010.10.004.

Roy, P.S., 1994, Holocene estuary evolution-stratigraphic studies from southeastern Australia, in Dalrymple, R.W., Boyd, R., and Zaitlin, B.A., eds., Incised-Valley Systems: Origin and Sedimentary Sequences: Society for Sedimentary Geology Special Publication 51, 217 p.

Sanford, L.P., and Gao, J., 2018, Influences of Wave Climate and Sea Level on Shoreline Erosion Rates in the Maryland Chesapeake Bay: Estuaries and Coasts, doi: 10.1007/s12237-017-0257-7.

Slaughter, T.H. 1967. Shore erosion control in tidewater Maryland. Journal of the Washington Academy of Sciences 57: 117–129.

Smith, G.L. and Zarillo, G.A., 1990, Calculating Long-Term Shoreline Recession Rates Using Aerial Photographic and Beach Profiling Techniques: Journal of Coastal Research, v. 6, p 111-120.

Schwartz, M., 1965, Study of Sea-Level Rise as a Cause of Shoreline Erosion: The Journal of Geology, v. 72, no. 3, p. 528–534.

State of Florida Department of Environmental Protection, 2018, Big Lagoon State Park, Tarkiln Bayou Preserve State Park, Perdido Key State Park Advisory Group Draft Unit Management Plan, p. 10,

https://floridadep.gov/sites/default/files/BL_TB_PK_AGDraft_Website.pdf (accessed December 2019).

Striggow, B., 2017, Field Measurement of Oxidation-Reduction Potential (ORP): U.S. Environmental Protection Agency Region 4, Science and Ecosystem Support Division Operating Procedure, 2017-SESDPROC-113-R2, 22 p., https://www.epa.gov/sites/production/files/2017-07/documents/field_measurement_of_orp113_af.r2.pdf (accessed January 2020).

SWRCB, 2002, Electrical Conductivity/Salinity Fact Sheet: The Clean Water Team Guidance Compendium for Watershed Monitoring and Assessment State Water Resources Control Board, 5 p., http://www.swrcb.ca.gov/water_issues/programs/swamp/docs/cwt/guidance/3130 en.pdf (accessed January 2020).

Tolhurst, T.J., Friend, P.L., Watts, C., Wakefield, R., Black, K.S., and Paterson, D.M., 2006, The effects of rain on the erosion threshold of intertidal cohesive sediments: Aquatic Ecology, doi:10.1007/s10452-004-8058-z.

Van Rijn, L.C., and Barr, D.I.H., 1990, Principles of fluid flow and surface waves in estuaries, seas and oceans: Journal of Hydraulic Research, doi:10.1080/00221689009499028.

Work, P., Charles, L., Dean, R., 1991, Perdido Key Historical Summary and Interpretation of Monitoring Programs: Submitted to Department of the Navy Southern Division Naval Facilities Engineering Command, Charleston, SC, 56 p.

Zhang, K., Douglas, B.C. and Leatherman, S.P., 2004, Global warming and coastal erosion: Climatic Change, v. 64, p.41–58.